UTILIZING BIOMASS AND WASTE FOR POWER PRODUCTION - A DECADE OF CONTRIBUTING TO THE UNDERSTANDING, INTERPRETATION AND ANALYSIS OF DEPOSITS AND CORROSION PRODUCTS

Flemming Jappe Frandsen

Associate Professor
Combustion and Harmful Emission Control Research Centre
Department of Chemical Engineering, Technical University of Denmark
Building 229, DK-2800 Lyngby, Denmark
Phone: +45 45 25 28 83, Fax: +45 45 88 22 58,
E-mail: ff@kt.dtu.dk

Through the years, Danish utilities have gained significant knowledge on how to minimize or even avoid ash deposition problems in utility boilers, firing worldwide high-volatile bituminous coals. In the early 90ties, the Danish Government decided on a 20 % reduction in the CO_2-emission before the year 2005, based on the 1988-level. Biomass is considered CO_2-neutral due to its short time of regeneration compared to fossil fuels. Thus, the Danish power producers are enjoined to burn 1.0 Mtons of straw, 0.2 Mtons of wood chips and 0.2 Mtons of straw/wood chips (free choice) every year beyond year 2005. As a consequence of this, the CHEC Research Centre, Department of Chemical Engineering, Technical University of Denmark, being partly funded by the Danish power utilities, has during the last decade, investigated ash and deposit formation, and corrosion, in utility boilers fired with coal, petcoke, orimulsion, and different types of biomass (straw (barley, rape and wheat), wood (beech, spruce, fibreboard, bark and waste wood), shea nuts, olive stones etc.).

This paper summarizes our findings, including recent activities on: 1) deposit formation during coal-wheat straw co-firing in a suspension-fired boiler, 2) a pilot-scale study of ash and deposit formation in the Sandia Multi-Fuel Combustor (MFC), 3) a full-scale measuring campaign dealing with the effect of co-firing of biomass on the ash and deposit formation, 4) a second full-scale measuring campaign addressing low-temperature corrosion of tubes in the air pre-heater of a straw-fired utility boiler, 5) a lab-scale study of the corrosion of superheater materials in straw-fired utility boilers, and, finally, 6) a fundamental study on ash and deposit formation in municipal solid waste incinerators. The paper provides insight into the experience gained on ash, deposit and corrosion formation in thermal fuel conversion systems fired with solid non-fossil fuels, and focuses attention on how these results fit into our current understanding of this subject. A complete and updated list of references covering our research activities within this area during the last decade is provided.

INVESTIGATION OF FORMATION PATHWAYS OF AEROSOL PARTICLES FORMED DURING FIXED BED COMBUSTION OF WOODY BIOMASS FUELS

Markus Jöller[1], Thomas Brunner[1], Ingwald Obernberger[1], Ilse Letofsky-Pabst[2]

[1] Institute for Resource Efficient and Sustainable Systems
Graz University of Technology, Inffeldgasse 25C, Graz, Austria
[2] Research Institute for Electron Microscopy
and Fine Structure Research
Graz University of Technology, Steyrergasse 17, Graz, Austria

Introduction

The use of biomass combustion for the production of heat and electric power has already become an important factor for energy supply. A big share of this kind of energy supply is covered by fixed bed combustion of woody biomass fuels in combustion plants with a size range from a few kW of thermal output to large plants in the MW range. But all of these plants suffer more or less from ash related problems, which are deposition of fly ashes and subsequent slagging and fouling and additionally, particle emissions have to be prevented.

In order to decrease the ash related problems inside the combustion plants as well as harmful emissions, detailed knowledge about fly ash formation and deposition mechanisms is required. The results from these investigations are expected to be helpful for the implementation of measures, which can influence the formation and deposition of ashes.

Fly ash formation during combustion of woody biomass. In order to get more information about fly ash formation and behavior and to determine possible influencing parameters, investigations of fly ashes were performed by many researchers in the past for coal combustion as well as for biomass combustion (e.g. 1-4).

At the Institute for Resource Efficient and Sustainable Systems (RNS) investigations concerning biomass combustion were performed for three woody biomass fuels, which are frequently used in fixed bed furnaces for energy production, namely chemically untreated wood, bark and waste wood (5). The results have shown a bimodal particle size distribution (PSD). One mode, the coarse fly ash particles, consists of particles with a diameter larger than 1 µm, the particles of the second mode, the aerosols, are submicron. Chemical analyses of coarse fly ashes showed mainly compounds, which have under the given conditions in biomass furnaces a low volatility. The coarse fly ashes investigated consisted mainly of oxides and sulphates of Ca, Mg, Si and K.

The average chemical composition of aerosol particles could be obtained by wet chemical analyses of particles sampled on Berner-type low-pressure impactor (BLPI) stages. It could be derived that low volatile elements were enriched in coarse fly ash particles in opposite to volatile elements, which were enriched in aerosol particles. At least the distribution of Zn followed the PSD, which suggested an even distribution in the particles. These results could also be gained from scanning electron microscopy (SEM)/ electron diffraction X-ray spectrometry (EDX) analyses of single particles, which provided average compositions.

Regarding the aerosols, three particle formation theories could be derived (6). The different chemical compositions of biomass fuels lead to different release behaviours of aerosol forming elements and in the following to different particle formation pathways.

During the combustion of chemically untreated wood chips mainly ash forming compounds of the elements K, S, and Cl are released to the gas phase. These compounds may react further and undergo gas to particle conversion processes during flue gas cooling. The supersaturated ash vapours may nucleate or condense on the surface of particles, which are entrained directly from the fuel bed (primary particles). Due to chemical analyses of aerosol particles, which showed K, S and Cl as the main components, the presence of considerable amounts of primary particles, which could suppress nucleation of new particles, could be ruled out. Therefore, nucleation and afterwards condensation should be the dominating particle formation mechanisms.

Compared to pure wood fuels bark contains considerably more low volatile compounds of the elements Ca and Mg, but also more K, Cl, S and Zn. During the combustion process a certain amount of the low volatile compounds is directly released as primary particles in the submicron as well as in the supermicron size range. Especially the submicron primary particles, which contain mainly CaO according to chemical analyses, may provide surface for further condensation of ash forming vapours. Additionally, Zn plays an important role for aerosol formation during bark combustion. According to thermodynamic equilibrium calculations Zn is expected to evaporate during combustion on the grate and as soon as oxidising conditions prevail in the flue gas ZnO should form. ZnO has a very low vapour pressure and therefore it should immediately form particles, which subsequently act as seeds for further condensation of aerosol forming matter. Therefore, during the combustion of bark nucleation of new particles may be suppressed partially by primary particles (CaO) and ZnO particles.

A third main pathway for aerosol formation could be derived for the combustion of waste wood, which contains considerably higher amounts of Zn than pure wood and bark. This surplus of Zn compared to other fuels mainly originates from paintings. Due to the great amount of ZnO particles, which form in the way as described for bark combustion, a further nucleation of ash forming vapours may be suppressed completely.

The condensation of ash forming vapours on aerosols containing Ca and Zn has not been proved yet. For that reason the analyses of aerosol particles regarding their composition in the core as well as in the outer layer were aspired. The only way to achieve a sufficiently high resolution for such particle analyses was the use of transmission electron microscopy (TEM) in combination with EDX analyses. Therefore, aerosol samples were taken on copper grids from combustion plants and subsequently analysed by TEM.

Experimental

Aerosol sampling. The particle sampling was performed during the combustion of chemically untreated wood (spruce) and bark at the boiler outlet of a combustion plant with a 440 kW_{th} flame tube boiler. The samples were taken in the way that copper grids, which were precoated with a carbon layer, were fixed on polycarbonate filters. After that, flue gas from the boiler outlet was sucked over the polycarbonate filters for some seconds. Then the copper grids were removed from the filter and forwarded to the Research Institute for Electron Microscopy and Fine Structure Research in order to perform the TEM/EDX analyses.

TEM/EDX Analyses. For the visual characterisation of the aerosol particles, pictures were taken with a CCD camera and evaluated. Furthermore, in order to detect the compositions of the aerosol particles EDX spectra were taken. Firstly, to detect the composition of the particles' cores the analysis point was set in the centre of the particle image. Secondly, for the outer layer analysis the electron beam was placed in a way that it touched the particle shells.

The instrument used for these investigations was a Philips CM20/STEM with an acceleration voltage of 200 kV and a LaB_6 cathode. The EDX spectra were recorded using a light element detector (HPGe).

Results and Discussion

The particles found on the TEM-grids had various sizes between several nanometres and about 0.2 µm. It seemed that bigger particles,

which were found during previous fly ash characterisation investigations could not be caught with the copper grids. Nevertheless, the particles captured were in the right size range for TEM analyses (< 0.3µm). The visual evaluation of the particles showed mostly small agglomerate-like particles as it can be seen in Figure 1.

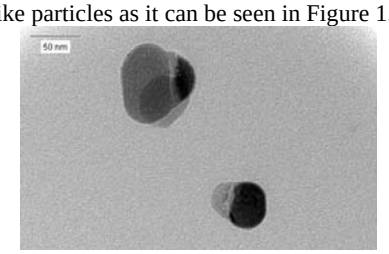

Figure 1. Picture of aerosol particles taken with a CCD camera

EDX analyses of aerosol particles from the combustion of wood chips (spruce) and bark showed that for chemically untreated wood the dominating species were K-compounds (mostly K_2SO_4) as it had been expected from former investigations. Also for aerosol particles from bark combustion K_2SO_4 and KCl were dominating the composition. Interestingly, no particles containing Ca could be found, which leads to the conclusion that Ca, although it had been detected in that particle size range by wet chemical analyses of impactor samples, originates from bigger particles, which could not be fixed on the TEM grids. The Ca in particles smaller than 200 nm in impactor samples was found most probably due to non-ideal particle precipitation efficiency of the impactor stages and particle bounce off to stages with smaller cut diameter.

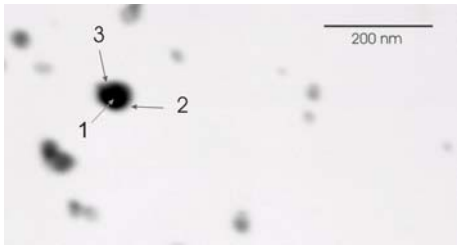

Figure 2. Locations of TEM analyses on aerosol particles

In order to determine if ZnO particles had been present before the formation of condensed K_2SO_4 and KCl, particles were investigated in more detail. During TEM analyses Zn was found in some aerosols from bark combustion. The particles were analysed at different points such as shown in Figure 2. The analyses of point 1 in Figure 2, which covered shell and core of the particle, showed a Zn/K mass ratio of 0.27 (± 20%). In contrast, the analysis of point 2, which just hit the particle shell, did not show any Zn. Point 3 showed a similar result as point 2. The analyses spectra of the points 1 and 2 are plotted in Figure 3. Generally, the Zn containing particles investigated showed this build-up. From that it could be concluded that Zn most probably had formed ZnO particles, which further acted as condensation seeds for other ash forming species. Regarding aerosol formation during waste wood combustion, chemical analyses of aerosol particles and simulation calculations suggest a higher suppression of nucleation of ash forming compounds by ZnO particles, but TEM/EDX analyses have still to be performed.

The formation pathways described could also be confirmed by aerosol formation simulations (7), which were performed in order to find the most influencing variables on formation mechanisms. Calculations of aerosol formation and behaviour in a biomass furnace with fixed grate and flame tube boiler were performed and the results were compared with measurements. In fact, modelling results similar to the measured results could be obtained when Ca and Zn were considered in the simulation as primary particles. Zn was inserted as peak of ZnO particles with a diameter < 0.1 µm and Ca was implemented as a broad peak of particles containing mainly CaO ranging from 0.3 to several hundred µm. Simulation results of PSDs and chemical compositions of the aerosols were similar to the measured values.

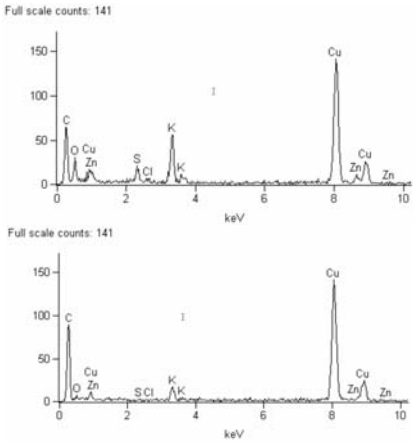

Figure 3. Spectra of point analyses no. 1 and 2 displayed in Figure 2

Conclusions

Investigations of aerosol formation during fixed bed combustion of chemically untreated wood, bark and waste wood were performed in order to derive influencing measures on particle formation and deposition. Three main aerosol formation pathways could be derived:

During the combustion of chemically untreated wood ash forming compounds of K, S and Cl are released into the gas phase and subsequently may react and further form particles by nucleation and condensation. During the combustion of bark submicron and supermicron Ca-containing particles are entrained from the fuel bed in considerable amounts. Especially the submicron particles provide condensation surface for further ash forming compounds and may suppress nucleation partly. For particle formation from bark combustion and especially from waste wood combustion Zn becomes important. As confirmed by thermodynamic data, the amounts of Zn released to the gas phase form mainly ZnO, which undergoes nucleation and condensation and forms particles with a diameter below 100 nm. These particles act as seeds for further condensation of alkali chlorides and sulphates as well as for gaseous heavy metal compounds and can therefore suppress nucleation to a certain extent depending on their concentration in the flue gas.

TEM analyses of aerosols in a size range below 200 nm from combustion of wood chips (spruce) and bark were performed in order to proof these theories. The results confirmed the expected particle formation pathways. Furthermore, these aerosol formation processes could be reproduced quite accurately by simulation calculations, which show results similar to measured PSDs and wet chemical analyses of aerosol particles.

References

(1) Wilemski, G., Srinivasachar, S., Sarofim, A.F. In *Inorganic transformations and ash deposition during combustion*; ASME, New York, 1992; pp. 545-564.
(2) Kauppinen, E.I., Pakkanen, T.A. *Environ. Sci. Technol.* **1990**, 24, 1811.
(3) Valmari, T., Kauppinen, E.I., Kurkela, J., Jokiniemi, J., Sfiris, G., Revitzer, H. *J. Aerosol Sci.* **1998**, 29, 445.
(4) Obernberger, I., Dahl, J., Brunner, T. In *Biomass: A growth opportunity in green energy and value added products, Vol. 2*; Overend, R.P., Chornet, E., Ed.; Pergamon-Elsevier Science Ltd., Oxford, 1999; pp. 1377-1383.
(5) Brunner, T.; Obernberger, I.; Jöller, M.; Arich, A.; Pölt, P. In *Aerosols from Biomass Combustion*; Nussbaumer, T., Ed.;Verenum, Zürich, 2001; pp. 75-80.
(6) Obernberger, I.; Brunner, T.; Jöller, M. In *Aerosols from Biomass Combustion*; Nussbaumer, T., Ed.; Verenum, Zürich, 2001; pp. 69-74.
(7) Jöller, M., Brunner, T., Obernberger, I.; Submitted for publication to *J. Aerosol Sci.* **2003**.

RELEASE OF INORGANIC ELEMENTS DURING WOOD COMBUSTION

Simone C. van Lith, Peter Arendt Jensen, Flemming J. Frandsen, and Peter Glarborg

CHEC Research Center
Department of Chemical Engineering
DTU-building 229
DK-2800 Lyngby, Denmark
E-mail: chec@kt.dtu.dk

Abstract

The objective of this work is to quantify the release of inorganic metal species, S and Cl from wood at combustion conditions that resemble grate combustion. This was done by performing lab-scale experiments at well-controlled conditions. The obtained quantitative release data are essential for the development of models for aerosol and fly-ash formation and behavior, aiming to understand the ash-related problems occurring during combustion of wood in power plants. Experimental release data obtained in the temperature range of 500-850^{o}C are presented for spruce and fiberboard. The results show that the release is strongly dependent on the temperature and on the inorganic composition of the fuel.

Introduction

Biomass fuels contain a certain amount of inorganic elements, of which a part may be released during combustion on the grate to form inorganic gases and particular matter (aerosols and fly-ashes), while the remaining part forms a bottom ash fraction. This formation of inorganic gases and particulate matter may lead to problems. First of all, the gases that are formed and emitted to the atmosphere include environmentally harmful gases (e.g. SO_2 and HCl). Inside combustion units, the formation of particular matter causes deposit formation on superheater tubes, which in turn leads to a reduction of the heat transfer efficiency to the water/steam system and may cause corrosion of the superheater tubes.

Although woody biomass fuels are often thought to be 'less problematic fuels' due to their relatively low ash content, ash-related problems are also observed in wood-fired boilers. Woody biomass generally has a low concentration of K, S and Cl compared to other solid fuels such as straw and coal, but the amount of Ca and heavy metals (such as Zn, Cu and Pb) is relatively high in most woody biomass fuels; especially bark contains a relatively high amount of Ca, and waste wood contains a relatively high amount of heavy metals. Combustion of wood may therefore lead to serious problems due to aerosol formation. Not only the quantity of ash, but also the composition of the ash and the volatility of the ash-forming matter are important when studying the release of inorganic elements during wood combustion.

Objectives

To be able to tackle problems involving aerosol and fly-ash formation and emissions of gaseous pollutants during the combustion of woody biomass, it is essential to understand the quantity and the mechanism of the release of the ash-forming matter from the fuel during combustion. The objective of this work is to quantify the release of inorganic metal species, S and Cl during combustion of woody biomass at well-controlled conditions.

Experimental

Equipment and Method. Combustion experiments were conducted in a lab-scale reactor, resembling the conditions in a grate-fired boiler. The experimental set-up was especially designed to study the release of inorganic elements during wood combustion, and consists of an electrically heated oven with an alumina tube inside, in which a fuel sample can be inserted and a gas can be introduced in order to provide a pyrolysis or combustion atmosphere around the fuel sample. Batch experiments with small sample sizes (30-45 g) were done at different temperatures in the range of 500-1150^{o}C. The release of various inorganic elements during combustion was quantified by performing accurate weight measurements and chemical analysis of the biomass feedstock and the residual ash samples, and performing mass balance calculations. Focus was on the alkali metals K and Na, the alkaline earth metals Ca and Mg, and the heavy metals Cu, Zn, Pb and Cd, since they were known to form aerosols during wood combustion. Furthermore, the non-metals S and Cl were studied, since they were expected to influence the volatility of the metal elements. The influence of fuel type and chemical composition of the fuel was investigated by using various types of woody biomass fuels.

Fuel samples. The fuels used in this experimental study are spruce (wood chips), beech (wood chips), bark and fiberboard. These wood biomass fuels are samples from the same batch as the fuels that were used in the EU-project 'Bio-Aerosols'[1], in the formation and behavior of aerosols from wood combustion on a grate were investigated. In the present paper results are given for spruce and fiberboard. The fuels were dried in open air at room temperature and milled using a 4 mm-screen before they were used in the experiments, in order to obtain physically and chemically homogenous samples. The chemical characteristics of the fuels are shown in Table 1.

Table 1. Chemical Characteristics of the Fuels Investigated

Fuel type	Spruce	Beech	Bark	Fiberboard
Moisture (wt%)	6.6	4.5	10.7	6.8
Ash (wt% d.b.)	0.95	0.52	4.41	1.24
Volatiles (wt% d.b.)	82.7	84.8	72.9	80.3
Cl (wt% d.b.)	<0.01	<0.01	0.01	0.05
S (mg/g d.b.)	0.1	0.12	0.42	0.3
K (mg/g d.b.)	0.85	0.92	2.4	0.64
Na (mg/g d.b.)	0.02	0.01	0.07	0.18
Ca (mg/g d.b.)	1.9	1	16	1.5
Mg (mg/g d.b.)	0.2	0.21	0.76	0.21
Si (mg/g d.b.)	0.43	0.03	2.2	0.55
Al (mg/g d.b.)	0.08	0.01	0.45	0.35
Fe (mg/g d.b.)	0.08	0.05	0.33	0.26
Ti (mg/g d.b.)				4.5
Cu (mg/kg d.b.)	2	1.6	5	3.9
Zn (mg/kg d.b.)	14	3.7	67	27
Cd (mg/kg d.b.)	0.14	0.032	0.25	0.18
Pb (mg/kg d.b.)	0.44	0.4	1.6	16

(d.b. = dry basis)

It can be observed that the main ash forming elements are Ca, K and Si in the case of all fuels. Furthermore, all fuels contain relatively low amounts of Cl and S. Heavy metals like Cu, Zn, Pb and Cd are also present in small amounts in the fuels, of which Zn is the most dominant element. Spruce and beech both have very low ash contents (< 1 wt% d.b.), fiberboard has a slightly higher ash content (around 1

wt% d.b.) and bark has the highest ash content (around 4 wt% d.b.). Bark contains a high amount of Si and Al, probably due to the presence of sand and clay minerals attached to the fuel. Fiberboard contains a high amount of Ti, originating from the pigments in the coating.

Results and Discussion

Quantitative release data were obtained for spruce and fiberboard in the temperature range of 500-1150°C. The experimental results show that the release of the studied elements is strongly dependent on the temperature and the inorganic composition of the fuel. In general, a high release of Cl, S, Zn, Pb, and Cd was observed, up to 100% at high temperature (above 850°C). The elements K, Na, and Mg were found to be released at lower levels, whereas no release was observed for the elements Ca, Si, Al and Fe.

Figure 1 shows the release of Cl, S and K during combustion of spruce and fiberboard as a function of temperature in the range of 500-850°C. In this temperature range, a very high release of Cl (~100%) and S (~75%) and a low release of K (up to ~30%) were observed for spruce. Cl was found to be (almost) completely released already at 500°C. Preliminary thermodynamic equilibrium studies of spruce indicated that Cl may start to be released around 500°C, in the form of $HCl_{(g)}$ or $KCl_{(g)}$. Since the concentration of Cl in the fuel is very low, a complete release of Cl around 500°C seems likely. The equilibrium calculations also showed that the release of K starts around 850-900°C, by the formation of $K_2SO_{4(g)}$. This may explain the steeper increase in the release observed between 800 and 850°C. The high release of S is not well understood yet. S is expected to be released mainly in the form of $SO_{2(g)}$ and $K_2SO_{4(g)}$, but the release of $SO_{2(g)}$ is also not expected to occur at temperatures below 900°C in the case of spruce.

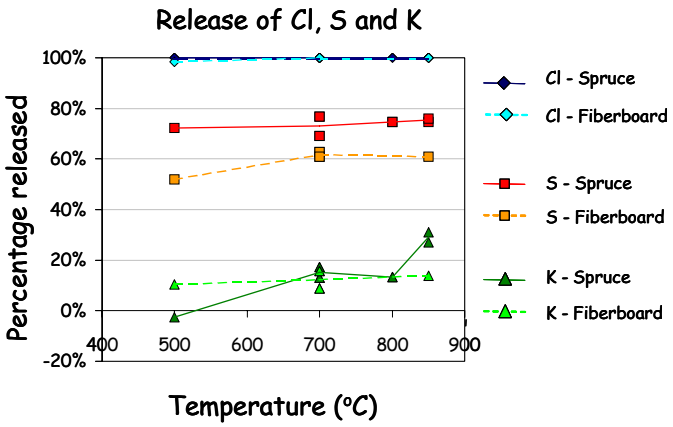

Figure 1. Release of Cl, S and K during combustion of spruce and fiberboard as a function of temperature in the range of 500-850°C.

Similar release trends were observed for fiberboard, although the release of S and K was lower in this case (see Figure 1). This may be due to a difference in speciation of these elements in the ash. The presence of certain inorganic elements may have an influence on the volatility of other elements. For example, in the case of fiberboard, the high content of Ti in the ash may play a role in decreasing the volatility of certain elements.

Figure 2 shows the release of Zn, Pb and Cd during combustion of spruce and fiberboard as a function of temperature in the range of 500-850°C. For spruce, it was found that the release of Zn and Pb increased form ~0 at 500°C to ~100% at 850°C, whereas Cd was released almost completely at 500°C. Completely different release trends were found for fiberboard, where the lower amounts of Zn, Pb and Cd released may again be due to the presence of other inorganic elements in the ash.

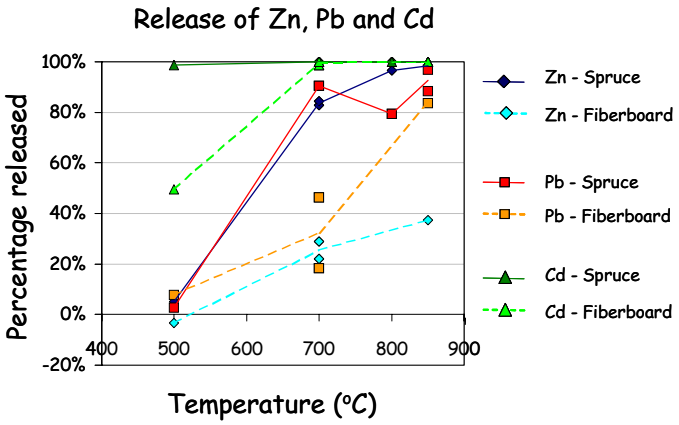

Figure 2. Release of Zn, Pb and Cd during combustion of spruce and fiberboard as a function of temperature in the range of 500-850°C.

Detailed thermodynamic equilibrium studies, as well as investigations of the structures and chemistry of the fuels and ashes will be performed in order to obtain a better understanding of the release data and the possible release mechanisms.

Conclusions

The release of inorganic elements during wood combustion was investigated by performing lab-scale experiments at well-controlled conditions and was found to be strongly dependent on the temperature and the inorganic composition of the fuel. In general, a high release of Cl, S, Zn, Pb, and Cd was observed, up to 100% at high temperature (above 850°C). The elements K, Na, and Mg were released at lower levels. This paper shows the results of the experimental release data for spruce and fiberboard in the temperature range of 500-850°C.

The obtained quantitative experimental data on the release of inorganic elements during wood combustion can be used as input data for aerosol and fly-ash formation and behavior models aiming to find solutions for ash-related problems during wood combustion.

Acknowledgements. The Danish Technical Research Council (STVF) is acknowledged for funding the project. Violeta Alonso Ramírez and Laura Lambea are acknowledged for their contributions to the experimental work.

References

(1) Aerosols in fixed-bed biomass combustion - formation, growth, chemical composition, deposition, precipitation and separation from flue gas', Final Report, EU Contract no. ERK6-CT-1999-00003, Project no. NNE5-1999-00114, 2003.

SLAG FORMATION AND POTASSIUM VOLATILIZATION FROM RICE STRAW BLENDED WOOD FUEL

P. Thy,[1] B.M. Jenkins,[2] R.B. Williams[2], and C.E. Lesher[1]

[1]Department of Geology
[2]Department of Biological and Agricultural Engineering University of California
One Shields Avenue
Davis, CA 95616

Introduction

There is experimental evidence that the addition of straw to conventional biomass boiler fuels in some instances may reduce potassium fouling. The results of an evaluation of urban wood fuel ash[1] show that potassium is strongly partitioned into the vapor phase. It is also known[2] that fundamental differences exist at superliquidus conditions between wood and rice straw ash melts. Contrary to expectations, potassium is retained in rice straw slag, but strongly volatilized from wood slag. The potential of these preliminary findings is that the addition of rice straw to conventional wood based fuels may be beneficial and may reduce potassium losses and thereby fouling.

We present the results of a systematic experimental study of the high temperature melting relations of ashes produced by mixing rice straw and wood. We use a high temperature vertical quench furnace that let us determine the phase relations at various temperatures by allowing run products to be rapidly quenched and recovered from the high-temperature environment. The predictions of the subscale ash experiments are tested using an atmospheric fluidized bed combustor (AFBC). The laboratory scale combustor allows us to better simulate the complexities of full-scale application than is possible with the atmospheric rapid quench furnace.[3,4]

Ash Melting Experiments

Experimental and Analytical Procedures

Starting materials for the melting experiments consist of two biomass fuels. The first is mixed whole tree chips of white fir and ponderosa pine, typical of clean fuel types received at commercial plants (ash content 1.1%, dry basis). The other is a M202 rice straw variety from California (ash content 20%). The two fuels were ashed at 525 °C using standard procedures. A total of six ash blends with from 10 to 50 % rice straw ash were prepared from the wood and rice straw ashes (Figure 1; Table 1). The compositions of the ashes and the ash blends are summarized in the Table 1, normalized to 100 % volatile free.

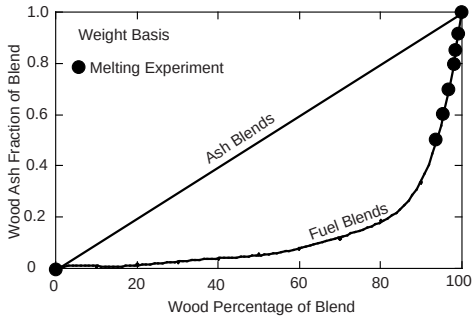

Figure 1. Wood ash fraction as a function of wood percentage in blend (ash or fuel) on a weight basis. Dots are the investigated fuel ash blends.

About 50-mg powder for each experiment were pressed in a pellet and mounted onto a 0.004" diameter Pt-wire. These mounted pellets were suspended into the furnace at the desired temperature. Temperature was monitored by a $Pt/^{90}Pt^{10}Rh$ thermocouple that was positioned near the ash pellet. Duration of the experiments varied to about 24 hours and temperature from the near solidus to the liquidus conditions. The experiments were terminated in air by pulling the sample out of the furnace.

Table 1. Summary of Ash Blends Used in the Experiments

	Rice Straw	R 50% W 50%	R 40% W 60%	R 30% W 70%	R 20% W 80%	R 15% W 85%	R 10% W 90%	Wood
SiO2	82.28	53.91	47.07	39.74	31.87	27.72	23.40	14.26
TiO2	0.01	0.09	0.11	0.13	0.15	0.16	0.17	0.20
Al2O3	0.10	2.04	2.51	3.01	3.55	3.84	4.13	4.76
Fe2O3	0.11	0.79	0.95	1.13	1.32	1.42	1.52	1.74
MnO	0.10	0.43	0.51	0.60	0.69	0.74	0.79	0.90
MgO	1.79	4.18	4.76	5.37	6.04	6.39	6.75	7.52
CaO	1.75	21.42	26.16	31.24	36.69	39.57	42.56	48.90
Na2O	0.15	0.34	0.38	0.43	0.48	0.51	0.54	0.59
K2O	13.04	14.42	14.76	15.11	15.50	15.70	15.91	16.35
P2O5	0.67	2.38	2.79	3.24	3.71	3.96	4.22	4.77
Total	100.00	100.00	100.00	100.00	100.00	100.00	100.00	100.00

R, rice straw ash; W, wood ash. Each blended composition is calculated to 100 %.

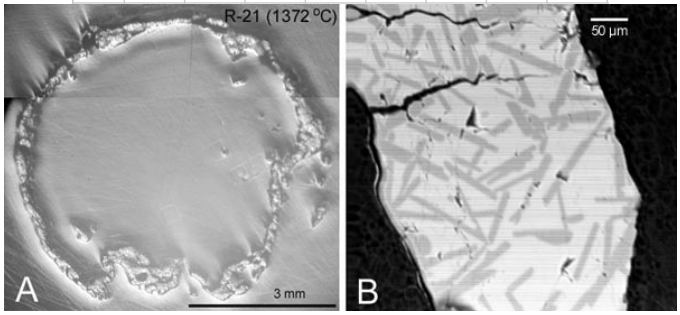

Figure 2. Rice straw ash products. (A) Reflected microscope image of experimental product at 1372°C. The product is composed of a large bubble with a thin outer wall. Scale bar is 3 mm. (B) Back-scattered electron image of the silicate wall in Figure 2A. The dark tabular grains are a quartz polymorph. Light gray is glass. Scale bar is 50 µm.

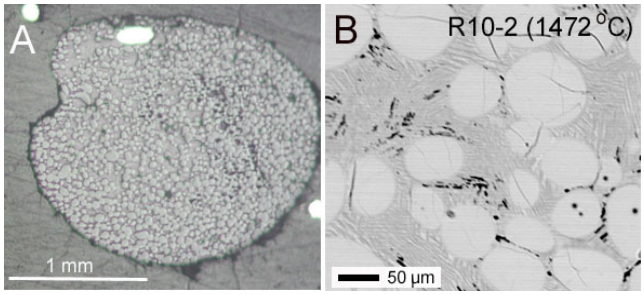

Figure 3. 10% rice straw ash blend products. (A) Reflected microscope image of the product heated at 1472°C. The experimental product is a compacted droplet of rounded larnitic grains and an interstitial quenched melt. Scale bar is 1 mm. (B) Back-scattered electron image of the center of the same experimental product as in Figure 3A. The lighter rounded grains are larnite. The quenched interstitial melt is composed of two unidentified phases. Scale bar is 50 µm.

Melting Results

The initial tests involve the characterization of the melting relations of the two pure ashes (rice straw and wood) as a function of temperature between their respective liquidus and solidus conditions.

These initial experiments form the basis for testing the effects on melting blends of the two ashes. Here we only show two examples of the experimental products. Figure 2A shows a reflected light microscope image of pure rice ash heated to 1372°C. This experimental product is composed of a large bubble with a thin outer wall, likely caused by the release of CO_2 during heating. The back-scattered electron image of the silicate wall indicates dark, needle-shaped quartz polymorphs and light gray glass.

The experimental products on an ash blend with 10 % rice straw ash are illustrated in Figure 3. Figure 3A shows a reflected microscope image of the product from 1472°C. This product is highly compacted and composed of droplets of rounded larnitic grains and an interstitial quenched melt. The back-scattered electron image of Figure 3B shows the textural relationships between rounded larnite grains and quenched interstitial melt composed of two unidentified phases.

Elemental Losses and Phase Appearances

The proportions of the solid phases and the coexisting liquid in the experimental products are estimated by least-squares, linear approximations of the compositions of the phases in the experimental products to the composition of the starting ash mixtures. In addition to the phase proportions in weight percentages, this type of calculation also allows estimates of the elemental losses, either directly from the deviations from the actual composition of ash mixtures or alternatively by including the element in question as an oxide in the calculations. This was done for K_2O and Na_2O for which the largest losses were detected.

The calculated losses of K_2O are illustrated in Figure 4. K_2O is strongly volatilized from the pure wood ash as well as from the wood ash blended with small amounts of rice straw ash (10 and 15 %). On the other hand, K_2O is partly retained in the blends with higher rice straw ash as well as in the pure rice straw ash. The loss correlates positively with the experimental temperature.

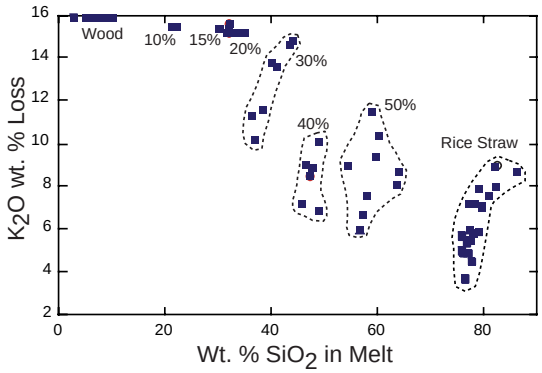

Figure 4. Losses of K_2O (wt. %, ash basis) from the experimental products as a function of SiO_2 content of melt.

The liquid-mineral relations for wood ash were only determined in a narrow interval between 1400 and 1550°C. Within this temperature interval, the melt proportion increases and the larnite proportion decreases with increasing temperature. The proportion of periclase is relatively constant except for a slight drop at the highest melting temperatures. We can extrapolate to a rather uncertain liquidus temperature of 1950-2050°C.

The addition of rice straw ash to the wood ash causes a strong drop in liquidus temperature. With 10 % added rice straw ash, the liquidus temperature is still too high to be directly determined. The mineral phases detected well below the liquidus are, as for the pure wood ash, larnite and periclase. With 15 % added rice straw ash, the liquidus has dropped sufficiently to allow an indication of the liquidus phase as larnite. Periclase is no longer detected at any melting temperature. With 20 % added rice straw ash, the liquidus mineral is larnite at 1403±11°C. Åkermanite appears at 1299±10°C. With 30 % added rice straw ash, wollastonite and åkermanite appear nearly simultaneously on the liquidus at 1264±11°C and are followed by leucite at 1217±11°C. With 40 % added rice straw ash, the liquidus phase is wollastonite at 1282±14°C and with leucite and diopside appearing nearly simultaneously at a temperature of 1212±11°C. With 50 % added rice straw ash, the liquidus phase is wollastonite at 1307±11°C and diopside appears at a temperature of 1263±11°C.

Because temperature dependent losses of K_2O are seen for some blends, it is possible that the estimated liquidus temperatures in part reflect the changing bulk composition of the slag. This mean that estimates of melting relations and liquidus temperature cannot be based on bulk ash compositions, as often done, but must take into consideration temperature dependent changes in bulk composition.

An important observation is that the retention in the slag of K_2O can be correlated with the appearance of leucite. Leucite is a K_2O and Al_2O_3 rich phase that is stabilized at relatively low temperature and low melt fraction in coexisting melts relatively enriched in Al_2O_3 and K_2O. The appearance of leucite, thus, strongly controls retention of K in the slag. This is seen for the 30 to 50 % rice straw blends. The observed variation in the behavior of potassium for the range of slag compositions investigated in this study can be explained by a marked decrease in potassium loss with increasing rice straw in the slag.

The liquidus temperature (or complete melting point) was bracketed in four series of experiments (50, 40, 30, and 20 %). The liquidus temperature for pure rice was extrapolated to approximately 1575°C. The true liquidus for a starting composition with 12 wt. % K_2O may very well be below 1100°C; however, for practical purposes the 'elevated' liquidus temperature shown on Figure 5 may be more relevant.

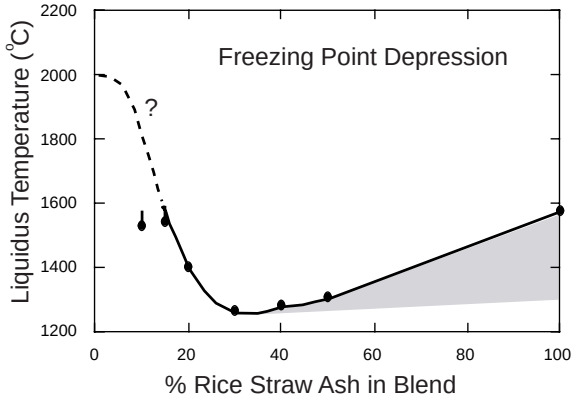

Figure 5. Experimentally determined liquidus temperatures as a function of weight % rice straw ash in the ash blend.

The resulting freezing point depression as a function of the percentage of rice straw ash in the blends is shown in Figure 5. It is seen that the addition of small amounts of rice straw ash to the blend will strongly affect the melting points until an amount of about 20 % rice straw ash (~25°C/wt.% rice ash). From about 20 % rice straw, the liquidus levels out and reaches a minimum at about 30 % rice (1264°C). With increasing rice straw ash, the liquidus temperature rises steadily to 50 % straw ash, and probably also beyond, to an apparent 1536°C for pure rice straw ash (4°C/wt.% rice ash).

Fluidized Bed Combustion

Combustion tests were conducted in an atmospheric laboratory scale fluidized bed combustor.[5,6] The first three experiments used the

2.4 % rice straw blend with either an 800-900°C or a 1000°C reactor wall temperature. The fourth experiment used the 9.6 % rice straw blend and a reactor wall temperature of 1000°C. Two control experiments were conducted using either a pure wood fuel or a leached rice straw fuel, both with a reactor wall temperature of 1000°C.

The fuel blends for the fluidized bed testing were selected based on the results of the bench top melting experiments on fuel ash blends. In these experiments, a minimum liquidus temperature was observed for a 30 % rice straw ash blend. We selected two fuel blends bracketing this ash composition: (1) 2.6 % rice straw and 97.4 % wood fuel and (2) 9.6 % rice straw and 90.4 % wood fuel. As control fuels, we selected two additional fuels; (3) 100 % wood fuel and (4) a 10.7 % leached rice straw and 89.3 % wood fuel blend. Pure rice straw fuel and higher straw blends were not tested since these fuels are well know readily to cause bed agglomeration.[6,7]

The main findings discussed here relate to observation of bed agglomeration. The experiment using the 9.6 % rice straw fuel blend was terminated by strong bed agglomeration that plugged the reactor and defluidized the bed. This was seen as a marked drop in differential bed pressure and rise in bed temperature. The agglomeration was estimated to have affected 25 % of the total bed material, but was concentrated in the central part of the reactor (Figure 6). This agglomeration estimate is based on the extracted bed after the experiment and is calculated on a weight basis relative to the original bed material. Figure 6 shows how silicate material forms as a film along the grain boundary and cements the bed particles together. The result is a highly porous bed cemented along a few grain boundaries. Minor agglomeration was observed in two other experiments, in both cases insufficient to have affected combustion. These were an experiment using the 2.4 % rice straw blend that indicate about 1 % agglomeration of the bed and an experiment using the leached rice straw blend likewise showed minor bed agglomeration (~0.1 %).

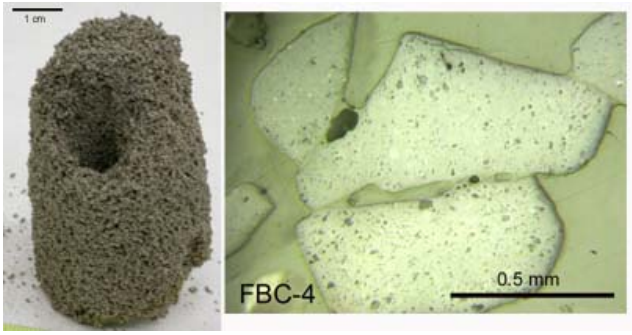

Figure 6. Agglomerated bed extracted from the fluidized bed reactor after termination of an experiment using a 9.6 % rice straw blend and a reactor temperature of 1030°C. The vertical channel is after a thermocouple rod. Right is shown bed agglomeration of bed particles (mullite) by silicate cement (Ca-K-Mg-P-Si).

The bed agglomeration percentages are summarized in Figure 7 as a function of percent rice straw content in the fuel blend. Bed agglomeration is expected to depend on fuel composition, combustion temperature, and duration. All experiments showing bed agglomeration were done with a 1000°C furnace wall temperature and maximum reactor temperature between 1030 and 1090°C. The highest reactor temperature was achieved for the experiment using the pure wood fuel (1090°C) without agglomeration. Minor agglomeration was found for the experiment using the leached straw fuel blend (1040-70°C). The highest agglomeration was found for the experiment using the 9.6 % rice straw blend (1030°C). Of the experiments based on the 2.6 % rice straw blend, only the experiment with the highest reactor temperature (1050°C) showed modest bed agglomeration. Two experiments using the same 2.6 % rice straw blend revealed no bed agglomeration (825 and 920°C, respectively). These results indicated that the fuel composition and combustion temperature control the extent of bed agglomeration. Figure 7 illustrates the effects on adding rice straw to a wood based fuel. The bed agglomeration measured as fraction of total bed on a weight basis increases exponentially with increasing rice straw in the fuel blend. The duration of the individual combustion experiments was not significantly different (2-6 hours) to allow the effect of continuous combustion and duration on agglomeration to be evaluated.

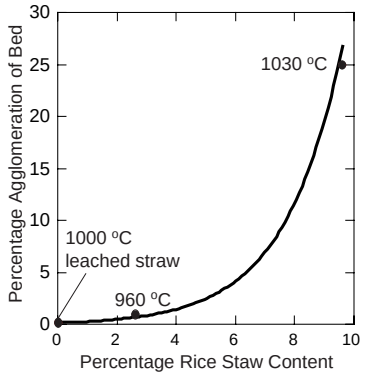

Figure 7. Estimated bed agglomeration as a function of rice straw in the fuel.

The combustion temperature also has a significant effect. For the 2.6 % rice straw blend, only the experiment with the highest combustion temperature showed minor agglomeration, while the lowest temperature experiments on the same fuel blend did not reveal agglomeration. The effect of duration was not investigated in the present study. The results for the short duration tests conducted reveal no clear correlation between duration and extent of bed agglomeration.

Analyses of the agglomerates revealed no significant mineralogical changes in the bed material with extent of agglomeration. Bed agglomeration is, therefore, attributed to either sintering of bed particles aided by potassium released during combustion or to the deposition of partially molten ash fragments or particles. Studies of the cause of agglomeration are currently in progress using the scanning electron microscope.

Conclusions

The blending of rice straw with wood based biomass fuels is shown to result in marked change in the behavior of potassium and its partitioning between the solid inorganic slag and the flue gas. Potassium is increasingly retained in the slag with increasing rice straw ash component. Strong retention is in addition controlled by low melting temperature approaching the solidus temperature for the slag and the saturation of potassium-aluminum-silicate minerals in the slag. The liquidus temperature shows a marked freezing point depression from above 2000°C to about 1260 °C for blends with a content of about 30 % rice straw ash. This content is equivalent to about 3 % rice straw content in the fuel. The complete melting intervals from liquidus to solidus conditions of ash blends are about 100-150°C.

These results suggest the addition of a small amount of straw to a predominantly wood fuel will have the effect of lowering melting temperature and the relative potassium loss to the flue gas. If combustion temperature can be controlled to within, or below, the

melting interval of the resultant ash/slag (<1260^{o}C), the loss of potassium can be minimized. An obvious drawback of adding straw materials is that the total volume of ash and slag will dramatically increase by a factor of 10-20 compared to clean wood. A pure wood fuel will loses most of its K_2O content, around 2 g K_2O/kg fuel. On the other hand, rice straw fuel will lose a lower fraction (0.3) of its original K_2O content, around 8 g K_2O/kg fuel. The determined (and interpolated) K_2O losses on a fuel intake basis are illustrated in Figure 8 showing a rapid increase in K_2O loss until a rice straw fraction of 20% after which the loss levels and remains fairly constant at 7-8 g/kg fuel.

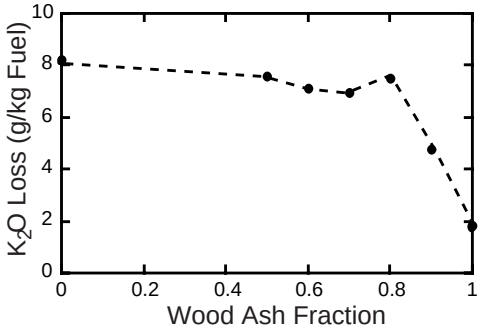

Figure 8. Experimental determined, near-solidus K_2O losses (g) on basis of fuel intake (kg) plotted as a function of wood ash fraction of blend. (wt. basis).

Fuel blend and bed medium composition, reactor temperature, and duration are the principal controls on bed agglomeration in fluidized bed combustors. The extent of bed agglomeration in our laboratory scale experimental combustor shows an exponential increase with rice straw component suggesting that a maximum of 7-8 % rice straw blends may be permissible for this type of biomass boiler. It is also shown that boiler operation below the minimum solidus temperature (~ 1050^{o}C) dramatically reduces potassium losses and therefore bed agglomeration.

Addition of rice straw to wood fuel decreases the fractional volatilization of potassium. However, because of the large difference in the ash fractions of the two fuel components, will not decrease the total fuel potassium volatilized that will rapidly increase until a straw fuel component of 20%. The principal problem in fluidized bed combustion thus appears not to be the fractional potassium loss to the flue gas, but rather the large increase in inorganic material that can severely affect the bed operation, may be deposited on firesides, and will be transported as ash particles to the heat exchange surfaces.

Acknowledgement. This work was supported by California Energy Commission's Energy innovation Small Grant (EISG) Program.

References

1 Thy, P., Jenkins, B.M., and Lesher, C.E., 1999. High temperature melting behavior of urban wood fuel ash. Energy and Fuels 13, 839-850.

2. Thy, P., Lesher, C.E., and Jenkins, B.M., 2000. Experimental determination of high temperature elemental losses from biomass fuel ashes. Fuel 79, 693-700.
3. Salour, D., Jenkins, B.M., Vafael, M., and Kayhanian, M., 1993. Control of in-bed agglomeration by fuel blending in a pilot scale straw and wood fueled AFBC. Biomass and Bioenergy 4, 117-133.
4. Jenkins, B.M., Baxter, L.L., Miles, T.R., Miles, T.R, Jr., Oden, L.L., Bryers, R.W., and Winther, E., 1994. Composition of ash deposits in biomass fueled boilers: results of full-scale experiments and laboratory simulations. ASAE International Summer Meeting, Kansas City, Kansas.
5. Bakker, R.R., Jenkins, B.M., and Williams, R.B., 2002. Fluidized bed combustion of leached rice straw. Energy and Fuels 16, 356-365.
6. Jenkins, B.M., Bakker, R.R., and Wei, J.B., 1996. On the properties of washed straw. Biomass and Bioenergy 10, 177-200.

QUANTIFICATION OF THE RELEASE OF Cl, K AND S TO THE GAS PHASE FROM COMBUSTION OF ANNUAL BIOMASS

Jacob N. Knudsen, Peter A. Jensen, and Kim Dam-Johansen

Department of Chemical Engineering
Building 229, Technical University of Denmark
2800 Kgs. Lyngby
Denmark

Introduction

The use of annual biomass such as straw, stalks and shells in heat and power generation is an interesting option in order to provide renewable energy and to reduce the net CO_2 emissions. In Europe and North America, straw is the most available biomass resource with a yearly production around 800 million tons[1]. In Denmark, straw is a particular interesting bio-fuel since it is an agricultural waste-product being available in surplus. However, the use of straw as a fuel in combined heat and power plants has proven to be a technical challenge. This is among other things, due to the relatively high concentrations of the elements: potassium, chlorine and sulfur. Formation of acidic pollutants and high mass loadings of aerosols together with deposition on heat transfer surfaces of potentially corrosive components are among the encountered problems[2-4].

During the conversion of annual biomass in grate-fired furnaces, Cl, K and S are partly released to the gas phase, but may also be partially retained in the bottom ash. Clearly, the extent of Cl, K and S release to the gas phase is directly related to the problems mentioned above. In order to predict the impacts of a given fuel in a combustion system, the release behavior of Cl, K and S needs to be investigated. In this work, the influence of combustion temperature and fuel composition on the gas phase release of Cl, K and S have been determined.

Experimental

Biomass fuels. Four biomass fuels with distinctive different ash composition were selected for the release investigation. As seen in Table 1, the concentration range of Cl, K, S and Si is particularly broad. Prior to use, the fuels were thoroughly homogenized in a hammer-mill and the fines were removed. The resulting particle-size fraction was 0.5-10 mm.

Table 1. Characteristics of the Biomass Fuels Applied in the Experimental Investigation.

Fuel	Wheat	Oat	Barley	Carinata
Moisture (%)	8.4	7.8	8.5	7.3
Ash (%, dry)	4.8	3.8	6.9	4.9
Ca (%, dry)	0.35	0.72	0.34	0.60
Cl %, dry)	0.27	0.05	0.79	0.05
K (%, dry)	1.2	0.55	2.3	1.4
P (%, dry)	0.05	0.11	0.06	0.14
S (%, dry)	0.17	0.14	0.20	0.26
Si (%, dry)	0.79	0.27	0.81	0.05
K/Si (mol/mol)	1.1	1.5	2.0	20
Cl/K (mol/mol)	0.25	0.10	0.38	0.04

Release quantification. An electrically heated laboratory flow-reactor was applied to combust small samples of biomass at well-controlled conditions. To simulate the heating rate of an industrial grate-fired boiler, an experimental procedure was utilized where the biomass sample was inserted into a preheated reactor. The release of Cl, K and S from the sample was subsequently quantified by a chemical analysis of the residual ash and a mass balance on the system. A series of experiments at different temperatures were conducted, in order to quantify the release as a function of combustion temperature. The influence of ash composition on the Cl, K and S release was investigated by conducting experiments with biomass fuels with different mineral content and composition.

Analytical. The residual ash samples were dissolved by pressurized digestion in a $HF/HNO_3/H_2O_2$ mixture, subsequently neutralized with boric acid and analyzed by ICP-OES.

Results and Discussion

Potassium. It is seen in **Figure 1** that potassium is released to the gas phase above 700°C and that the release increases with the applied combustion temperature for all biomass fuels regardless of the ash composition. Between 20 and 50% of the total potassium has been released at 900ºC. At temperatures above 900ºC the relative potassium release increases almost linearly with temperature until 60 to 90% is released at 1150ºC. The local temperature on the grate in grate-fired furnaces is fluctuating, but frequently above 900-1000ºC[5]. This implies that significant amounts of the fuel-potassium are released to the gas phase during grate combustion of annual biomass.

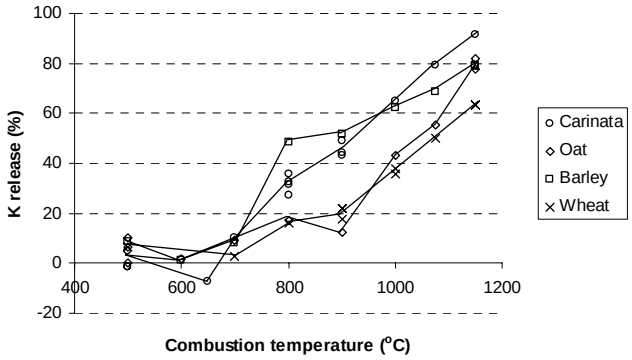

Figure 1. Release of potassium as a function of temperature.

It is furthermore seen in **Figure 1** that the release of potassium is greatly affected by the ash composition. The biomass fuels with the higher Si and lower Cl content relative to K (oat and wheat straw) display the lower potassium release. Potassium can be incorporated into silicate structures[6]. The vapor pressure of potassium fixed in silicate structures is relatively low, which implies that less potassium is released from biomass fuels having a low K/Si ratio. According to Table 1, the K/Si molar ratio of the wheat, oat and barley straw is low compared to the one of carinata and a lower potassium release is expected. However, a high concentration of chlorine relative to potassium may increase the volatility of potassium, due to the relatively high vapor pressure of KCl at combustion relevant temperatures. This indicates that chlorine promotes the release of potassium to the gas phase. A significant fraction of the potassium in the chlorine-rich barley straw is released between 700 and 800°C, the interval where KCl is found to evaporate[6]. This implies that chlorine may facilitate the release of potassium, although the biomass contains substantial amounts of silicon relative to potassium.

Thus, at grate combustion conditions it is expected that the release of potassium to the gas phase will be considerable for biomass fuels containing high amounts of chlorine and/or potassium relative to silicon. On the contrary, the potassium release is expected to be low for high-silicate fuels with low chlorine content.

Chlorine. It appears in **Figure 2** that chlorine is released in two steps for the samples which contain substantial Cl (barley and wheat). Between 30 and 60% is released in the first step below 500ºC. The remaining Cl is released in the second step between 650 and 800ºC. The observed two-step chlorine release is in agreement with observations in the literature[6]. It has been demonstrated that chlorine is released as HCl during the fuel devolatilization at 200-400ºC. The second release-step of chlorine is linked to the evaporation of KCl[6], which mainly occurs between 700 and 800ºC as seen in **Figure 2**. This is consistent with the observed step-like increase in the potassium release between 700 and 800ºC for the chlorine-rich fuels as shown in **Figure 1**.

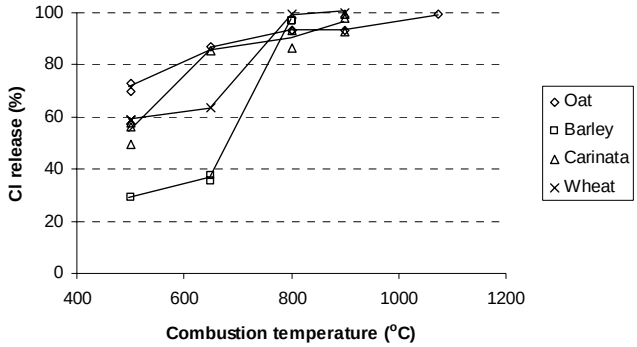

Figure 2. Release of chlorine as a function of temperature.

For the samples which have a relatively low Cl content (oat and carinata), the chlorine release is gradually increasing as a function of combustion temperature. In general a higher fraction of the fuel-chlorine appears to be released at lower temperatures for the low-chlorine fuels. This is most likely an effect of concentration rather than a true mechanistic difference. Significantly less KCl must be evaporated from the low-chlorine fuels, thus the evaporation rate becomes important at lower temperatures.

Nevertheless, the investigation indicates that combustion of annual biomass above 800ºC results in nearly complete release of Cl to the gas phase. The ash composition or the absolute Cl content of the fuel does not affect this fact. The temperature on the grate in grate-fired furnaces is typically significantly above 800ºC[5], which implies that most fuel-chlorine will be released to the gas phase during grate-combustion of annual biomass.

Sulfur. Unlike the observed release behavior of Cl and K, **Figure 3** reveals that the sulfur release appears to be more sensitive to the ash composition than the combustion temperature.

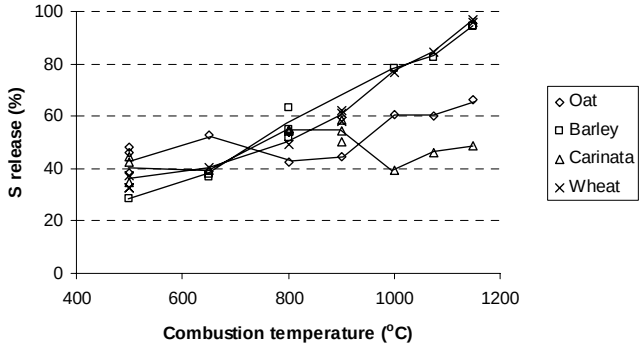

Figure 3. Release of sulfur as a function of temperature.

In case the biomass fuel contains relatively high amounts of Ca and K compared to Si, (oat and carinata), approximately 50% of the sulfur is released almost independently of the applied combustion temperature. On the other hand, if the Si concentration is high, the sulfur release increases with combustion temperature. Calcium and potassium are the elements facilitating sulfur capture in the residual ash. It appears in Table 1, that the content of Ca and K in the fuels is sufficient to retain all fuel-sulfur. However, in the high-silicate fuels, calcium and potassium are to a large extent incorporated into glassy silicate structures. The retention of sulfur in Ca-K-silicates is low, hence, the sulfur release to the gas phase is observed to be higher for high-silicate fuels.

It appears in **Figure 3** that the sulfur release is greater than 40% at all temperatures and for all of the investigated biomass fuels. This is related to the occurrence of substantial amounts of volatile organic sulfur in annual biomass. Earlier work[7] has indicated that annual biomass fuels contain both organic sulfur and inorganic sulfate. The organic sulfur is released to the gas phase during devolatilization at 200-400ºC, whereas the inorganic sulfate is retained in the char.

Altogether, the experimental work indicates that the sulfur release in grate-fired boilers is controlled by the organic-to-inorganic sulfur ratio in the fuels and the accessibility of potassium and calcium. The accessibility of potassium and calcium is largely determined by the relative concentration of silicate in the fuel.

Conclusions

The experimental investigation revealed that both the combustion temperature and the ash composition greatly affected the extent of Cl, K and S release to the gas phase at grate combustion conditions. The release of potassium was largely determined by the fuels content of chlorine and silicon along with the combustion temperature. The fuel-chlorine was found to be completely released to the gas phase at combustion temperatures above 800°C, regardless of the ash composition. The sulfur release was predominantly controlled by the association of sulfur in the fuel together with the accessibility of Ca and K.

Acknowledgement. This work is part of the CHEC (Combustion and Harmful Emission Control) research centre funded by Elsam, Elkraft, the Danish and Nordic Energy Research programs, the Technical Research Council of Denmark and the Technical University of Denmark.

References

(1) Hall, D. O.; Overend, R. P. Biomass. *Regenerable energy*, John Wiley & sons, Chichester, 1987, Chapter 4.

(2) Michelsen, H. P.; Frandsen, F. J.; Dam-Johansen, K.; Larsen, O. H. *Fuel Processing Technology*. **1998**, *54*, 95-08.

(3) Sander, B.; Henriksen, N.; Larsen, O. H.; Skriver, A.; Ramsgaard-Nielsen, C.; Jensen, J. N.; Stærkind, K.; Livbjerg, H.; Thellefsen, M.; Dam-Johansen, K.; Frandsen, F. J.; van der Lans, R.; Hansen, J. *Emissions, Corrosion and Alkali Chemistry in Straw-Fired Combined Heat and Power Plants*, 1st World Conference on Biomass for Energy and Industry. June 2000, Sevilla, Spain.

(4) Christensen, K. A.; Stenholm, M.; Livbjerg, H. *J. Aerosol Sci*. **1998**, *29*, 421-444.

(5) Van der Lans, R.; Pedersen, L.T.; Jensen, A.; Glarborg, P.; Dam-Johansen, K. *Biomass and Bioenergy*. **2000**, *19*, 199-208.

(6) Jensen, P.A.; Frandsen F.J.; Dam-Johansen, K.; Sander, B. *Energy & Fuels*, **2000**, *14*, 1280-1285.

(7) Knudsen, J.N.; Lin, W.; Frandsen, F.J.; Dam-Johansen, K. *Sulfur Transformations during Thermal Conversion of Biomass, Power Production in the 21st Century*, Engineering Foundation Conference, Snowbird, Utah, USA, 28 Oct. - 2 Nov. **2001**.

SLAGGING BEHAVIOUR OF WOOD ASH UPON ENTRAINED-FLOW GASIFICATION CONDITIONS: PRELIMINARY STUDIES

B. Coda, M.K. Cieplik, J.H.A. Kiel

Energy Research Centre of the Netherlands, ECN
P.O. Box 1, 1755 ZG Petten, The Netherlands

Introduction

Entrained flow gasification is one of the most promising technologies to convert biomass streams for large-scale applications aimed at (integrated) production of power, hydrogen and chemicals (e.g. Fischer-Tropsch diesel fuels). Application of biomass streams in entrained-flow gasifiers similar to those employed in coal gasification (e.g. slagging gasifiers) requires R&D concerning fuel feeding and ash behavior, especially with regard to ash slagging tendencies.

This paper present results related to characterization of slag behaviour of selected wood streams - beech, willow, wood mixture - under simulated (pressurized, oxygen blown) entrained-flow gasification conditions. Wood ash in the fuel is very low (about 1% fuel weight), and characterized by high alkaline-earth and alkali metals content. Therefore its application upon conditions typical of slagging gasifiers requires careful adaptation, since the latter are designed for higher fuel ash content (typically > 6% fuel weight) and operate at a temperature where coal ash can form a molten slag (typically 1300-1500 °C).

Methods

The approach is based on experimental and modeling work. Experiments were performed in an atmospheric-pressure entrained-flow reactor, equipped with an integrated, premixed and multi-stage flat flame gas burner[1]. A scheme of the reactor is shown in **Figure 1**.

The ring-shaped, concentric, staged gas burner is used to simulate the (high) initial heating rates, and serves as a source for the reaction atmosphere. The alumina reactor, placed in a two-stage electrically-heated furnace, is designed to mimic the temperature-time history that coal/biomass/char particles experience in entrained-flow gasifiers. The flamefront temperature can be set as high as 2600 °C, while the reactor/furnace can withstand 1750 °C. The residence times possible to achieve in the system are a couple of hundreds milliseconds scale, allowing for high degrees of conversion of biomass fuels. The slagging behavior of the ash has been characterized by means of a deposition probe, on which top an alumina plate was placed, kept uncooled. The probe was set axially at different positions along the reactor, thus simulating different particle residence times. For this experimental campaign, the reactor furnace temperature was set at 1450 °C, while flame temperature has reached approx. 2050 °C (see **Figure 2**).

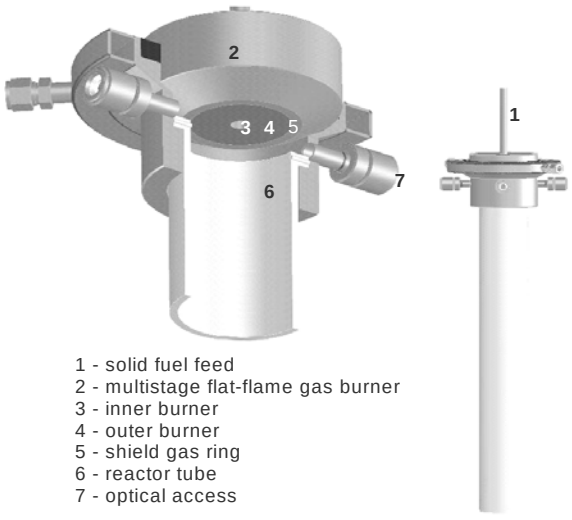

Figure 1. Schematic of the LCS test rig

SEM/EDX techniques have been applied to characterize the slag sample obtained. In addition, knowledge on slagging/melting tendencies of the selected fuels has been studied using an equilibrium model (FACTSAGE computer model) minimizing Gibbs free energy of an hypothetical (pressurized) entrained-flow gasification system, as well as simulating operation conditions close to the experimental ones.

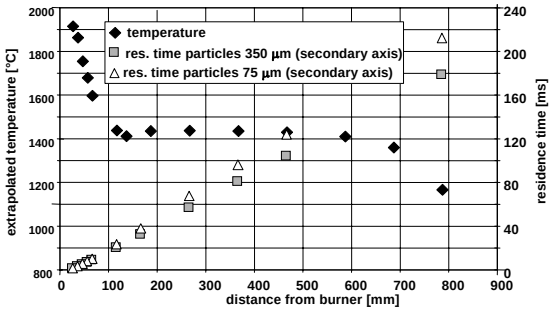

Figure 2. Experimental Temperature/Residence Time Profiles

Fuels. Experiments have been performed with three different woods: beech, willow, and a mixed wood that is commonly utilized in a Dutch power station. Fuel ash composition is shown in **Table 1**.

	beech	willow	wood mixture
Ash content (wt%)	1.01	1.9	1.51
Cl (wt% daf)	0.0037	0.02	0.19
S (wt% daf)	0.017	0.057	0.4
Si (mg/kg fuel)	171	618	417
Al (mg/kg fuel)	48	60	94
P (mg/kg fuel)	89	708	192
Mg(mg/kg fuel)	366	524	252
K(mg/kg fuel)	1151	2894	974
Ca(mg/kg fuel)	3096	5720	2417
Fe (mg/kg fuel)	47	68	116
Na(mg/kg fuel)	8	210	53

Table 1. Fuel Ash Content and Fuel Ash Composition

Results and Discussion

The results of the experimental campaign have shown that wood ash is not prone to form a fluid slag at typical operating temperatures of slagging gasifiers (e.g. 1300-1500 °C). **Figure 3** shows a SEM picture of a particle of beech ash slag after an experiment of 2 hrs. duration time. On the top of the deposit probe no uniform melt/ash layer was found, but rather single (clusters of) ash particles in which the original wood particle structure is still recognizable. Shifting the deposit probe position from 300 to 760 mm (corresponding to changing the residence time from 80 to 220 ms) does not improve the melting behavior of the ash. Only a small share of particles undergoes an enhanced melt formation due to formation of a Ca-silicate structure.

The results of the experimental campaign were well correlating with the predictions of the FACT-SAGE thermodynamic equilibrium program in terms of molten slag composition, which predict that overall at 1400 °C only 17% of the total ash-forming constituents in

the wood will form a molten slag. Condensation of CaO is predicted to begin in the temperature window 1800-1700 °C. At 1000 °C, 74% of the total Ca in the fuel will form condensed CaO. Alkalis will exclusively form gaseous species overall the temperature range 2000-1000 °C, over a wide pressure range 5-30 bars. The experimental results were similar for the three types of wood ash investigated. For willow, it has been experimentally found out that the higher fuel phosphor content might partly enhance the melting behavior of the slag. **Figure 4** shows a typical (cluster of) particles upon gasification of willow: a molten slag structure, phosphor-enriched, is recognizable, whereas the non-molten structure is composed predominantly by CaO.

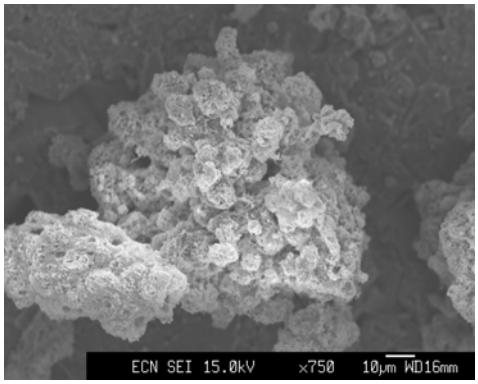

Figure 3: Micrograph of a beech gasification slag deposit

Changing the material substrate of the deposit probe plate was seen not to influence the melting behavior of the ash; on the contrary, wood ash particles have been homogeneously encapsulated in the melt when a pre-existing melt on the deposit probe-plate was present.

Since the wood ashes are not prone to melt under typical operating process temperatures of entrained flow slagging gasifiers, additives will be required which will lower the melting point of the ash.

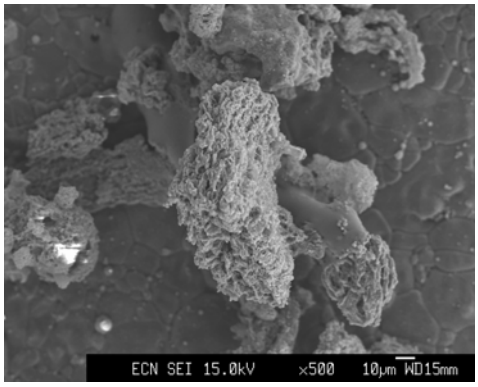

Figure 4: Micrograph of a willow gasification slag deposit

In this respect, additives rich in quartz or clay may enhance the overall fluidity of the slag. Experiments performed with beech wood mixed with SiO_2, (~99% purity), in agreement with thermodynamic calculations and with standard ash fusion test (DIN 51730), have shown that adding quartz on a molar ratio Si: Ca_{fuel} = 1:1; 2:1 (correspondent to 600 g – 1200 g quartz/kg fuel ash) may be sufficient to decrease the melting point of the ash system down to typical process operating temperatures.

Under experimental conditions, a layer of molten slag, (Ca-Silicate) was found on the deposit probe plate. When adding quartz, alkaline earth (and, to a less extent, alkali) metals will tend to be encapsulated in the silicon-based melt. Clay compounds have been predicted by thermodynamic calculations to perform in a similar way as SiO_2 in terms of increasing the total molten slag amount in the system.

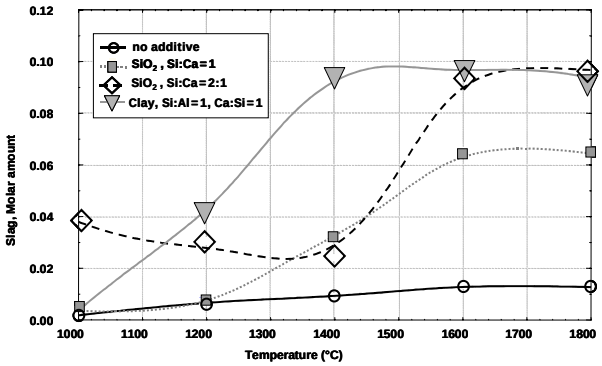

Figure 5: Influence of different additives on slag amount

Figure 5 shows the results of the thermodynamic equilibrium predictions plotting the molten slag amount versus temperature.

When adding a clay with a share of Al: Si=1:1 and Si: Ca_{fuel}=1:1 molar ratio), 90% of the total ash forming constituents will constitute a liquid melt at 1400 °C, according to thermodynamic predictions. This is due to the fact that Ca will be effectively encapsulated in the Al/Si based matrix.

Application of empirical viscosity models, such as Urbain-Kalmanovitch[2], to the investigated optimal wood/flux mixtures, show that viscosity may reach values in the range 8-15 Pa*s, thus achieving both sufficient fluidity to allow free flow and easy slag tapping is possible over typical temperature conditions. However, availability of data on slag flow properties in the composition range of wood ash with flux streams is limited[3], and more work is needed to assess quantitatively the characteristics of the slag flow in terms of viscosity versus slag composition and temperature.

Conclusions

Wood ash is not prone to form a fluid molten slag at typical operating conditions of (pressurized, oxygen-blown) entrained-flow gasifiers due to the formation of high-temperature melting compounds (e.g. CaO). Flux addition with quartz-based or clay-based compounds is a promising option to improve slag behavior by reducing the melting point of the slag. Further work is required to assess quantitatively the characteristics of the slag flow, especially in terms of viscosity versus slag composition and temperature.

Acknowledgement. The financial contribution of SDE (Agency for research in Sustainable Energy) is gratefully acknowledged. The authors express their thanks to B. van der Drift and H. Boerrigter, ECN Biomass, for fruitful discussions.

References

(1) Kiel, J.H.A.; Eenkhoorn, S.; and Heere, P.G.T., Ash behaviour in entrained flow gasification: preliminary studies, EC*N. Brandstoffen, Conversie en Milieu [BCM]* ECN-C--99-037, 1999.

(2) Browning, G.J.;Bryant, G.w.;Hurst, H.J; Lucas, J.A.; and Wall, T.F., *Energy &Fuels*, **2003**,*17*, 731-737.

(3) Vargas, S.; Frandsen, F.J.; and Dam-Johansen, K., *Progress in Energy and Combustion Science*, **2001**, *27*, 237-429.

EXTENDING THE CAPABILITY OF CFD CODES TO ASSESS ASH RELATED PROBLEMS IN BIOMASS FIRED BOILERS

Søren K. Kær[1], Lasse A. Rosendahl[1], and Larry L. Baxter[2]

[1] Aalborg University
Institute of Energy Technology
DK-9220 Aalborg Ø.
Denmark

[2] Brigham Young University
Dep. Chemical Engineering
350 Clyde Building
Provo, UT 84602

Abstract

This paper discusses the application of FLUENT™ in the analysis of grate-fired biomass boilers. A short description of the concept used to model fuel conversion on the grate and the coupling to the CFD code is offered. The development and implementation of a CFD-based deposition model is presented in the reminder of the paper. The growth of deposits on furnace walls and super heater tubes is treated including the impact on heat transfer rates determined by the CFD code. Based on the commercial CFD code FLUENT™, the overall model is fully implemented through the User Defined Functions. The model is configured entirely through a graphical user interface integrated in the standard FLUENT™ interface. The model considers fine and coarse mode ash deposition and sticking mechanisms for the complete deposit growth, as well as an influence on the local boundary conditions for heat transfer due to thermal resistance changes. The model is applied to the straw-fired Masnedø boiler. Results are in good qualitative agreement with both measurements and observations at the plants.

Nomenclature

A	Area [m]
C_c	Cunningham slip correction [-]
C_f	Friction factor [-]
C_v	Constant volume specific heat [J/(kg K)]
d	Diameter [m]
d_m	Molecular diameter [m]
dt	Incremental time [s]
f	Fraction [-]
F	Force [N]
k	Thermal conductivity [W/(m K)]
k_B	Boltzmann's constant [J/K]
k^+	Dimensionless roughness height [-]
Kn	Knudsen number [-]
L_1	Lift force on particle [N]
m	Mass [kg]
$\dot{m}$	Mass flow rate [kg/s]
Nu	Nusselt number [-]
p	Probability [-]
Pr	Prandtl number [-]
r	Reflectance [-]
R	Conduction resistance coefficient [m^2K/W]
R_g	Gas constant [J/(kg K)]
Re	Reynolds number [-]
s_n	Norm. momentum accommodation coef. [-]
s_t	Tang. momentum accommodation coef. [-]
S	Particle to gas density ratio [-]
Stk	Stokes number [-]
t	Time [s]
T	Temperature [K]
u	Velocity [m/s]
u^*	Friction velocity [m/s]
U	Gas velocity [m/s]
V	Volume [m^3]

Greek letters:

ε_s	Surface roughness height [m]
$\varepsilon_{deposit}$	Deposit porosity [-]
ϕ_p	Particle concentration [kg/m^3]
γ	Specific heat ratio [-]
η	Efficiency [-]
ν	Kinematic viscosity [m^2/s]
ρ	Density [kg/m^3]
τ_p	Particle relaxation time [s]
τ_w	Wall shear stress [Pa]

Subscripts:

cell	Computational cell property
d	Deposition, deposit
g	Gas property
imp.	Impaction
in	Inlet property
liq.	Liquid
out	Outlet property
p	Particle property
s	Surface property
stick	Sticking
Tu	Turbulent
Th	Thermophoresis
vol	Volume
+	Boundary layer property

Introduction

In Denmark, as well as internationally, boiler manufacturers are set increasing demands for fuel-flexible and efficient boilers. To meet these demands still more advanced design tools are needed and the use of Computational Fluid Dynamics (CFD) is increasing. To improve the design tools used by Danish boiler manufacturers and operators in design, operation optimisation and trouble-shooting of biomass fired boilers a Computational Fluid Dynamics (CFD) based tool is under development. Mechanistic models are developed and integrated into the commercial CFD code FLUENT™ to tailor the predictive capabilities of the code to the specific needs of the boiler industry and power utility companies.

This paper discusses an overall modelling concept for grate-fired boilers and outlines a model that relates ash deposition behaviour during biomass combustion in grate-fired furnaces to fuel properties, boiler operating conditions, and boiler design. In this paper focus is on straw combustion, however, the long-term objective is for the model to embrace a wide range of fuel types and mixes.

The accumulation of deposits on heating surfaces reduces heat transfer rates from the flue gas to the steam circuit causing a decrease in plant efficiency if they cannot be removed according to the design assumptions of the boiler. In case of severe slagging and fouling unscheduled plant shutdown may result due to the formation of unmanageable amounts or forms of deposits. A typical example of super heater deposits from Masnedø CHP plant, Denmark is illustrated in **Figure 1**.

Figure 1 Super heater deposits formed during straw combustion at Masnedø CHP plant (picture taken from the grate looking upwards). Courtesy of Lars Fenger, ENERGI E2.

In recent years, attention has been given to mechanistic descriptions of deposit formation [1,2,3,4,5,6] however, with only limited attention directed towards biomass firing in grate-based boilers. The fluid mechanics and thermodynamics of the flow and combustion processes influence the deposition processes through particle residence times, particle motion, mixing processes, temperature patterns and heat transfer rates. Comprehensive investigation and modelling of the interaction of these mechanisms can only be obtained by incorporating deposit formation models into Computational Fluid Dynamics (CFD) codes.

Model setup

The commercial CFD code FLUENT™ is used as the framework to solve the turbulent fluid flow, gas and particle combustion, heat transfer and particle transport. The deposition model was implemented through the User Defined Functions (UDF) and a Graphical User Interface (GUI) was included in the standard FLUENT™ interface to ensure ease of use. This allows the user to choose any of the standard FLUENT™ models to solve the fluid dynamics and combustion processes while at the same time being able to include the deposition model. **Figures 2** and **3** illustrate two of the deposition model menu items integrated into FLUENT™.

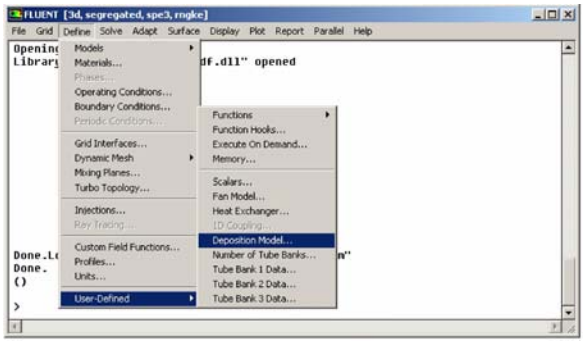

Figure 2 The Graphical User Interface integrated into FLUENT™ for easy configuration of the deposition model.

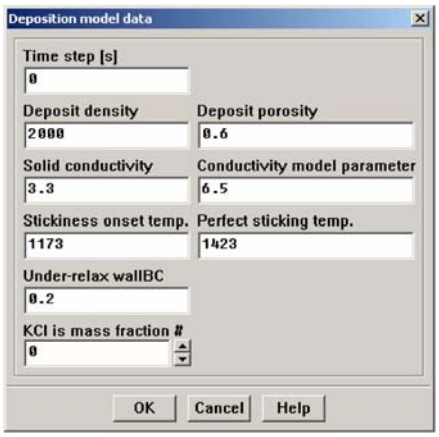

Figure 3 The deposition model configuration panel in FLUENT™.

In the predictions presented in this paper, the steady-state governing equations were solved using the SIMPLE algorithm and the effect of turbulence on the mean flow field was accounted for using the RNG k-ε model. Radiative heat transfer was modelled using the Discrete Ordinates model available in FLUENT™. A two-step reaction mechanism was used for the gas combustion with CO as the intermediate species. The reaction rates were modelled using a combination of chemical kinetics and turbulent mixing (Eddy-Break-Up).

In terms of the geometrical model, the secondary and tertiary platen super heaters in the first and second passes were approximated as slabs and the primary super heater and economizer tube banks in the third pass were accounted for using source terms in the momentum and energy equations. **Figure 4** illustrates the approach used.

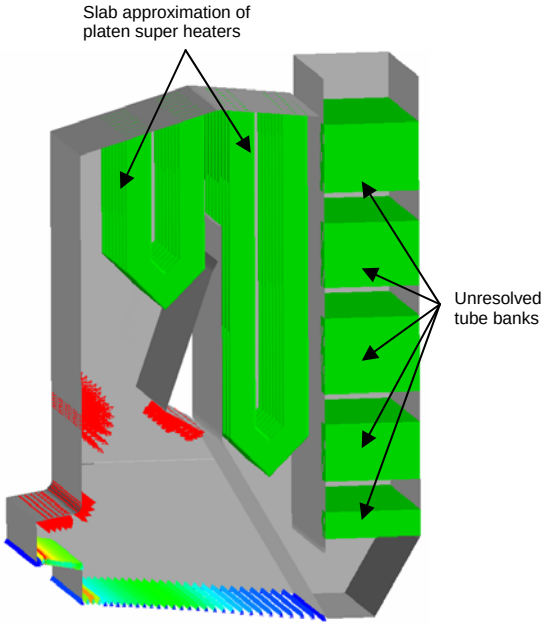

Figure 4 Illustration of the slab approximation used for platen super heaters and the source term approach used for tube banks.

Fuel conversion in bed

Fuel conversion on the grate plays a key-role as boundary conditions in the analysis of the boiler free-board processes. A stand-

alone model[7] was used to predict fuel conversion on the grate. The bed model uses a moving column approach where a three dimensional package of fuel is tracked along the grate while the conversion processes are taking place. In the horizontal direction gas and fuel properties are represented at discrete node points. The principle is illustrated in **Figure 5**.

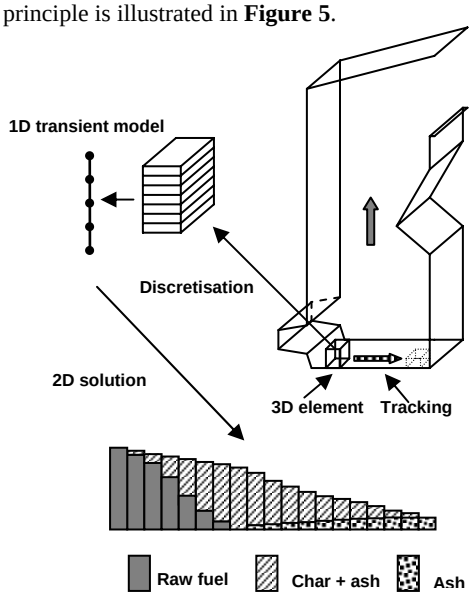

Figure 5 Schematic of the bed combustion modelling concept applied.

This approach results in a two dimensional picture of the bed composition and temperature patterns as indicated at the bottom of **Figure 5**. Profiles of gas velocity, temperature and composition at the bed surface are transferred to the CFD model as boundary conditions. This is discussed in more details in a later section.

Ash formation and transport

In biomass combustion the release of volatile ash fractions (mainly alkali) and entrainment of non-volatile mineral matter lead to a characteristic bimodal fly ash size distribution. **Figure 6** illustrates the ash formations paths.

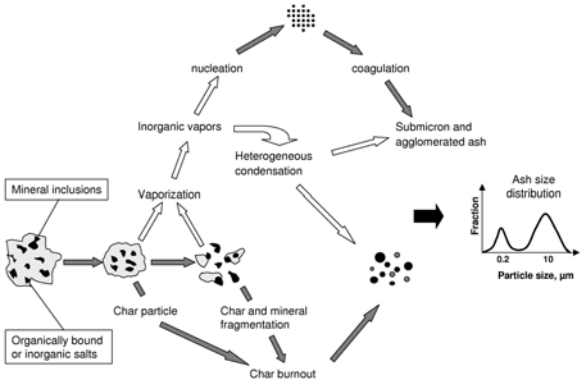

Figure 6 Schematic of the ash formation routes leading to a bimodal fly ash size distribution.

Information about the local flux of ash leaving the grate in the form of vapours and entrained particles is required by the deposition model. This is illustrated in **Figure 7**.

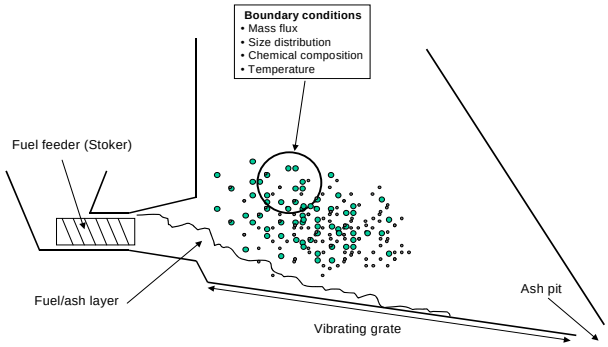

Figure 7 Schematic illustration of boundary conditions required at the grate.

For the entrained particles, the chemical composition as well as the particle size distribution are also required.

Vapour release. During straw combustion alkali salts are the main vapour forming species. Potassium chloride is the predominant stable alkali-bearing species released from the fuel bed at the prevailing combustion temperatures[8]. Chlorine and potassium is released from the fuel matrix early in the combustion process at temperatures around 200-400°C[9]. Potassium re-deposits at the particle surface as discrete KCl particles or intercalates into the char[10]. The amount of potassium that subsequently vaporizes is often determined by the amount of chlorine available to form stable vapours rather than the amount of potassium in the fuel[8]. The mechanisms controlling potassium release rates are not sufficiently well understood to model the conversion and release processes in detail. As a first-order approximation in this paper, the evaporation rate was predicted using mass transfer correlations subject to the constraint that 70 wt% of the total chlorine is released to the gas phase.

Entrainment of coarse non-volatile ash. The chemical composition as well as the particle size distribution of the entrained ash fraction originating from non-volatile species is difficult to determine at a location just above the grate. The chemical composition of fly ash samples collected at locations where the flue gas temperature is below the dew point of alkali vapours cannot be used due to enrichment in these species. The ash composition at high temperatures was approximated from bottom ash chemical analyses[11]. A density of 2000 kg/m^3 was used for these particles. Table 1 presents the major species found in the bottom- and fly ashes from Slagelse CHP plant, Denmark.

Table 1, Major Species in Bottom and Fly Ash Samples Collected from a Straw-Fired Boiler[11].

Species [wt%]	SiO_2	Fe_2O_3	CaO	MgO	Na_2O	K_2O
Bottom ash	68	0.56	10	2	0.4	11
Fly ash	27	0.66	4.7	0.82	0.7	32

A size distribution obtained from CCSEM analysis of the bottom ash is used for the entrained particles. This is a fairly rough approximation however, pending more detailed measurements; it seems to be the best option available. **Figure 8** shows the size distribution used for the entrained non-volatile ash fraction.

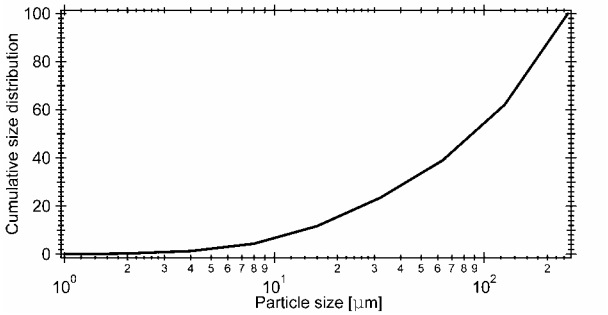

Figure 8 Measured cumulative size distribution from the bottom ash of a straw fired boiler[11].

Based on field measurements, 20 wt% of the total fuel ash is assumed to be entrained in the flue gas. The local flux of ash particles entrained from the grate is approximated from a linear dependence on the local velocity of air through the fuel layer i.e. proportional to the Stokes drag force. The temperature is assumed to equal the temperature of the fuel bed predicted by the bed model.

Ash transport modelling. An Eulerian mass fraction equation is used to represent KCl vapour and sub-micron particles formed by condensation of these vapours. The entrained, relatively coarse, particles dominated by silicates are represented in a Lagrangian frame by the Stochastic Separated Flow model[12] by numerical integration of the particle equation of motion:

$$\frac{d\left(m_p \vec{u}_p\right)}{dt} = \sum_i \vec{F}_i \qquad (1)$$

Ash deposition model

Special attention was given to the deposition mechanisms governed by boundary layer phenomena. Due to limited computational resources these mechanisms cannot be accounted for in full-scale simulations of utility boilers by traditional Lagrangian particle tracking. The computational grid insufficiently resolves the details of the boundary layer and modelling of the complex turbulence patterns requires closures that are not feasible or even non-existent. To resolve these problems, this work adapts the approach based on deposition velocity correlations suggested by[3]. **Figure 9** illustrates the modelling concept.

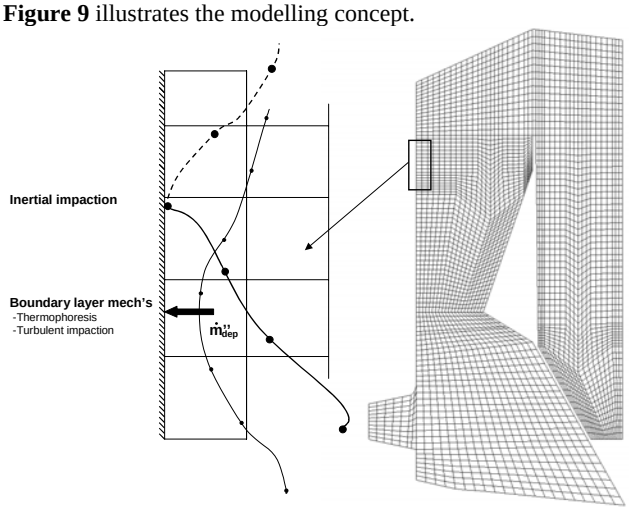

Figure 9 Schematic of the CFD-based ash deposition modelling concept.

The modelling concept used to represent deposition by boundary layer phenomena relies on dimensionless deposition velocities as defined in Equation 2.

$$u_d^+ = \frac{u_d}{u^*} \qquad u^* = \sqrt{\frac{\tau_w}{\rho_g}} \qquad (2)$$

As such this approach follows the same basic idea as in turbulence modelling where wall functions have been used with great success for decades to predict shear stresses, heat and mass transfer. The deposition mass flux is found from multiplication of the deposition velocity with the near-wall particle concentration:

$$\dot{m}''_d = u_d \, \phi_p \qquad (3)$$

The total deposition velocity is calculated by adding the deposition velocities due to turbulent impaction and thermophoresis:

$$u^+_{d,total} = u^+_{d,Tu} + u^+_{d,Th} \qquad (4)$$

The near-wall particle concentration is predicted from the Eulerian transport equation for the sub-micron particles and the Lagrangian trajectories for the particles in the micron-range. Specifically, for the Lagrangian model, the contribution from one trajectory to the particle concentration in a next-to-wall cell is given by:

$$\phi_p = \int_{t_{cell,in}}^{t_{cell,out}} \frac{\dot{m}_{trajectory}}{V_{cell}} \, dt \qquad (5)$$

Boundary layer deposition in tube banks. For water walls and platen super heaters the shear velocity (required in Equation 2) is calculated directly using wall functions in the CFD model. This information is not available for the unresolved tube banks. Instead, an estimate is made from Reynolds analogy using a Nusselt number correlation for circular tubes in cross-flow:

$$\tau_w = \frac{C_f}{2} \rho U_g{}^2 \qquad (6)$$

and

$$\frac{C_f}{2} = \frac{Nu}{\mathrm{Re}\,\mathrm{Pr}} \qquad (7)$$

Boundary layer deposition takes place on all tubes in the tube bank. The tube surface area available for deposition in each cell inside the tube bank is taken to be the ratio of the total surface area of all tubes in the bank to the tube bank volume (this ratio is termed A_{vol}) multiplied by the cell volume. At each time step in the trajectory calculation (Δt) the deposited mass is removed from the trajectory:

$$\dot{m}_{out} = \dot{m}_{in} - u_{d,total} \, \phi_p \, A_{vol} \, V_{cell} \, \eta_{stick} \qquad (8)$$

with

$$\phi_p = \frac{\dot{m}_{trajectory} \, \Delta t}{V_{cell}} \qquad (9)$$

For the sub-micron particles forming from vapour condensation, the concentration is calculated from the Eulerian transport equation as mentioned above.

Turbulent deposition. Detailed numerical predictions[13,14] and experimental studies[15] of particle transport in boundary layers support the original idea[16] that deposition of particles with dimensionless relaxation times between 0.25 and 20 occurs due to the interaction with coherent structures (turbulent bursts). The dimensionless particle relaxation time is defined as:

$$\tau_p^+ = \frac{1}{18} C_c \, S \, d_p^+ \quad with \quad d_p^+ = \frac{d_p u^*}{\nu} \qquad (10)$$

Using numerical methods to establish a limiting trajectory

leading to deposition in a viscous plane stagnation point flow representing the coherent eddies in the boundary layer a model that considers the surface roughness introduced by deposited particles was derived[17]:

$$u^+_{d,Tu} = \left[\frac{\left(0.64k^+ + \frac{d^+}{2}\right)^2}{3.42}\right]^{\frac{1}{(1+\tau_p^{+2}L_1^+)}} \times \frac{1+8\exp\left(-\frac{(\tau_p^+-10)^2}{32}\right)}{27.03\ \ (1-\tau_p^{+2}L_1^+)} \quad (11)$$

with the following definitions of the non-dimensional lift force and roughness height:

$$L_1^+ = \frac{3.08}{S\,d_p^+} \qquad k^+ = \frac{\varepsilon_s u^*}{\nu} \quad (12)$$

Figure 10 presents the dimensionless deposition velocity as a function of dimensionless relaxation time based on Equation 11:

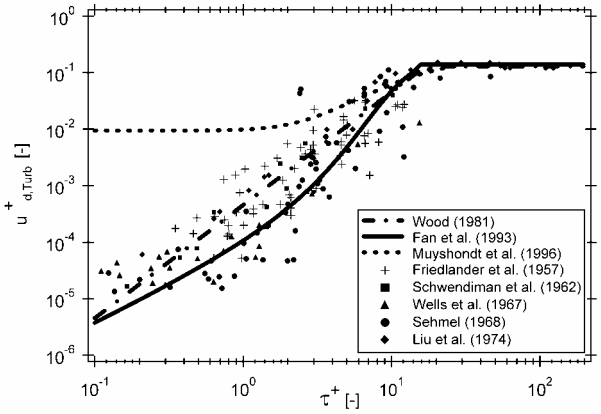

Figure 10 Comparison of dimensionless turbulent deposition velocity correlations with measurements.

It is worthwhile noting that turbulent eddy impaction should not be confused with the deposition caused by vortex shedding at the downstream side of a tube. Turbulent eddy impaction is the result of coherent structures associated with spontaneous turbulent bursts in the boundary layer whereas vortex shedding behind a tube is a bulk flow feature.

Thermophoretic deposition. In most combustion applications a significant temperature gradient exists across the viscous boundary sub-layer causing an enhanced deposition rate of particles with dimensionless relaxation times less than ≈1 (at typical combustion conditions) due to a significant thermophoretic force[18].

A number of correlations giving the thermophoretic force as a function of the Knudsen number have been suggested and that given in Equation 12 is adopted in this work[19].

$$F_{Th} = \frac{1.15\,Kn\left(1-\exp\left(-\frac{\alpha}{Kn}\right)\right)\sqrt{\frac{4}{3\pi}\phi\pi_1 Kn}\,\frac{k_B}{d_m^2}\nabla T d_p^2}{4\sqrt{2}\,\alpha\left(1+\frac{\pi_1}{2}Kn\right)} \quad (13)$$

where

$$\phi = 0.25(9\gamma - 5)\frac{c_v}{R_g}$$

$$\alpha = 0.22\left(\frac{\frac{\pi}{6}\phi}{1+\frac{\pi_1}{2}Kn}\right)^{\frac{1}{2}} \quad (14)$$

$$\pi_1 = 0.18\frac{\frac{36}{\pi}}{(2-S_n+S_t)\frac{4}{\pi}+S_n}$$

The thermophoretic force calculated from Equation 13 was non-dimensionalised as given by Equation 15 and is shown as a function of the Knudsen number in **Figure 11**. Correlations suggested by other investigators as well as measurements are also included.

$$F^*_{Th} = \frac{F_{Th}}{\left(d_p/2\right)^2|\nabla T|}10^5 \quad (15)$$

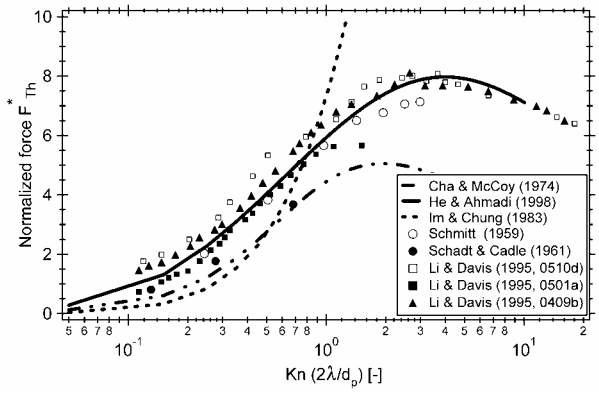

Figure 11 Comparison of predicted dimensionless thermophoretic forces with measurements.

The dimensionless deposition velocity due to thermophoresis relates to the thermophoretic force as given by Equation 16[19].

$$u^+_{Th} = \frac{F_{Th}\tau_p}{m_p u^*} \quad (16)$$

Inertial impaction. The inertia of particles larger than about 10 μm is sufficient for their trajectories to deviate from the gas streamlines in regions of strong streamline curvature (e.g. around super heater tubes). Inertial impaction is often the major transport mechanism contributing to deposit build-up. The characteristic time scales of the particle motion and the flow field, expressed through the Stokes number, govern the rate of inertial impaction. The rate of inertial impaction onto a tube in cross flow becomes significant at Stokes numbers larger than unity[20]. For water walls and pendant super heaters, the inertial impaction rate is calculated by monitoring when a particle trajectory meets the surface.

For the tube banks represented by three-dimensional volumes, the approach outlined above is not applicable. Instead, an empirical correlation is used that relates the Stokes number to the impaction efficiency, η_{imp}. The Stokes number is given as:

$$Stk = \frac{\rho_p d_p^2 U_g}{9\,\mu_g\,d_{tube}} \quad (17)$$

The impaction efficiency is defined as the ratio of the number of particles that strike the surface to the number directed towards the surface in the free stream. For a circular tube, the impaction efficiency can be related to the Stokes number as:

$$\eta_{imp} \approx \frac{1}{1 + b(\Phi)^{-1} - c(\Phi)^{-2} + d(\Phi)^{-3}} \quad (18)$$

where

$$\Phi = Stk - a \quad (19)$$

with the following values of the constants: a=0.125, b=1.25, c=-0.014 and d=0.00508. This approach is only used for the first row of tubes in a tube bank. For an in-line tube arrangement, subsequent rows are subject to much slower inertial impaction rates. The ratio of the surface area of tubes in the flow direction to the total flow area gives the probability that a particle is directed towards a tube. Taking the sticking propensity into account, the overall deposition efficiency is:

$$\eta_{bank} = \frac{N_{tubes,\,per}\, d_{tube}}{L} \eta_{imp}\, \eta_{stick} \quad (20)$$

where $N_{tubes,\,per}$ (the number of tubes perpendicular to the flow direction) and L (tube bank dim. 1) are defined as shown in **Figure 12**. After passing the first row of tubes in the bank, the mass flow of particles represented by the trajectory is:

$$\dot{m}_{out} = \dot{m}_{in}(1 - \eta_{bank}) \quad (21)$$

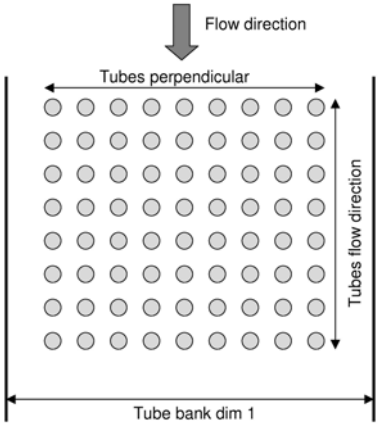

Figure 12 Geometric data required for tube banks.

Ash sticking propensity

The subject of ash sticking propensity has been given considerable attention in the literature, however, so far no generally accepted modelling methodology has been developed, especially not focusing on conditions typical for biomass combustion. In mechanistic modelling approaches to ash deposition in coal combustion, the most frequently used approach is that of[21]. Neglecting resuspension and other deposit removing mechanisms, the net fraction of particles contributing to deposit growth is given by:

$$\eta_{stick} = \underbrace{p(T_p)}_{\text{particles}} + \underbrace{\left[1 - p(T_p)\right] p(T_s)}_{\text{deposit surface}} \quad (22)$$

The influence from condensed alkali vapours on the sticking propensity cannot be disregarded in straw-fired boilers[22]. Deposit growth in the presence of condensed material has been discussed by for example[23,24,25] and [26]. It has been found that molten alkali salts (predominantly KCl in straw combustion) at the deposit and particle surfaces efficiently capture the silica-rich particles[27,28]. Based on this observation it was suggested that the sticking propensity is proportional to the fraction of melt at the surface[27]. In this work the melt fraction based sticking concept is developed further towards a form applicable in the context of a CFD analysis.

It was found by[27] that biomass ashes collected from the super heaters, the furnace walls and the bottom ash exhibit a characteristic melting behaviour. Roughly, melting occurs in two temperature regimes; one corresponding to melting of alkali salts; and one to melting of silicates. This was approximated as given in **Figure 13**:

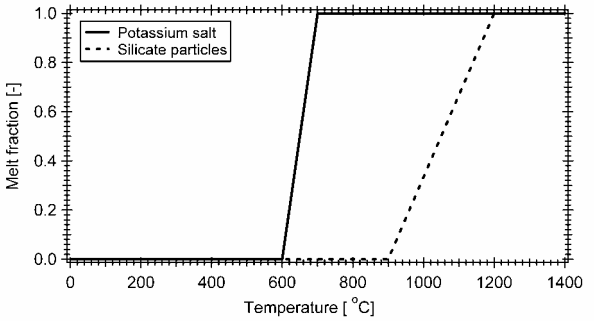

Figure 13 Approximated melting curves of potassium salt and silica-rich particles.

From these assumptions, the local temperature and composition (indicated by T and X in Equation 23) dependent melt fraction can be estimated and used in the prediction of sticking propensity for the particle as well as the deposit surfaces.

$$f_{melt}(T,X) = f_{melt,KCl}(T)\frac{m_{KCl}}{m_{total}} + f_{melt,silicate}(T)\frac{m_{silicate}}{m_{total}} \quad (23)$$

As an alternative to this approach the particle viscosity can be used for silica-rich particles. This approach was applied in the original paper[21] where a reference viscosity is defined and the sticking propensity modelled as:

$$p(T,X) = \begin{cases} \dfrac{\eta_{ref}}{\eta} & \eta > \eta_{ref} \\ 1 & \eta \le \eta_{ref} \end{cases} \quad (24)$$

Particles that are predicted to stick to the heating surface are removed from the prediction such that, statistically, particles cannot deposit twice.

Deposit physical properties

The deposit porosity varies depending on temperature and chemical composition. Experimental findings suggest the porosity of the inner layer of potassium salt may be as high as 0.9[29]. A deposit consisting of coarse weakly sintered silicate particles typically has a porosity of around 0.6[1]. The fractions of liquid and solid phases influence the local porosity. A simple correlation based on the ratio of liquid to solid volumes was proposed by[1] and adopted by[4,5]:

$$\varepsilon_{deposit} = 1 - \left[(1-\varepsilon_0) + \frac{V_{liq}}{V_{solid}}(1-\varepsilon_0)\right] \quad (26)$$

The thermal conductivity of deposits is a complex function of many parameters including the deposit microstructure and the degree of connectedness between individual particles in the deposit. In the literature, a large number of correlations have been proposed giving the thermal conductivity of ash[30]. In the present work, the simple correlation proposed by[1] in a study of deposit heat transfer is used:

$$k = (1-F)\,k_{solid} + F\,k_{gas} \quad (27)$$

where the weighting factor, F, is defined as:

$$F = \frac{2^n}{2^n - 1}\left(1 - \frac{1}{(1+\varepsilon_{deposit})^n}\right) \quad (28)$$

Based on the heat flux predicted by the CFD code, the deposit layer thickness, the thermal conductivity, and the clean tube temperature (T_{tube}) the deposit surface temperature can be determined from:

$$T_d = \dot{q}'' R + T_{tube} \quad (29)$$

where the conduction resistance coefficient (R) is determined as:

$$R = \sum_{i=1}^{N} \frac{dx_{i,deposit}}{k_{i,deposit}} \quad (30)$$

The summation is over the deposit layers generated in each time step.

A model is currently being implemented in FLUENT™ that allows the radiative properties of the deposit to be determined from the optical properties of the deposited material. In the meantime a constant emissivity was estimated in the simulations presented in this paper. In the new model, the emittance of the initial particulate layers is determined using the theory of imbedded invariance[31]. The single particle properties required by this approach are determined from Mie theory. The spherical reflectance of the particulate deposit is given as[31]:

$$r_s = 1 - 2\gamma H_1 \quad (31)$$

with

$$\gamma = \sqrt{(1-w)} \quad (32)$$

Where w is the single-scattering albedo. H_1 is the first moment of the H-function. The H-function is defined as[31]:

$$H(x) = 1 + \frac{w}{2} x H(x) \int_0^1 \frac{H(x')}{x + x'} dx' \quad (33)$$

The H function is complicated to evaluate, however good approximations exist for practical applications. **Figure 14** presents a comparison of predicted and measured emittance of a particulate deposit.

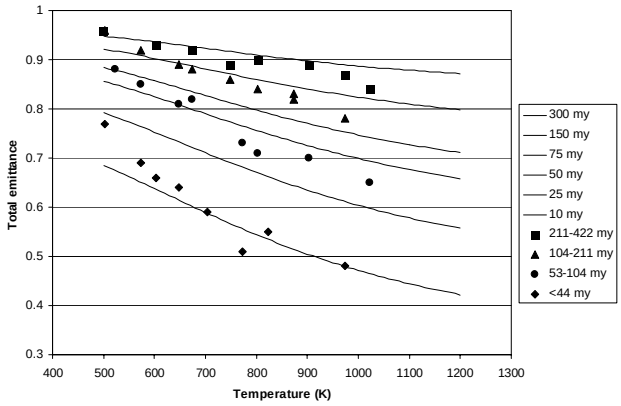

Figure 14 Comparison of predicted and measured emittance of a particulate deposit.

The properties of a completely fused slag with a smooth surface may be approximated as an optically smooth surface. The normal reflectance of a smooth surface is given by[32].

$$r_n = \frac{(n_\lambda - 1)^2 + k_\lambda^2}{(n_\lambda + 1)^2 + k_\lambda^2} \quad (34)$$

where n and k are the real and complex parts of the refractive index, respectively. The spherical reflectance can be found from a similar expression although with a somewhat more complicated functional dependence on n and k[32].

Full-scale model demonstration

The applicability of the deposition models described is demonstrated using the straw-fired boiler at Masnedø CHP plant as a test case. In this context some of the most significant results will be presented. For further discussions of the results please refer to[7].

Gas and fuel inlet conditions. The combustion air inlet conditions and locations are indicated in **Figure 15** showing the lower part of the furnace.

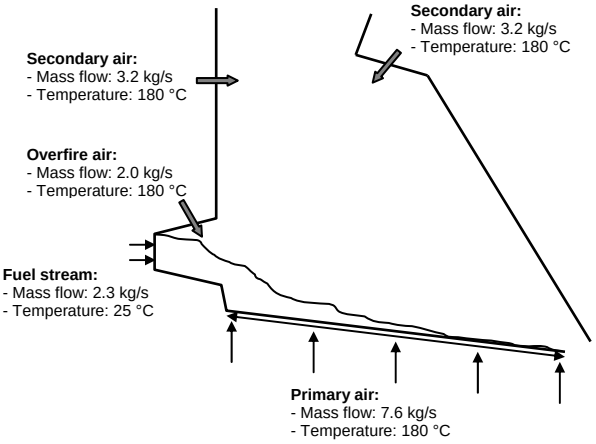

Figure 15 Boundary conditions used for the Masnedø simulations.

Approximately 50% of the total air is primary air supplied from under the grate. In this particular case, the grate air includes ignition air injected close to the fuel feeder. The remaining 50% is split between over fire air and secondary air with the major fraction being secondary air.

Inlet condition for the CFD model. Predicted profiles of gas velocity, temperature and composition at the top of the fuel bed is used as boundary condition for the CFD analysis of the free-board. **Figure 16** illustrates velocity and temperature profiles.

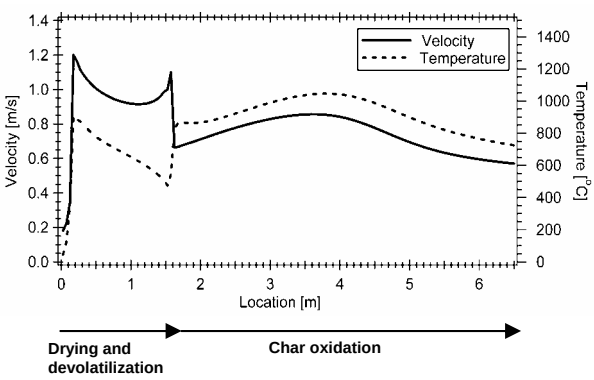

Figure 16 Predicted velocity and temperature profiles at the bed surface.

The drying and devolatilisation phases are characterised by high velocities due to rapid mass release from the fuel, and relatively low temperatures. At the onset of char oxidation, the temperature increases whereas the velocity decreases. **Figure 17** shows the composition of the evolving gases.

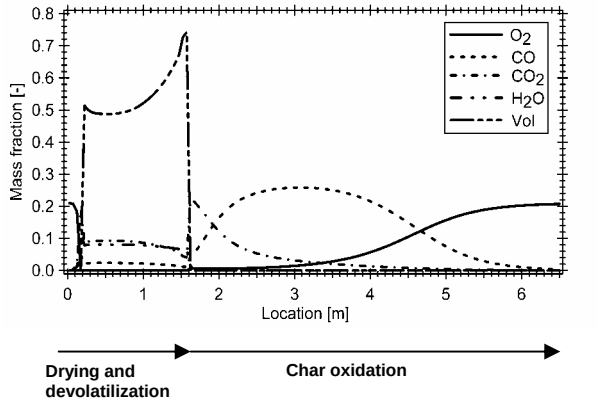

Figure 17 Predicted gas composition at the fuel bed surface.

The devolatilisation zone is dominated by volatiles (approximated as a pseudo-gas with a given C, H and O content), water vapour and carbon dioxide evolution. In the char oxidation region carbon monoxide and dioxide are the primary products. Towards the end of the grate, an increasing amount of oxygen leaves the bed as char conversion is nearly completed.

Measured and predicted gas properties. Sampling of gas phase species and temperature measurements were undertaken at Masnedø CHP plant in November 1998 during straw firing[33]. Approximate locations of the measurement ports are illustrated in **Figure 18**. The exact locations were difficult to establish except for the insertion length of the probe, which was reported to be 1.3m. To illustrate the implications of not knowing the exact probe locations, the variation in predicted values within a distance of ±0.5m (worst-case) from the estimated probe location is indicated by error bars.

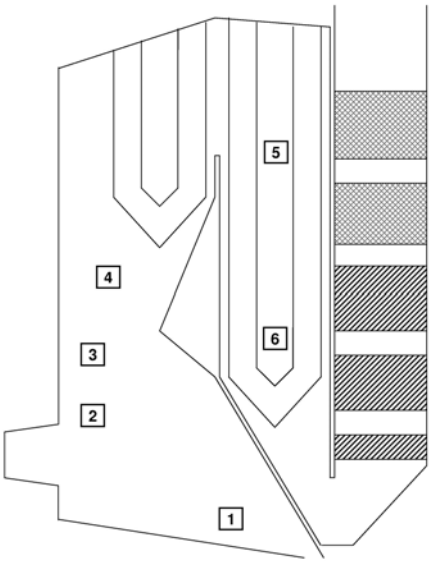

Figure 18 Estimated measurement locations for the full-scale data.

Figure 19 compares measured temperatures with calculated values. An error bar is given for each of the calculated temperatures illustrating the variation within a distance of ±0.5m of the estimated port location. In regions of strong gradients, the uncertainty is considerable.

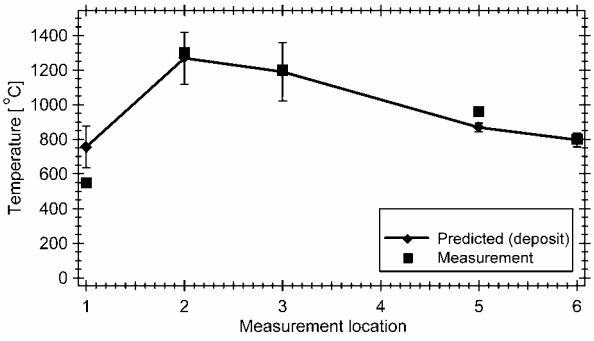

Figure 19 Comparison of predicted and measured temperatures.

The predicted temperatures are in very good correspondence with the measurements except at location 1, which is just above the grate. The calculated value is about 200 °C too high mainly due to the inlet value predicted by the bed model being too high. The measurement port is located approximately at the location where char burnout is completed on the grate. Most likely the difference can be ascribed to an inaccurate prediction of this location. This is supported by the observation that, during the measurements, the temperature at this measurement location varied several hundreds of degrees depending on the fuel load on the grate[33]. The standard deviations of the measurements have not been reported for the case of 100% straw firing, however, from standard deviations reported from measurements during co-firing with other biofuels it was estimated to be within ±50 °C.

Figure 20 shows calculated and measured oxygen and carbon dioxide concentrations at the same locations. Error bars in Figure 16 indicate the standard deviations of the concentration measurements. The uncertainty of the calculated value (related to the port location) is not included but from the variation of temperature it was estimated to be within ±15% of the local value.

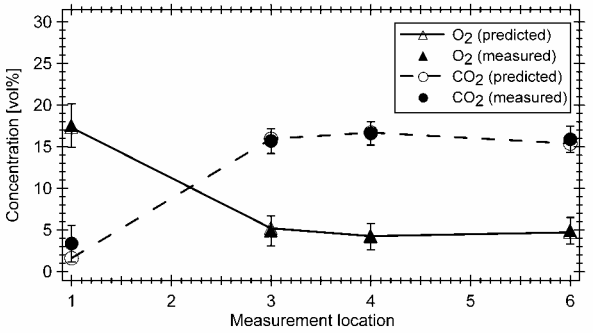

Figure 20 Comparison of measured and predicted oxygen and carbon dioxide concentrations.

As for the temperatures, the agreement with measurements is favourable and in this case also at the first measurement port. The concentrations at location 6 and to a lesser extent location 4 are given almost exclusively by the overall stoichiometry of the combustion process and consequently they are fairly easy to capture by the model. At locations 1 and 3, the concentrations are influenced by local mixing rates and finite reaction rates and as such they are considerably more difficult to predict accurately. The influence from

finite reaction rates can be identified from the co-existence of oxygen, carbon monoxide and volatiles at ports 1 and 3. Carbon monoxide and volatiles concentrations are compared to measured values in **Figure 21**.

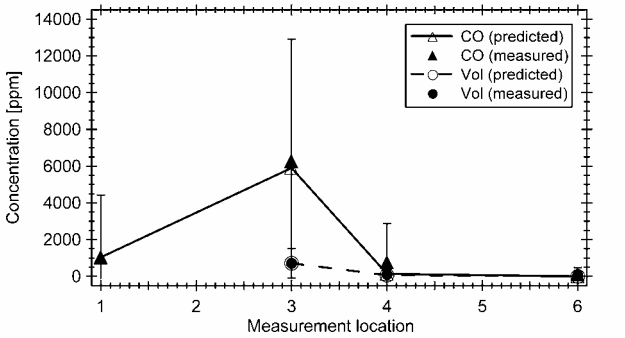

Figure 21 Comparison of measured and predicted carbon monoxide and volatiles concentrations.

When compared to the oxygen and carbon dioxide concentrations, the carbon monoxide and volatiles concentrations exhibit much larger standard deviations in the measurements. This is mainly due to combustion fluctuations introduced by grate vibrations[33]. Obviously, the steady state model used in this work cannot capture such time dependent phenomena. Still, the time-averaged solution obtained by the CFD model is in good correspondence with the time-averaged measurements.

Deposit formation predictions. The predictions presented here assume the contribution to the sticking propensity from the deposit surface is zero and shedding mechanisms were not accounted for. **Figure 22** illustrates the deposition mass flux. The unit of the legend is $gm^{-2}h^{-1}$.

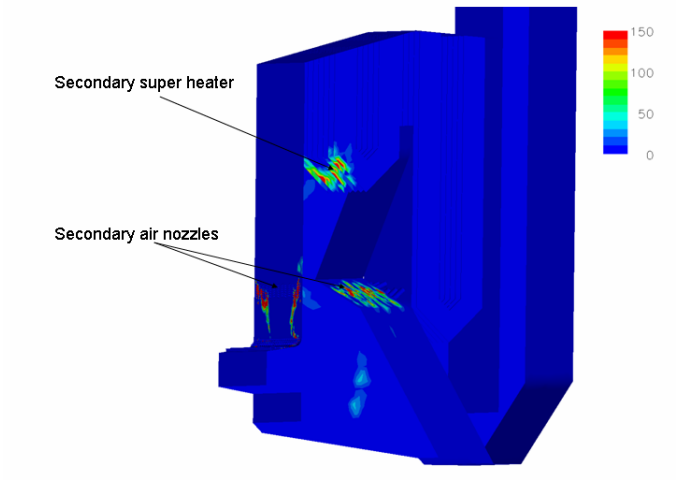

Figure 22 Predicted deposition mass flux in $gm^{-2}h^{-1}$.

It is difficult to undertake a quantitative validation of the predicted deposition rates as sufficiently detailed experimental data are not available. As such, the predictions should mostly be used to get an idea about areas of potential deposit formation problems.

Overall, the fastest deposition rates are found around the secondary air nozzles, located at the front and back walls just below the level of the nose, and on the windward part of the secondary super heater. These locations are characterized by strong streamline curvature that leads to inertial impaction of particles larger than about 10-20 μm. These locations of rapid deposit growth are consistent with observations from the plant.

The contributions to the deposition flux from inertial impaction and boundary layer controlled mechanisms (mainly turbulent eddy impaction and thermophoresis) are illustrated in **Figures 23** and **24** focusing on the secondary super heater.

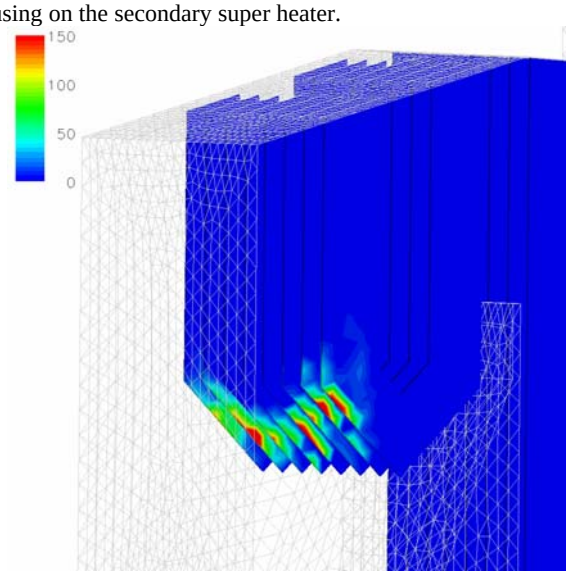

Figure 23 Close-up of the secondary super heater showing inertial impaction flux in $gm^{-2}h^{-1}$.

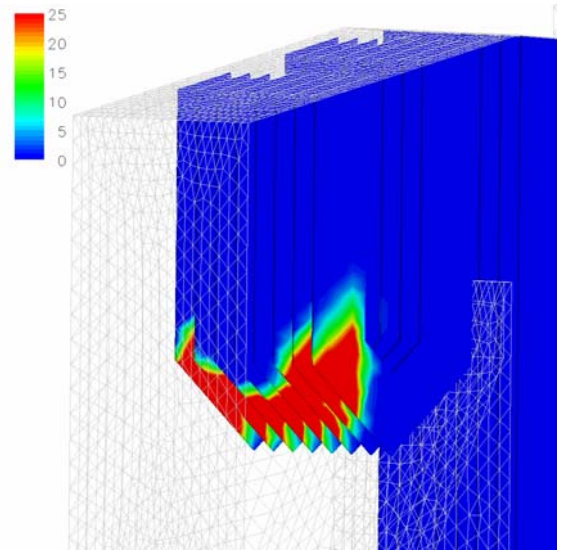

Figure 24 Close-up of the secondary super heater showing boundary layer controlled deposition flux in $gm^{-2}h^{-1}$.

It is seen that the inertial impaction is highly localized at the forward part of the super heater whereas deposition by boundary layer controlled mechanisms is more evenly distributed around the perimeter of the super heater panel. The inertial impaction flux is almost an order of magnitude higher than the boundary layer rate. Deposition probes were used to determine deposition fluxes in a Danish straw-fired boiler located in Slagelse[22]. This boiler uses the same firing technology as the one for which predictions are reported in this paper. Depending on exposure time rates in the range 60-100 $gm^{-2}h^{-1}$ were reported[22]. This is in good overall agreement with the results shown in **Figures 23** and **24**.

The model also considers deposition of vapours (assumed to

form aerosols before deposition). Although this mechanisms is not significant in terms of the total mass deposited it does provide a "glue" that influences the sticking of larger particles. The rates of this mechanism are shown in **Figure 25**.

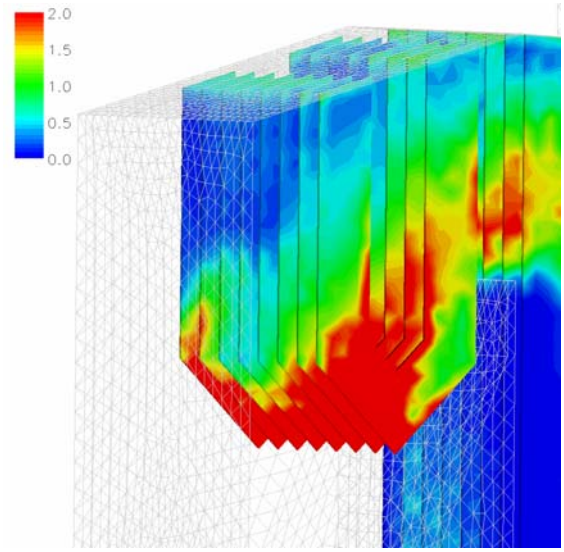

Figure 25 Close-up of the secondary super heater showing vapour deposition flux in $gm^{-2}h^{-1}$.

Compared to the two previous plots, the vapour deposition fluxes are significantly lower but most of the super heater is influenced. This mechanism is important as an initiator for subsequent capture of larger particles. The increase in heat transfer surface temperature (at the deposit surface) after 24 hours of operation is shown in **Figure 26**.

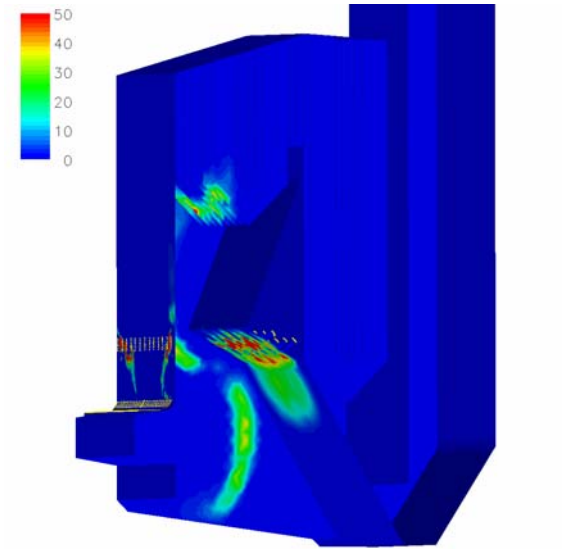

Figure 26 Heat transfer surface temperature increase after 24 hours of exposure to ash deposition.

It is seen that a 50 degrees increase in surface temperature results from the first 24 hours of exposure to ash deposition. The resulting influence on heat transfer rates in the furnace is still only minor; however, a beginning change in surface stickiness will occur as the temperature is approaching the melting temperature of the alkali dominated deposits.

To validate predicted deposit compositions qualitatively, comparison is made with deposits collected from the secondary super heater (mature deposits) and from deposition probes at Masnedø CHP plant[28]. The mature deposits all had the characteristic structure with; an inner part rich in potassium and chlorine; a middle layer dominated by potassium and chlorine but with increasing amounts of silicon and calcium; and an outer part predominantly formed from potassium, silicon and calcium. The major elements found in the layers are given in Table 2.

Table 2, Major Elements found in the Mature Deposits from the Secondary Super Heater in wt%[28].

Location/species [%wt]	Cl	S	K	Ca	Si
Full	5.6	3.8	20.9	8.1	17.1
Inner layer	34.4	2.9	47.0	1.1	1.7
Middle layer	29.4	1.6	39.5	4.9	5.5
Outer layer	0.1	1.1	16.0	11.2	26.2

There is no information about the exact location on the super heater from where the deposits were collected and the predictions show a significant variation between locations. Therefore, detailed comparison with the model predictions is not meaningful; however, some overall qualitative conclusions can still be drawn.

For the inner layer, the model predictions indicate that, in a relatively small region, Ca and Si-rich particles deposit in significant amounts. This region is characterized by a high loading of Ca and Si-rich particles (entrained from the grate) and at the same time the temperature level is sufficient for these particles to be sticky. Elsewhere on the super heater, KCl dominates the deposit. On a mass basis, about 60% of the inner layer has been predicted to consist of KCl. However, on an area basis this ratio is significantly higher.

For the outer layer, the model predictions show a reduction of the fraction of KCl to about 4-5% on a mass basis. In terms of the deposit surface, a sticking propensity of 0.5 has been assumed for these predictions. The presence of K in the outer deposit layer in the measurements reflects the reaction of K with Si and Ca in the deposit. This reaction has not been accounted for by the model.

Overall for the second case, the deposit accumulation rates have increased by a factor of 10-15 compared to those found during the formation of the inner layer. This trend, which is consistent with experimental observations, has been indicated by the time evolution of the deposited mass shown in **Figure 26**.

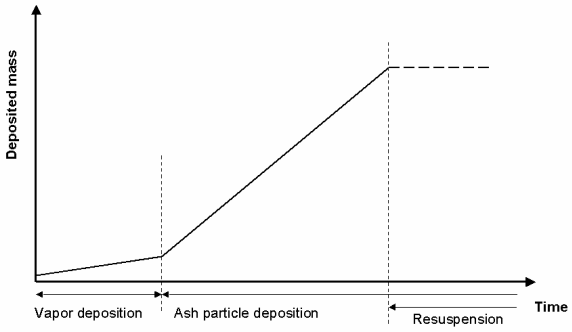

Figure 26 Illustrative trends in the deposited mass as a function of time.

Mixing pattern and operational implications. As mentioned above, the overall oxygen concentration in the stack is approximately 5 vol% (see **Figure 16**) suggesting relatively high overall excess oxygen. Based on the predictions reported here, and a number of similar boilers modelled by the authors, there are significant indications that poor mixing between the bulk flue gas flow and the air being injected through the secondary air ports result in locally reducing conditions. **Figure 27** shows predicted oxygen concentrations in a cross-section of the furnace. Dark areas represent low oxygen concentrations. Please note that the colouring was chosen to provide good resolution of low concentration regions by decreasing the maximum value to a mass fraction of 0.06.

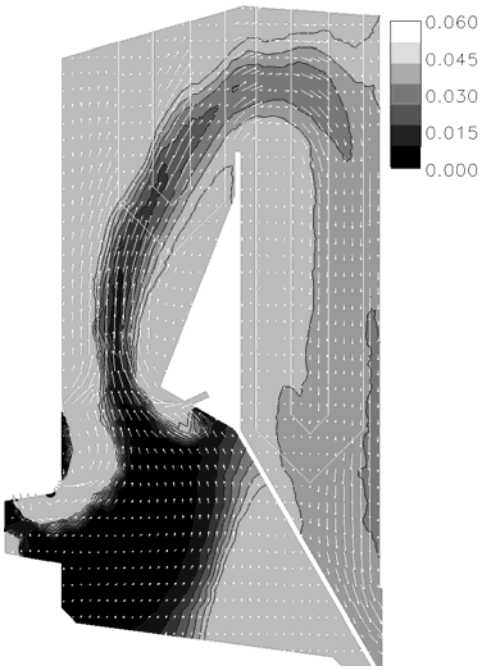

Figure 24 Contour plot illustrating the existence of a striated flow pattern with a near-zero oxygen concentration in the main flow path.

There is a clear striation of the flow with very low oxygen concentrations in the centre part of the boiler and relatively high concentrations near the walls. The low oxygen region in the centre has, at the same time, high velocities and high temperatures.

The low oxygen, high velocity and high temperature alley potentially increases problems related to ash deposition and associated corrosion of the platen super heaters. Under reducing conditions chemical equilibrium predictions show that a larger fraction of the potassium reacts with silica[27] increasing the stickiness of fly ash particles. The high gas temperature adds further to increase the particle stickiness. Due to the high gas velocity, particles deposit efficiently by inertial impaction.

In terms of corrosion risk, the reducing conditions change the most stable form of potassium from sulphates to chlorides at typical heat transfer surface temperatures. Chlorides are much more aggressive towards the boiler tubing compared to the sulphates. These concerns become more important as still more exotic fuel blends are burned to follow developments in fuel prices.

Conclusions

A numerical modelling approach to predict ash deposition and the influence on heat transfer rates in straw-fired boilers has been developed and demonstrated. The model was implemented in the commercial CFD programme FLUENT™. Using a Danish straw-fired boiler as test case, the model was found to correctly predict operational trends observed at the facility. In the future, a significant effort will be put into further improvements and validation of the modelling concept. Planned extensions include the ability to handle co-firing conditions, and inclusion of the model to predict radiative properties.

Acknowledgement. This work was funded by the Danish Energy Research Programme, the Danish Public Service Obligations programme, ELSAM A/S and Babcock & Wilcox Vølund Aps.

References

(1) Richards, G., Slater, P. and Harb, J. (1993) "Simulation of ash deposit growth in a pulverized coal-fired pilot scale reactor", Energy & Fuels, 7, 774-781.
(2) Baxter, L. (1993) "Ash deposition during biomass and coal combustion: A mechanistic approach", Biomass and Bioenergy, 4 (2), 85-102.
(3) Pyykönen, J. and Jokiniemi, J. (1997) "Development of a prediction scheme for pulverized coal-fired boiler slagging", The Engineering Foundation Conference on: Impact of mineral impurities in solid fuel combustion, November 2-7, Kona, Hawaii.
(4) Wang, H., Harb, J. (1997) "Modeling of ash deposition in large-scale combustion facilities burning pulverized coal", Progress in Energy and Combustion Science, 23, 267-282.
(5) Hecken, M., Reichelt, L. and Renz, U. (1999) "Numerical simulation of slagging films in the pressurized coal combustion facility Aachen", Proceedings of the 4th International Symposium on Coal Combustion, Peking.
(6) Lee, F., Lockwood, F. (1999) "Modelling ash deposition in pulverized coal-fired applications", Progress in Energy and Combustion Science, 25, 117, 132.
(7) Kær, S. K. (2001) "Numerical investigation of deposit formation in straw-fired boilers", Ph.D. Thesis, Institute of Energy Technology, Aalborg University, Denmark.
(8) Baxter, L. et al. (1998) "The behavior of inorganic material in biomass-fired power boilers: field and laboratory experiences", Fuel Processing Technology, 54, 47-78.
(9) Jensen, P., Sander, B., Dam-Johansen, K. (1999) "Release of potassium and chlorine during straw pyrolysis", In Overend, R. and Chornet, E. (Eds.), Proceedings of the Fourth biomass conference of the Americas, Pergamon, 1169-1175.
(10) Wornat, M. et al. (1995) "Structural and compositional transformations of biomass during combustion", Combustion and Flame, 100, 131-143.
(11) Frandsen, F., Hansen, L., Sørensen, L., Hjuler, K. (1998) "Characterisation of ashes from biofuels",Final report EFP-95, The Danish Energy Research Programme, ISBN 87-7782-000-2.
(12) Shuen, J.-S., Chen, L.-D., Faeth, G. (1983) "Evaluation of stochastical model of particle dispersion in turbulent round jet", AIChE Journal, 29 (1), 167-170.
(13) McLaughlin, J. (1989) "Aerosol particle deposition in numerically simulated channel flow", Physics of Fluids A, 1 (7), 1211-1224.
(14) Brooke, J.W., Kontomaris, K., Hanratty, T.J. and McLaughlin, J.B. (1989) "Turbulent deposition and trapping of aerosols at a wall", Physics of Fluids A, 4 (4), 825-834.
(15) Kaftori, D., Hetsroni, G. and Banerjee, S. (1995) "Particle behavior in the turbulent boundary layer. I. Motion, deposition, and entrainment", Physics of Fluids, 7 (5), 1095-1106.

(16) Owen, P. (1969) “Pneumatic Transport”, Journal of Fluid Mechanics, 39, 407-432.
(17) Fan, F.G. and Ahmadi, G. (1993) “A sublayer model for turbulent deposition of particles in vertical ducts with smooth and rough surfaces”, Journal of Aerosol Science, 24, 45-64.
(18) Cameron, J.H., Goerg-Wood, K. (1999) “Role of thermophoresis in the deposition of fume particles resulting from the combustion of high inorganic containing fuels with reference to kraft black liquor”, Fuel Proc. Tech., 60, 49-68.
(19) He, C. and Ahmadi, G. (1998) “Particle deposition with thermophoresis in laminar and turbulent duct flows”, Aerosol Science and Technology, 29 (6), 525-546.
(20) Rosner, D. and Tandon, P. (1995) “Rational prediction of inertially induced particle deposition rates for a cylindrical target in a dust-laden stream”, Chem. Eng. Science, 50 (21), 3409-3431.
(21) Walsh, P. et al. (1990) “Deposition of bituminous coal ash on an isolated heat exchanger tube: Effect of coal properties on deposit growth”, Progress in Energy and Combustion Science, 16, 327-346.
(22) Jensen, P., Stenholm, M. and Hald, P. (1997) “Deposition investigation in straw-fired boilers”, Energy & Fuels, 11, 1048-1055.
(23) Rosner, D., Nagarajan, R. (1987) “Towards a mechanistic theory of net deposit growth from ash-laden flowing combustion gases: self-regulated sticking of impacting particles and deposit erosion in the presence of vapor deposited - or submicron mist - 'glue'”, AIChE Symposium Series, 289-296, Heat Transfer - Pittsburg 1987.
(24) Ross, J., Anderson, R., Nagarajan, R. (1988) “Effect of sodium on deposition in a simulated combustion gas turbine environment”, Energy & Fuels, 2 (3), 282-289.
(25) Nagarajan, R., Anderson, R. (1988) “Effect of coal constituents on the liquid-assisted capture of impacting ash particles in direct coal-fired gas turbines”, The Gas Turbine and Aeroengine Congress, Volume 88-GT-192, Amsterdam, The Netherlands, ASME.
(26) Hansen, L. (1998, March) “Melting and sintering of ashes”, Ph.D. Thesis, Department of Chemical Engineering, DTU, Denmark.
(27) Nielsen, H. P. (1998, November) “Deposition and high-temperature corrosion in biomass-fired boilers”, Ph.D. Thesis, Department of Chemical Engineering, DTU, Denmark.
(28) Hansen, L. et al. (2000) “Influence of deposit formation on corrosion at a straw-fired boiler”, Fuel Processing Technology, 64, 189-200.
(29) Robinson, A., Buckley, S., Yang, N., Baxter, L. (2000) “Experimental measurements of the thermal conductivity of ash deposits: Part 2. Effects of sintering and deposit microstructure”, Technical Report SAND2000-8600, Sandia National Laboratories.
(30) Rezaei, H. et al. (2000) “Thermal conductivity of coal ash and slags and models used”, Fuel, 79, 1697-1710.
(31) Hapke, B. (1993). “Theory of reflectance and emittance spectroscopy”, Cambridge University Press
(32) Siegel, R. and Howell, J. R., (2001), Thermal Radiation Heat Transfer, 4th ed., Taylor and Francis-Hemisphere, Washington.
(33) van der Lans, R. (1999) “Gas concentrations and temperature measurements during straw and biomass co-firing in the grate furnace of Masnedø combined heat and power plant”, CHEC report 9914, Department of Chemical Engineering, Danish Technical University, Denmark.

Modeling Fireside Slag Formation and Deposition in Tangentially-Coal-Fired Boilers

Edmundo Vásquez
Alliant Energy Corporate Services
744 Heartland Trail
Madison, WI 53717-1934

Zhanhua Ma
RMT Incorporated
744 Heartland Trail
Madison, WI 53717-1934

Steven A. Benson, Donald P.McCollor, Robert Jensen, Li Yan, A.S.M. Rokanuzzaman, and Lingbu Kong
Energy & Environmental Research Center
University of North Dakota
P.O. Box 9018
Grand Forks, ND 58202-9018

Introduction

Fireside ash deposition is a major problem that impacts the efficiency and operability of coal-fired utility boiler. The ash deposition problem is dependent on fuel composition, boiler design, and operating conditions. In general many of the chemical and physical processes involved in ash formation and deposition are understood and this understanding has assisted many utilities in minimizing ash deposition problems in utility boilers. Many of these processes have been formulated into computer codes. For example, computer codes exist to predict the particle-size and composition distribution (PSCD) of the ash produced upon combustion (1) and simplified transport deposition and growth programs for specific locations in the boiler (2). However, no integration of these programs with boiler models to predict the effects of deposit growth on heat transfer has occurred.

The advances made over the past several years in predicting ash behavior have been made possible as a result of more detailed and better analysis of coal and ash materials. These advanced techniques, such as computer-controlled scanning electron microscopy (CCSEM), are able to quantitatively determine the chemical and physical characteristics of the inorganic components in coal and ash (fly ash and deposits) on a microscopic scale (3). Many of the mechanisms of ash formation, ash deposition, and ash collection in combustion systems are more clearly understood as a result of these new data. This understanding has led to the development of better methods of prediction that include advanced indices and phenomenological models.

Advanced indices programs provide coal ranking with respect to a coals potential to cause deposition in various sections of the boiler such as the waterwalls and high-temperature and low- temperature convective pass. The index is based on advanced methods of analysis, detailed understanding of key processes that influence fouling, and full-scale performance data (4).

Phenomenological or mechanistic models have been developed and are being used to predict the effects of ash-forming constituents as a function of coal composition, combustion conditions, systems geometry, and operating conditions. ATRAN is a model that has been developed to predict the PSCD of ash produced in utility boilers. The results achieved with this model have been verified with full-scale experience for both pulverized coal (pc) and cyclone-fired boilers with a favorable outcome. ATRAN is a vital part of other methods used to predict the effects of ash species, since the PSCD is needed to predict ash deposition (5).

Recently work has been conducted to integrate the predictive methods and incorporate them into a computational fluid dynamics code. The results presented here will illustrate the ability of the model to predict upper wall slagging in a tangentially fired boiler utilizing. Black Thunder, a Powder River Basin coal.

Computational Fluid Dynamics

SmartBurn® uses numerical simulations of processes to compare design and operational alternatives and to identify the underlying limitations of boiler performance. Once these limitations are identified, a cause and effect relationship can be established and a more complete understanding of the combustion process is obtained. The tool of choice for performing such an investigation for pulverized coal combustion in an enclosed fluid atmosphere is computational fluid dynamics (CFD). This type of numerical simulation resolves the Navier-Stokes equations and incorporates several numerical schemes for fluid flow, heat transfer, turbulence, and chemistry within the given geometry and for a set of operating conditions and, most importantly, solves the coupled solution of these equations.

Coal particles are simulated with the Discrete Phase Model (DPM) in a two way coupled solution utilizing stochastic tracking for turbulence interaction in a Lagrangian reference frame. The DPM model is defined to simulate the moisture evaporation, de-volatilization, and char burnout of the coal particles. Seven chemical species are solved for the gas phase in which the Magnussen-Hjertajer turbulence-chemistry interaction model is employed. Radiation is modeled using the Discrete Ordinate (DO) model, which provides for particle radiation interaction.

A CFD model was built for Columbia Unit 1 (6,7) a tangentially fired 1975-vintage 512 MW boiler. Columbia Unit 1 was one of the first-generation T-fired units designed to burn PRB coal and therefore has a small firebox with a high heat release. The output of the CFD model provides the basic information used in the ash behavior model.

Results and Discussion

A diagram of the boiler modeled is illustrated in Figure 1 (7). The portion of the boiler that will be used to illustrate the ability of the model to predict performance is the upper wall section above the burner level. The ash impaction rates are shown in Figure 2.

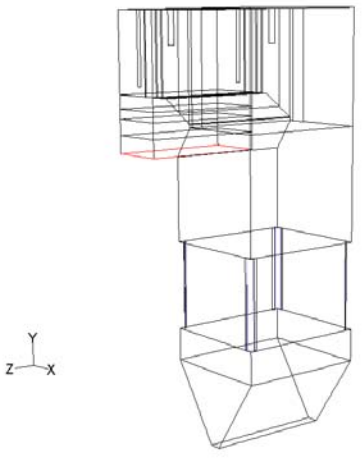

Figure 1. Schematic diagram of tangentially-fired boiler.

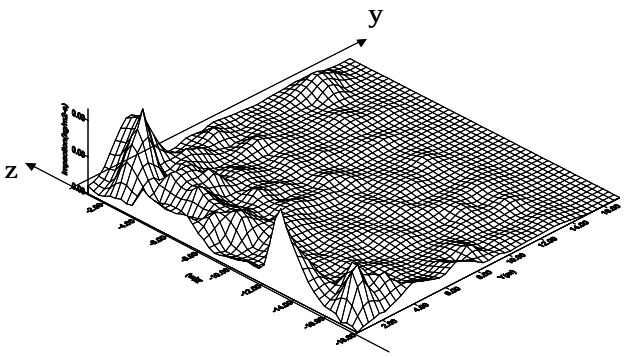

Figure 2. Ash Particle Impaction Rate Distribution on Furnace Upper-Front Wall

Currently work is being conducted to validate the model. Figure 3 shows the heat flux measurements made at several locations on the upper wall panel that is being modeled. Figure 4 shows the results from the model.

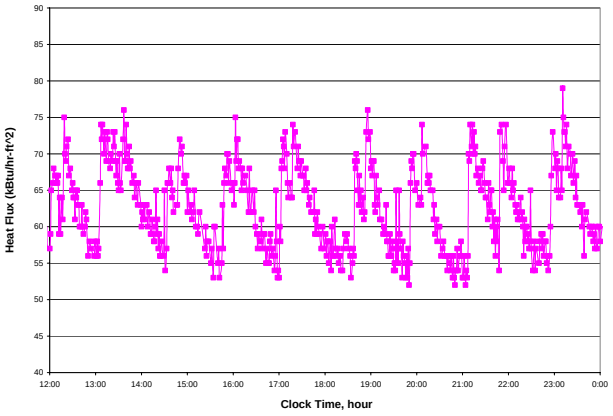

Figure 3. Measured Heat flux at the full scale utility on the wall panel is illustrated in Figure 2.

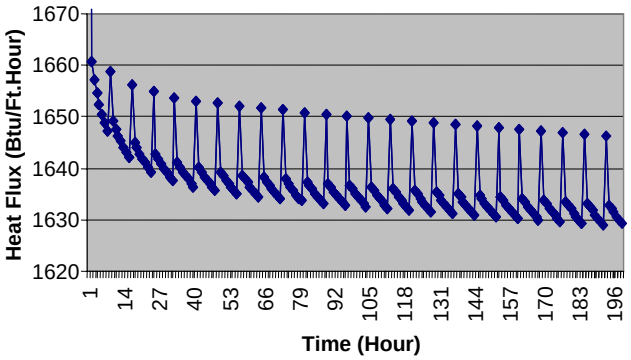

Figure 4. Predicted heat flux based on fuel quality, boiler design, and operating conditions.

Currently the modeling efforts show promise in being a very valuable tool to predict plant performance.

Conclusions

The resulting integration of CFD simulations with predictive methods for ash behavior in tangentially coal-fired boilers, provide a quantitative and qualitative description of the fireside slag formation and deposition processes within the furnace. As a result, the method permits the determination of the deposit thickness; chemical composition; physical properties and heat transfer properties. The utilization of this procedure to different types of boilers, fuel types and operating conditions is in progress.

References

1. Benson, S.A.; Steadman, E.N.; Zygarlicke, C.J.; Erickson, T.A. Ash Formation, Deposition, Corrosion, and Erosion in Conventional Boilers. In Applications of Advanced Technology to Ash-Related Problems in Boilers; Baxter, L.; DeSollar, R., Eds.; Plenum Press: New York, 1996; pp 1-15.
2. Benson, S.A.; Sondreal, E.A. Impact of Low-Rank Coal Properties on Advanced Power Systems. In Ash Chemistry: Phase Relationships in Ashes, Special Issue of Fuel Process. Technol. 1998, 56 (1-2), 129-142.
3. Steadman, E.N.; Zygarlicke, C.J.; Benson, S.A.; Jones, M.L. A Micro analytical Approach to the Characterization of Coal, Ash, and Deposits. In Seminar on Fireside Fouling Problems; ASME Research Comm. on Corrosion & Deposits from Combustion Gases: Washington, DC, 1990.
4. Zygarlicke, C.J. Predicting Ash Behavior in Conventional and Advanced Power Systems: Putting Models to Work. In Impact of Mineral Impurities in Solid Fuel Combustion; Gupta, R. .Ed.; Kluwer Academic/Plenum Publishers: New York, 1999; pp 709-722.
5. Yan, L., Jensen, R.R., Laumb, J.D. and Benson, S.A. Predicting Ash Particle Size and Composition Distribution From Coal Biomass Cofiring, Proceedings of Engineering Foundation Conference, Production in the 21st Century: Impacts of Fuel Quality and Operations, October 28 November 2, 2001, Snowbird, Utah.
6. Vásquez, E; Sears, R., Combustion Control Techniques achieve 0.15 lbs/MMBtu NO_x levels without SCR, Power Engineering, Vol 107, No 1, 39-42, January 2003.
7. Vásquez, E.; Mara, F.; Maas, D.J.; Ma Z.; McQuistan, K.; Gadalla, H.; Iman, F. Application of SmartBurn^{SM} Technology for NO_x Control in Tangentially Fired Coal Boilers, PowerGen International, December 9-11, 2003, Las Vegas, Nevada USA

EVOLUTION OF FLAME-BORNE MINERAL MATTER IN A 350 MW_e PULVERISED COAL-FIRED BOILER

Glenn P. Devir[a]
Co-operative Research Centre for Coal in Sustainable Development
School of Chemical Engineering
University of Queensland
Sir Fred Schonell Drive
St Lucia QLD 4072 AUSTRALIA

John H. Pohl
Alexandria Research Institute
Department of Mechanical Engineering
Virginia Tech
Suite 400, 206 N. Washington St
Alexandria VA 22314

Introduction

The mineral matter present in burning pulverised coal particles will experience rapid, high temperature transformations in the gas path of a utility boiler. These inorganic combustion residues may remain inert, melt, spheroidise, coalesce, vesiculate, fragment, freeze, crystallise, vapourise, and/or condense during transport from the bulk gas phase, across the cooler boundary layer, to heat transfer surfaces. The evolution of such flame-borne mineral matter will be dependent upon the size, composition and time-temperature history of each mineral inclusion in the parent coal particle.

The local gas environment is likely to be reducing for flame-transformed mineral matter on or beneath the surface of receding char particles. Conversely, mineral particles which have been liberated from the coal substance during milling will experience oxidising conditions in the gas path of a boiler, as will flame-transformed mineral matter which is released from the char during char burnout.

The evolution of flame-borne mineral matter during pulverised coal combustion is being studied as part of an investigation into the mechanisms of slagging in a 350 MW_e opposed-fired boiler. The observed transformation phenomena of mineral matter in the gas phase are described in terms of classical sintering theory. Possible explanations for the observed absence of various transformation phenomena are also proposed. It is hoped that the interpretation accompanying the images presented in this paper will contribute to a qualitative understanding of particulate transformations in pulverised coal-fired boilers. This paper concludes by identifying future research directions to hopefully resolve the uncertainties of such transformations.

Methodology

The mineralogy of the sub-bituminous coals fired in this minemouth power station typically consist of 60-70% kaolinite ($4SiO_2.2Al_2O_3.4H_2O$), 10-20% siderite ($FeCO_3$) and 5-15% quartz (SiO_2), with minor quantities (<2%) of other minerals present. The mineral matter transformations occurring in the hottest region of the furnace are assessed by using a water-cooled probe to quench and withdraw particulates through a port eight metres above the top row of burners. Particles are examined under the scanning electron microscope (SEM) to ascertain probable physical and chemical transformation mechanisms.

[a] Present address (and to where all correspondence should be addressed): Process Engineer, HRL Technology, 1 Acirl St, Riverview QLD 4303, AUSTRALIA, gdevir@acirl.com.au

Results and Discussion

The most predominant type of particle sampled was glassy sub-micron non-porous aluminosilicates. However, considerable evidence was found to support the notion that kaolinite-derived particles coalesced to various degrees with other kaolinite-derived particles.

An approximate solution for the rate of surface tension driven coalescence of two spheres with single point contact was first proposed by Frenkel[1]. The rate of neck growth, relative to the instantaneous radius a of one of the growing spheres, was shown to be proportional to $(\gamma)^{-}$, and inversely proportional to $(a\eta)^{-}$, where γ and η are the surface tension and viscosity of the coalescing species. However, this approach, and many subsequent attempts to model coalescence, both empirically and theoretically, have been based on non-porous particles of like composition.

The time required for pore closure in a viscous body due to capillary forces was shown by Frenkel[1] to be proportional to $a_o\eta$ and inversely proportional to γ, where a_o is the initial pore radius. A kaolinite-derived particle in the furnace of a boiler may possess[2] a pore-free viscosity of 10 Pa.s and a surface tension of 0.4 Nm^{-1}. For a 5 μm initial pore radius, the time required for pore closure would therefore be anticipated to be less than one millisecond. However, it is evident from Figures 1 to 3 that pore closure is not complete in the residence time of the furnace, which is likely to be somewhere in the order of one second.

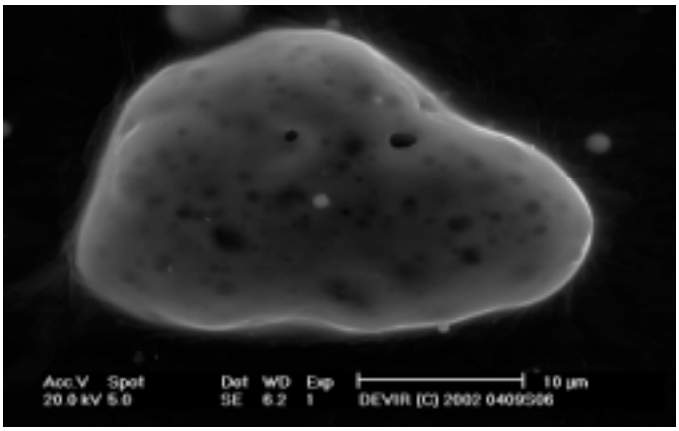

Figure 1. Partial coalescence of several large kaolinite-derived particles. Secondary electron image.

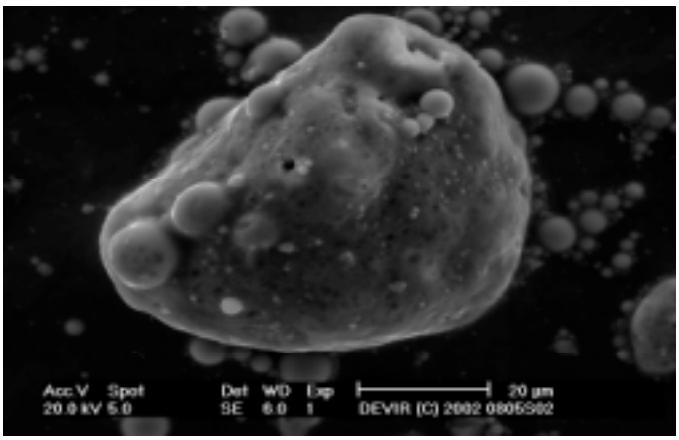

Figure 2. Partial coalescence of many various-sized kaolinite-derived particles. Secondary electron image.

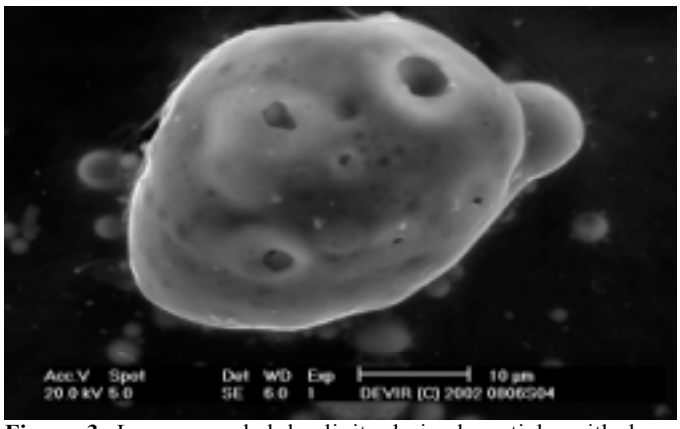

Figure 3. Large rounded kaolinite-derived particle with large pores. Secondary electron image.

The interfaces of real coalescing fluids possess complex rheological properties, and may exhibit viscous, viscoelastic or even elastic behaviour, with both spatial and temporal variations[3]. It is apparent from these images that the kinetics of pore closure in flame-borne kaolinite-derived particles are somewhat slower than that predicted by viscous sintering theory. The retardation of pore closure may explain the incomplete coalescence of large kaolinite-derived particles in the furnace, as evidenced in Figures 1 to 3.

The presence of pores may either increase or decrease the effective viscosity, depending upon the pore morphology. Spherical pores are thought to decrease the effective viscosity, due to the much lower viscosity of the gas phase. Non-spherical pores, however, may increase the effective viscosity of the particle due to their higher resistance to shearing stress, and hence viscous flow.

Many large irregularly-shaped, slightly rounded particles were observed, with varying degrees of surface porosity. Qualitative analysis of various points on each particle was performed using energy dispersive x-ray analysis (EDXRA). It was found that spot compositions ranged from almost pure silica (SiO_2) to the composition of metakaolinite ($4SiO_2.2Al_2O_3$), with regions of low surface porosity corresponding to high silica point concentrations. It was concluded that kaolinite-derived particles had wet the inert surface of large quartz particles, forming a molten porous layer. Figure 4 shows one of these particles.

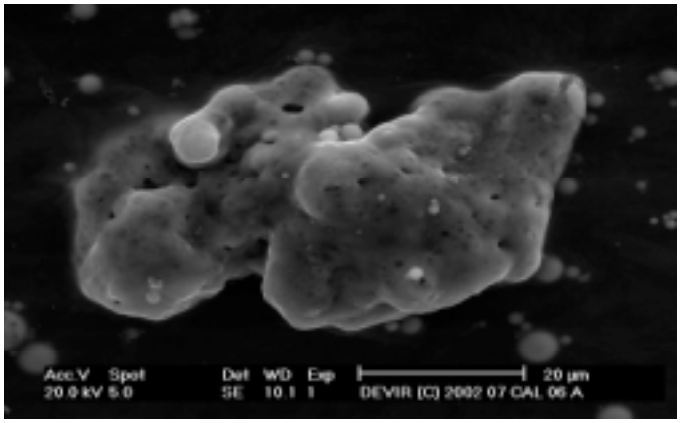

Figure 4. Wetting of inert quartz particle by mobile porous aluminosilicate layer. Secondary electron image.

There was no conclusive evidence to ascertain the primary transformation mechanism of siderite-derived ('FeO_n') particles in the boiler furnace. Iron oxide particles were predominantly less than 1 μm in diameter, suggesting that fragmentation may have been a dominant mechanism. Raask[4] documented the fragmentation of siderite-derived particles into sub-micron particulates, and attributed this phenomenon to the rapid evolution of carbon dioxide from a low viscosity liquid. Iron oxide particles between 5 and 10 μm were rarely observed, suggesting that coalescence of siderite-derived particles was not likely.

There was no evidence found to support the idea that kaolinite-derived particles coalesced with siderite-derived particles to form low melting temperature aluminosilicate particles. Sintering literature suggests that a broad range of responses are possible in mixed powder systems, depending upon the physical and chemical properties of each component[5]. Sintering and coalescence will occur readily where there is intersolubility between the mixed powders, thereby allowing chemical potential gradients to dominate the surface energy driving force for viscous flow. However, resistance to coalescence will occur when at least one of the species possesses a low solubility in the other, or indeed if one or more species is very porous.

SEM images of cross-sectioned boiler deposits suggest that siderite-derived particles are very soluble in aluminosilicate regions, but not vice versa[6]. This observation may provide a qualitative explanation as to why coalescence is observed in some coal mineralogical systems and not others.

Conclusions

This paper examined the evolution of flame-borne mineral matter during the combustion of sub-bituminous coals in a 350 MW_e pulverised coal-fired boiler. The observed transformation phenomena were documented and described in terms of viscous sintering theory. It was concluded that the thermodynamic data currently available in the literature to help describe the high temperature mineral matter transformations occurring in coal combustion is inadequate. This data is largely restricted to compositions and temperatures of interest to metallurgists and ceramists, and therefore is of limited use to combustion engineers. It is recommended that a database of thermodynamic properties (e.g., viscosity of solid-liquid and liquid-gas mixtures, solubility, diffusivity, activity coefficients, etc.) be generated for slag compositions and temperatures of interest to combustion engineers. The high temperature transformations of mineral matter occurring in the gas phase of the boiler may then be better understood.

Acknowledgements The authors gratefully acknowledge the interest and co-operation shown by Dr Chris Spero and Mr Adrian Hughes of CS Energy. We also wish to acknowledge the financial assistance provided by the Co-operative Research Centre for Coal in Sustainable Development, which is funded in part by the CRC Programme of the Commonwealth Government of Australia.

References

(1) Frenkel, J. *J. Phys.*, **1945**, *9* (5), 385.
(2) Verein Deustcher Eisenhüttenleute, *Slag Atlas*, 2nd Edition, Verlag Stahleisen GmbH, Dusseldorf, Germany, 1995
(3) Hiram, Y and Nir, A. *J. Coll. Int. Sc*. **1983**, *95 (2)*, 462.
(4) Raask, E. *Mineral Impurities in Coal Combustion – Behaviour, Problems and Remedial Measures*, Hemisphere Publishing Corporation, Washington, D.C., USA, 1985
(5) German, R. M. *Sintering Theory and Practice*, John Wiley & Sons, Inc., New York, NY, USA, 1996
(6) Devir, G.P. *Ph. D. Thesis in Progress*, University of Queensland, St Lucia, QLD, Australia, 2004

PREDICTION OF PHASE EQUILIBRIA AND VISCOSITY IN COMPLEX COAL ASH SLAG SYSTEMS

*E.Jak, *D.Saulov, **A.Kondratiev, and **P.C.Hayes

*Centre for Coal in Sustainable Development (CCSD),
** Pyrometallurgy Research Centre, School of Engineering,
The University of Queensland, Brisbane, QLD, 4072, Australia
http://pyrosearch.minmet.uq.edu.au; E.Jak@minmet.uq.edu.au

Abstract

Significant improvements in predictive capabilities in relation to the melting behaviour of the mineral matter in coal have been achieved through the use of i) thermodynamic modelling of phase equilibria, and ii) viscosity modelling studies.

The thermodynamic modelling has been carried out using the computer system FactSage, which is used for the calculation of multi-phase slag / solid / gas / matte / alloy / salt equilibria in multi-component systems of industrial interest. A modified quasi-chemical solution model is used for the liquid slag phase. New model optimisations have been carried out, which have significantly improved the accuracy of the thermodynamic models for coal combustion processes. The database for the Al-Ca-Fe-O-Si system has recently been extended to characterise effects of Mg, K and Na. Viscosity modelling, using a modified Urbain formalism, is carried out in conjunction with FactSage calculations to predict the viscosities of fully liquid as well as heterogeneous, partly crystallised slags.

The solution of a range of problems in coal utilisation technologies, including ash slag flow in slagging gasifiers, deposit formation, slagging, fouling, fusibility tests, fluxing, blending etc related to the melting behaviour of the mineral matter in the coal can be obtained with the assistance of the new models.

Introduction

Many coal companies and electrical power utilities are faced with difficult technical issues associated with the melting and flow behaviour of coal mineral matter. A range of problems in coal utilisation technologies, including ash slag flow in slagging gasifiers, deposit formation, slagging, fouling, fusibility tests, fluxing, blending etc, are related to the melting behaviour of the mineral matter in the coal. The wide ranges of coal mineralogies, ash compositions and process conditions experienced in the various parts of each reactor and in different coal utilisation technologies highlight the need for powerful tools to predict the behaviour of the mineral matter. Fundamental knowledge of the melting and flow behaviour of coal mineral matter/flux mixtures can greatly assist in the design and operation of these power generation technologies.

The prediction of phase equilibria and viscosities of the coal ash following combustion is a longstanding problem for users of various coal-based power generation technologies. The empirical "ash fusion tests", such as the cone deformation tests, thermo-mechanical tests (e.g. TMA) and empirical slagging indices are widely used to estimate and compare the relative behaviours of coal ashes. Recent scientific approaches to the prediction of these properties are, however, starting to produce results that will have a significant impact on the industry. Improvements in chemical thermodynamic and viscosity models of oxide systems, the development of computational methods, computer software and hardware now make it possible to predict the phase equilibrium and flow behaviour in complex multi-component coal ash slag systems. The purpose of this paper is to demonstrate how the latest advances in chemical thermodynamic and viscosity modelling can be used to characterise the melting and flow behaviour of mineral matter present in coal combustion systems.

Development of modelling tools

FactSage Database. One of the predictive tools used successfully in coal ash applications is the computer package FactSage[1]. FactSage is used worldwide in various industries to predict chemical equilibria, the proportions of liquid and solid phases as a function of temperature, composition and atmospheric conditions. One of the strengths of FactSage is its ability to describe the melting behaviour of the oxide systems, commonly referred to as slags. Accurate and reliable prediction, however, requires the development of a thermodynamic database with model parameters for all possible liquid and solid phases.

A new thermodynamic database of the system Al-Ca-Fe-O-Si has been completed by researchers at the Pyrometallurgy Research Centre (PYROSEARCH), The University of Queensland, in collaboration with the Centre for Research in Computational Thermochemistry, Polytechnique de Montreal, Canada[2]. This database has recently been extended to characterise effects of Mg, K and Na on liquidus temperatures[3-4]. The new thermodynamic database incorporates the latest experimental data and more advanced thermodynamic models of the oxide phases. The new database is the result of the systematic thermodynamic optimisation of the multi-component systems, and it provides improved accuracy and reliability in the description of phase equilibria in the coal ash system.

Viscosity Model. A new slag viscosity model for the system Al_2O_3-CaO-'FeO'-SiO_2 used in conjunction with FactSage has recently been completed by the present authors[5-7]. The model enables the viscosities of homogeneous (completely molten) liquid slag systems as well as heterogeneous (partially crystallised) slag systems, to be predicted as a function of the bulk slag composition and operating temperature over the complete range of conditions at metallic iron saturation. FactSage is used to calculate the proportions of solids and the composition of the remaining liquid in the partly crystallised slag systems. The original Urbain formalism[8-11] has been modified to make viscosity predictions possible over the whole composition and temperature ranges. This was achieved by taking into account the different contributions of various oxides (in this particular case, CaO and FeO) on the viscosity of the slag[6]. The model parameters for the individual oxides have been derived from critically reviewed experimental data. The Roscoe equation[12], with parameters obtained by fitting model predictions into experimental points by Hurst[13-15], is used to characterise the "slurry" effect in partly crystallised slag. Examples of the application of the new viscosity model have been reported in the literature[5-7].

Table 1. Comparison of Different Viscosity Models Using the Mills' Parameter

System	Modified Urbain model[5-7]	Watt-Fereday model[17]	T-shift model[18]	Kalmanovich-Frank model[19]
SiO_2	19.1	99.9	N/A	99.9
Al_2O_3-SiO_2	30.1	66.9	N/A	41.5
CaO-SiO_2	10.9	84.3	40.3	24.3
'FeO'-SiO_2	8.1	213.8	378.1	717.6
Al_2O_3-CaO-SiO_2	31.2	49.5	49.2	24.6
CaO-'FeO'-SiO_2	9.9	115.4	339.8	594.4
Al_2O_3-CaO-'FeO'-SiO_2	29.2	96.0	94.0	169.6

The agreement between experimental data and model predictions was evaluated using the parameter proposed by Mills et al.[16]: $\Delta = \frac{1}{N}\sum^{N}\left|\frac{(\eta_n)_{calc} - (\eta_n)_{ex}}{(\eta_n)_{ex}}\right|$, where N is a number of points and n is a particular slag system, the subscripts *calc* and *ex* refer to the calculated and experimental viscosities at a given composition and process condition. Table 1 shows the comparison of the viscosity models[5-7,17-19] for a number of chemical systems.

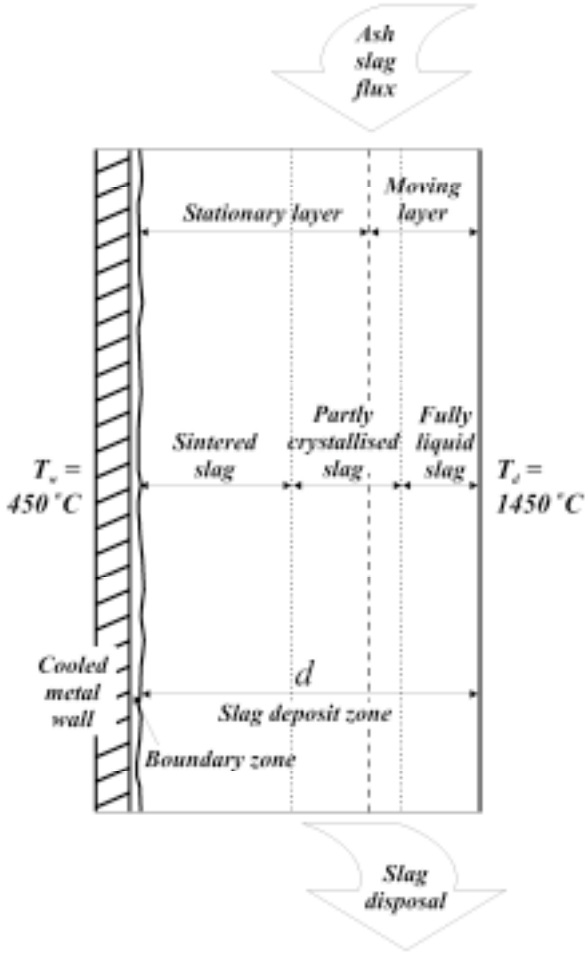

Figure 1. Schematic of the flowing slag deposit.

Applications of the models to entrained flow coal gasification systems

A number of examples of the application of the FactSage computer package and viscosity models to coal ash related problems by the authors can be found in recent scientific literature[2,3,5,20-25]. Increasing attention is being given to the development of entrained flow coal (slagging) gasifiers since they offer potential advantages in terms of improved energy efficiencies and environmental outcomes. A key factor in the operation of these technologies is the flow properties of the slags; these properties are principally dependent on

- liquid composition,
- proportion of liquid,
- proportion of solids,
- oxygen partial pressure, and
- temperature.

These in turn can be controlled or varied in the process by adjustments to

- coal blending,
- flux addition and
- gasifier temperature and operating oxygen partial pressure.

Depending on the gasifier type, the limiting requirements for slag viscosity and temperature can vary from 5 to 25 Pa.s and from 1100^{O}C to 1500^{O}C, respectively[26-28]. These requirements are usually determined empirically by the tappability of the slag in a gasifier. Exact specifications should be identified by individual power generation utilities. Provided the slag can flow from the reactor, and can also fulfil any requirements, such as the incorporation of other minor elements, then it is possible to operate at sub-liquidus conditions.

Using the new thermodynamic and viscosity models described above it is now possible to predict the stability of the liquid slag and solid crystalline phases as well as the viscosity of the liquid slag for the complex coal ash slag systems. This is illustrated in the present paper with analysis of the use of two coals A and B (see Table 2) in a slagging gasifier.

Table 2. Compositions of the Coal Ash Slags (wt pct)

#	Al_2O_3	CaO	'FeO'	SiO_2
Ash A	25.44	27.53	12.50	34.53
Ash B	30.51	25.87	6.26	37.36

One of the common problems in coal gasification is the formation of slag deposit on the walls of a slagging gasifier; these deposits affect the overall heat balance, temperature of the out-gases and tappability of slag (i.e. ability of slag to flow freely from a gasifier)[26,29-30]. The following example shows the application of the thermodynamic and viscosity models developed in the Pyrosearch Centre to the problem of deposit formation in the slagging zone of a gasifier.

A typical section of flowing slag deposit on a reactor wall in the slagging zone[29] is shown in Figure 1. The temperature of the slag at the water-cooled wall of a gasifier T_w is taken ~450^{o}C, while temperature of the slag surface T_d is ~1450^{o}C. The temperature gradient across the slag deposit leads to the formation of different sub-layers across the deposit: 1) a stationary layer of sintered slag (glass and crystalline phases) and partly crystallised slag with high proportion of solids, and 2) a moving layer, which also contains partly liquid slag but with lower percentage of solids, and fully liquid slag. Assuming the linear temperature profile across the slag layer, the proportion of solids across the layer was calculated by FactSage[1] with the new thermodynamic database[4]. The slurry viscosity was predicted by the model developed in PyroSearch Centre[5-7]. Using the Navier-Stokes equation for steady-state, laminar flow of a slag layer of constant thickness under gravity force the slag velocity across the layer was predicted. Thickness of the deposit layer was then calculated from mass balance and geometry of a gasifier. The examples of these calculations for two different coal ash slags (marked Ash A and Ash B) are shown in Figure 2.

Figure 3 shows the thickness of the deposit layer for coal ash slags A and B as a function of the temperature of slag surface determined by the temperature of the reaction zone. It can be seen that ash A has wider operational range of temperatures than ash B.

The conditions of the operations always fluctuate. The analysis of the effects of different factors on crystallisation and viscous flow behaviour therefore is important. Figures 4 through 6 give detailed analysis of the effects of temperature, atmospheric conditions(reducing / oxidising) and composition changes on proportions of liquid and solid phases and on viscosities of the slags corresponding to coals A and B.

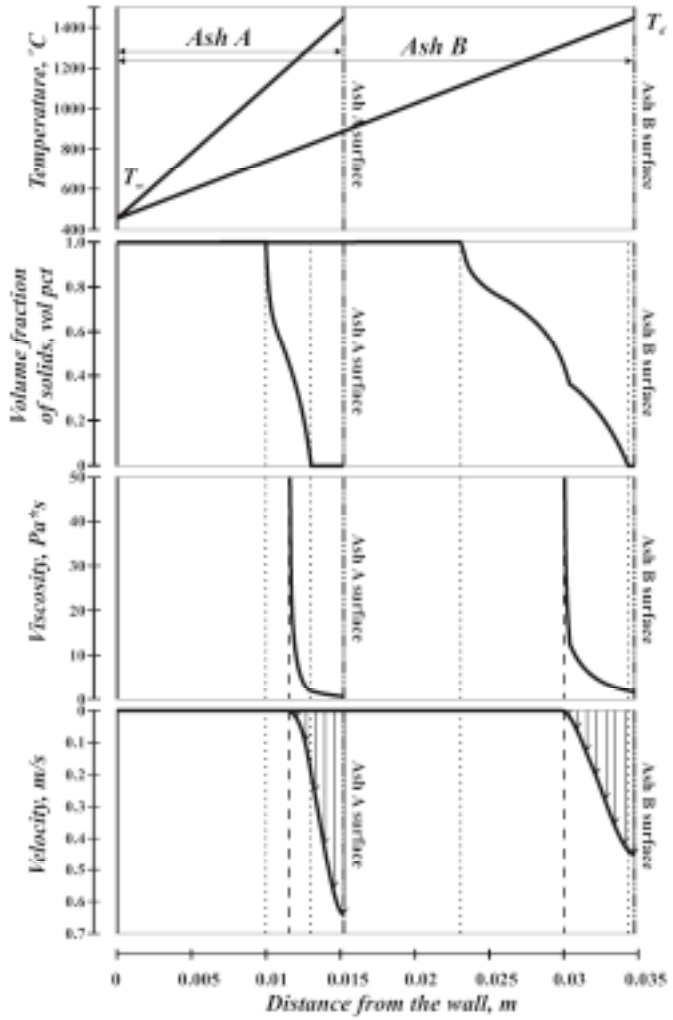

Figure 2. Temperature, proportions of solids, viscosity and slag flow velocity profiles predicted with new models for coals A and B.

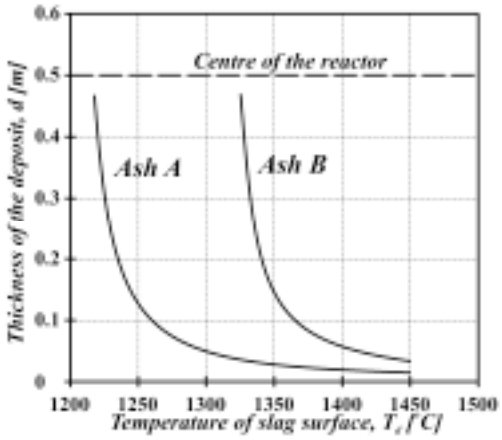

Figure 3. Thickness of the deposit as a function of temperature of the slag surface for coals A and B.

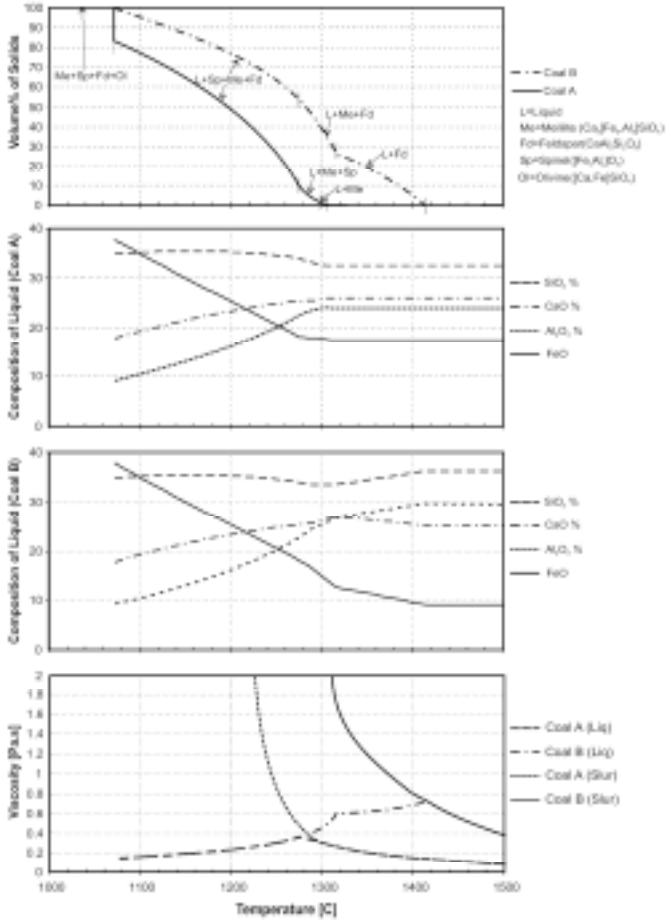

Figure 4. Crystallisation characteristics and viscosities of the coals A and B at metallic iron saturation as a function of temperature.

Conclusions

Using new chemical thermodynamic and viscosity models it is now possible to predict the behaviour of complex slag systems relevant to coal utilisation technologies. Properties such as phase equilibria, liquidus temperatures and viscosities of single and multiphase slags can be systematically analysed as functions of a given compositional variable through the selection of appropriate sections in compositional space. This has been illustrated with examples for the system FeO-Fe_2O_3-CaO-SiO_2-Al_2O_3 for a range of compositions and temperatures relevant to entrained coal gasification technologies. Effects of MgO, Na_2O and K_2O on phase equilibria can also be now predicted.

Acknowledgement. The authors would like to acknowledge the support of the Centre for Coal in Sustainable Development for the financial support of the development of the FactSage database; staff of the Centre for Research in Computational Thermochemistry, Montreal in particular Dr S. Degterov and Prof. A.D. Pelton for their contributions to the development of the thermodynamic database; the Australian Research Council for financial support for the viscosity model development, Dr A. Klimenko for his contribution to the deposit flow modelling.

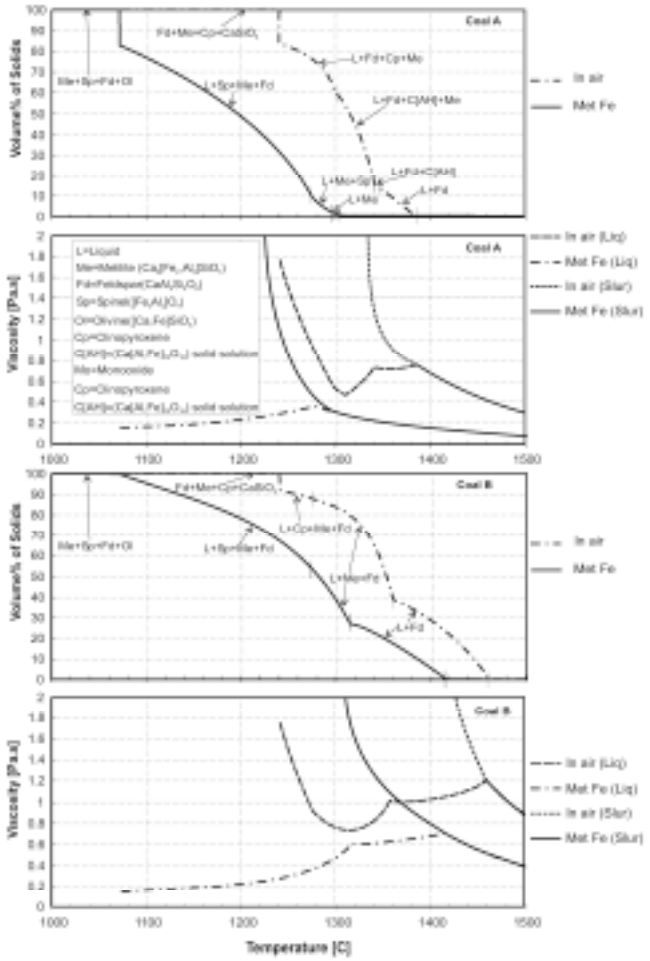

Figure 5. Effect of atmosphere conditions on crystallisation characteristics and viscosities of the coals A and B (at metallic iron saturation compared to air) as a function of temperature.

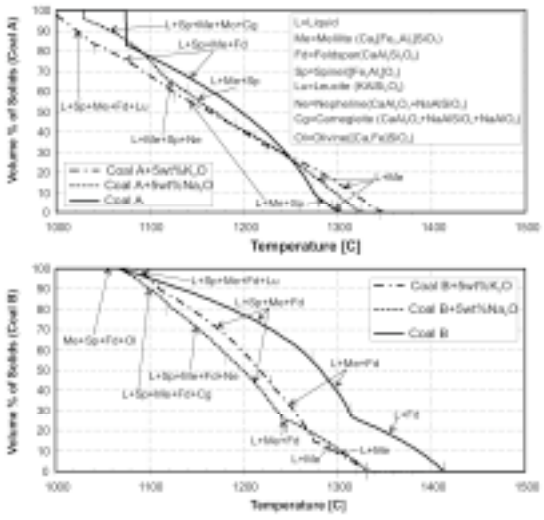

Figure 6. Effect of Na2O and K2O on crystallisation behaviour of the coals A and B at metallic iron saturation as a function of temperature.

References

(1) Bale C.W., Chartrand P., Degterov S.A., Eriksson G., Hack K., Mahfoud R. Ben, Melançon J., Pelton A.D., and Petersen S.: *Calphad*, **2002**, 26 (2), 189-228.

(2) Jak E. and Hayes P.C.: *Applications of the new FACT database for the prediction of melting behaviour of coal mineral matter*, 9th Australian Coal Sci. Conf. "Solutions for Industry", Brisbane, Nov. 2000, ed. J.H.Pohl, publ. Australian Institute of Energy, Toukley, NSW, Australia, http://www.aie.org.au , ISBN # 1864993960.

(3) Jak E. and Hayes P.C.: *Thermodynamic Modelling of the Coal Ash Systems in Black Coal Utilisation (a new FactSage database of the SiO_2-Al_2O_3-CaO-FeO-Fe_2O_3 system and the effects of MgO, K_2O and Na_2O on liquidus)*, 18th Annual Intl. Pittsburgh Coal Conf., Newcastle, NSW, Australia, 4-7 Dec. 2001, ISBN 1-890977-18-7, publ. Pittsburgh Coal Conference, Univ. of Pittsburgh, Pittsburgh, PA, USA.

(4) Jak E., D.Saulov and Hayes P.C.: *New thermodynamic database for prediction of high temperature phase equilibria for the SiO_2-Al_2O_3-CaO-FeO-Fe_2O_3 system with addition of MgO, K_2O and Na_2O with FactSage computer package*, Report, 2003, Centre for Coal in Sustainable Development, Brisbane, Australia.

(5) Kondratiev A. and Jak E.: *Fuel*, **2001**, 80(14), 1989-2000.

(6) Kondratiev A. and Jak E.: *Metall. Trans. B*, **2001**, 32B, 1027 - 1032.

(7) Kondratiev A. and Jak E.: *Metall. Trans. B*, **2001**, 32B, 1015 - 1025.

(8) Urbain G., Cambier F., Deletter M. and Anseau M.R.: *Trans. J. Br. Ceram. Soc.*, **1981**, 80, 139-141.

(9) Urbain G.: *Steel Res.*, **1987**, 58, 111-116.

(10) Mills K.C. *Viscosities of molten slags*, Chapter 9, Slag Atlas, 2nd edition, Berlin, Springer-Verlag, 1995, pp. 349-402.

(11) Urbain G. and Boiret M.: *Ironmaking & Steelmaking*, **1990**, 17, 255-260.

(12) Roscoe R.: *Br. J. Appl. Phys.*, **1952**, 3, 267-269.

(13) Hurst H.J. *Personal communication*, 1999, CSIRO DET, North Ryde, Sydney, Australia.

(14) Hurst H.J., Novak F. and Patterson J.H.: *Fuel*, **1999**, 78, 439-444.

(15) Hurst H.J., Novak F. and Patterson J.H.: *Fuel*, **1999**, 78, 1831-1840.

(16) Mills K.C., Chapman L., Fox A.B., Sridhar S.: *6th Int. Conf. Slags Fluxes Molt. Salts*, 2000, KTH, Stockholm, CD-ROM, paper #433.

(17) Watt J. D. and Fereday F.: *J. Inst. Fuel*, **1969**, 42, 99-103.

(18) Browning G.J., Bryant G.W., Hurst H.J., Lucas J.A., and Wall T.F.: *Energy & Fuels*, **2003**, 17, 731-737.

(19) Kalmanovich D.P. and Frank M.: *Proc. Eng. Foundation Conf., Miner. Matter Ash Deposition*, **1988**, pp. 89-101

.(20) Jak E., Degterov S., Hayes P.C. and Pelton A.D.: *Fuel*, **1997**, 77,77-84.

(21) Jak E., Degterov S., Pelton A., Happ J. and Hayes P.: In *Impact of Miner. Impurities in Solid Fuel Combust.*, ed. Gupta R.P., Wall T.F., Baxter L., Kluwer Academic/Plenum Publ., NY, USA, 1999, pp. 723-734.

(22) Jak E., Degterov S., Zhao B., Pelton A. and Hayes P.: *Metall. Trans. B*, **2000**, 31B, 621-630.

(23) Vladimirov I., Christie S. and Jak E.: *Computer modelling of physical-chemical properties of complex coal ash slag systems in multi-dimensional compositional space*, 18th Annual Intl. Pittsburgh Coal Conf., Newcastle, NSW, Australia, 4-7 Dec. 2001, ISBN 1-890977-18-7, publ. Pittsburgh Coal Conference, Univ. of Pittsburgh, Pittsburgh, PA, USA.

(24) Jak E. (2002): *Fuel*, **2002**, 81 (13), 1655-1668.

(25) Jak E., Kondratiev A., Christie S. and Hayes P.C.: *Metall. Trans. B*, **2003**, 34B, 595-603.

(26) Hoy H.R., Roberts A.G., and Wilkins D.M.: *Inst. Gas Engrs. J.*, **1965**, 5, 444-469.

(27) Patterson J.H., and Hurst H.J.: *Slag characteristics of Australian bituminous coals for utilization in slagging gasifiers*, Proceedings of the Workshop "Impact of Coal Quality on Thermal Coal Utilisation", 1996, CRC Black Coal Utilisation, Brisbane, Australia.

(28) Harris D.J. and Patterson J.H.: *Aust. Inst. Energy News J.*, **1995**, 13, 22-32.

(29) Reid W.T. and Cohen P.: *Trans. ASME*, **1944**, 66, 685-690.

(30) Reid W.T. and Cohen P.: *Trans. ASME*, **1944**, 66, 83-97.

SLAG FOAMING IN ENTRAINED FLOW GASIFIERS

Chulbum Cho and Myongsook S. Oh

Department of Chemical Engineering
Hongik University
72-1 Sangsudong Mapogu, Seoul, Korea

Introduction

In the entrained flow type of gasifiers, the slag viscosity is an important parameter which determines gasification conditions.[1] The slag viscosity has been measured experimentally under a reducing condition, and also estimated by various empirical models.[2-4] Most viscosity measurements were conducted under isothermal conditions or very low cooling rates such as 2 or 3°C/min. These data were used to determine the gasification temperature in the slurry-feed gasifiers to ensure continuous flow and, therefore, continuous removal of slag. In the dry-feed gasifiers which operate at temperatures well above 1500°C, the viscosity is used as a guide for minimizing the refractory wear. The isothermal measurements, however, do not render any information on slag behavior under rapid cooling conditions at the slag tap.

As the cooling rate increases, the viscosity at a given temperature decreases,[5] and the slag remains fluid to quite low temperatures. The low viscosity helps the slag flow out of the slag tap, so it was not a concern until one particular coal, Denisovsky coal, was tested. Denisovsky coal was a Russian sub-bituminous coal and was one of the nine coals tested under the project, "Development of fundamental Technologies for the IGCC systems," funded by Korean Ministry of commerce, Industry and Energy.[5] All nine coals were tested in two pilot scale entrained flow gasifiers: a 3-ton/day dry-feed gasifier at the Institute of Advanced Engineering (IAE), Suwon, Korea, and an 1-ton/day slurry-feed gasifier at Korean Institute of Energy Research (KIER), Taejeon, Korea. While the Denisovsky coal slag didn't cause any operational problem at the high temperature of the dry-feed gasifier, slag foaming filled up most volume of the slurry-feed gasifier vessel, resulting a major repair of the unit.

The cause of foaming was investigated in the laboratory. The slag viscosity was measured at two cooling rates, 2 and 10°C/min, and the cooled slag was examined using (a) Scanning Electron Microscope (SEM).

Experimental

Slag sample: The slag produced from the IAE dry-feed gasifier was used. The composition of the slag is shown in Table 1. The Denisovsky slag contains high concentrations of SiO_2 and Al_2O_3, and low concentration of CaO. The numbers in Table 1 were normalized to give 100, excluding refractory components such as Cr_2O_3 and ZrO. The concentration of refractory components varied widely from sample to sample. The average concentration of refractory components was 3-4%, but some contains over 10% of Cr_2O_3.

Table 1. Normalized Composition of Denisovsky Coal Slag

Al_2O_3	SiO_2	Fe_2O_3	CaO	MnO	TiO_2	MgO	K_2O	Na_2O	P_2O_5
30.5	49.3	9.13	5.63	0.19	0.99	1.70	1.68	0.53	0.44

Viscometer: Brookfield HB-DVIII viscometer with Searle type coaxial cylindrical cell was used in viscosity measurements.[6] The cell(stationary crucible and the rotor) was made of high density alumina and was placed in a high temperature furnace with the maximum attainable temperature of 1600°C. In order to simulate a reducing atmosphere, 80/20 (volume %) mix of CO_2/CO was injected from the bottom of the furnace at 1000cm^3/min. Approximately 70g of slag samples were broken into the sizes less than 2mm and slowly fed to the crucible at 1550°C. When all the slag was fed and the rotor was assembled, the temperature of the furnace was lowered at the rate of 2 or 10°C/min. The viscosity was measured every 30s at the shear rate of 10 rpm, until the torque on the rotor reached the 90% of the viscometer limit. Then, the rotor was removed from the molten slag and the whole assembly was allowed to cool down naturally. The cooled slag was cut as needed and examined using a SEM (Hitachi model).

Results and Discussion

Figure 1 shows the viscosity of Denisovsky coal slag as a function of temperature at two cooling rates. The viscosity was typical of a glassy slag at both cooling rates, and, as expected, shows lower values at 10°C/min. Under 2°C/min cooling rate, the maximum viscosity measured was about 5000 poise at 1380°C, while at 10°C/min, was 4000 poise at 1350°C. Measurements at a higher cooling rate were not possible due to the large mass of the cell and slag employed, and also due to excessive swelling, as discussed below. Once the hot slag boils over the crucible, it damages the furnace seriously.

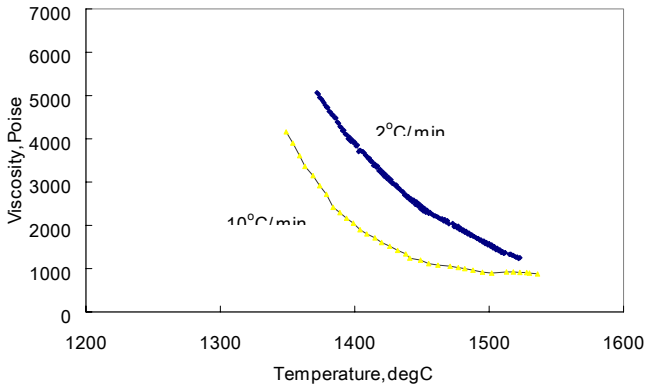

Figure 1. Viscosity of Denisovsky coal slag as a function of temperature at two cooling rates.

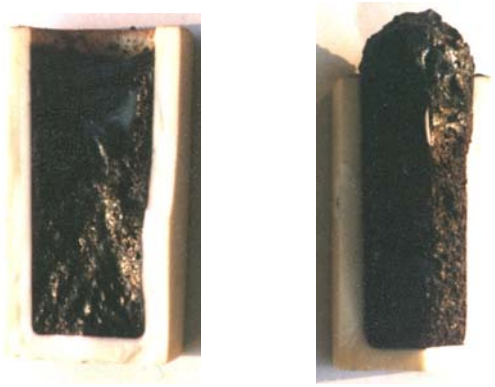

(a) After 2℃/min Cooling (b) After 10℃/min Cooling

Figure 2. Photographs of Denisovsky coal slag after viscosity measurements.

Figure 2 shows the shape of Denisovsky coal slag after viscosity measurements. At 2°C/min cooling, the slag remained inside the crucible, but filled the space which had been occupied by the rotor. The slag contained large number of small spherical pores though out the sample. At 10°C/min, the slag shows excess swelling. The slag not only filled out the rotor space, but also expanded above the crucible. The portion extruded above the crucible had rusty color coating and relatively high strength. The hardness decreased towards the bottom of crucible, becoming very brittle to the point that it could be crushed by hand. Many big spherical pores were observed at the bottom of crucible. Excess swelling or foaming of the slag after viscosity measurements was not observed in any other coal slags tested.

The SEM micrographs of the extruded top portion of the slag cooled at 10°C/min are shown in Figure 3. The overall area (Figure 3(a)) shows glassy background with needle-shape crystalline phases. The analysis by SEM/EDX identified these crystals as Al-Cr-oxide, a phase found in the refractory of the IAE gasifier. SEM/EDX composition analysis of a pore (Figures 3.b and 3.c) revealed that the pore had higher concentration of Fe than the glassy matrix, and the Fe concentration decreased towards the edge of the pore.

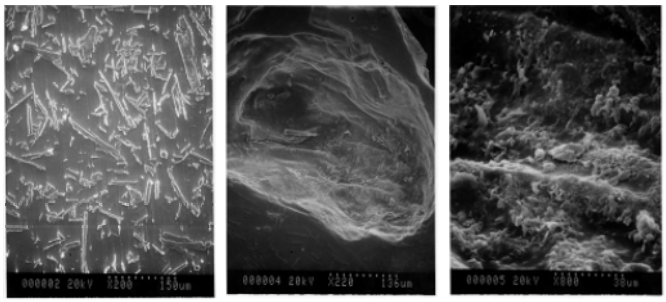

(a) Glassy Matrix (b) Pore (c) Inside of Pore

Figure 3. SEM micrographs from the top of Denisovsky coal slag cooled at 10°C/min.

The SEM micrographs of the bottom part of the slag are shown in Figure 4. The large spherical pores at the bottom have smooth, clear boundary which indicates their origin as gas bubbles in molten state. Figure 4(b) is the center area of Figure 4(a), magnified by 10 times, and shows the glassy matrix with Al-Cr-oxides and spherical droplets with white boundary. The SEM/EDX revealed that the droplets were made of metallic Fe. Metallic Fe droplets were also found in the large pores shown in Figure 4(c) and (d). Therefore, one can conclude that the pores were from O_2 gas bubbles which were released from Fe-oxides as they were reduced to Fe in a reducing gas atmosphere.

The SEM micrographs of the slag cooled at 2°C/min were similar to those in Figure 3. The top was also coated with the hard rusty red layer. The slag contained a high concentration of refractory components. Although the pores were smaller in size and number than those in 10°C/min slag, they also contained metallic iron inside.

The compositions of the top, middle, and bottom portion of 10°C/min slag cooled at 10°C/min, and one sample from 2°C/min slag were determined by XRF analysis. The compositions of 4 samples were very close to those shown in Table 1, confirming that there was no difference in composition between the hard top portion and porous bottom of the 10°C/min cooled slag, and also between the slags from two cooling rates.

The difference in pore size was resulted from the different actual cooling rates. When the cell assembly was allowed to cool down naturally after viscosity measurements, the cooling rate of the extruded portion of the slag is expected to be much faster than that of the bottom. The fast quenching and subsequent solidification of the slag inhibited the reduction of iron oxides and growth of bubbles, while, at the bottom, slow cooling allowed bubbles to expand to larger sizes.

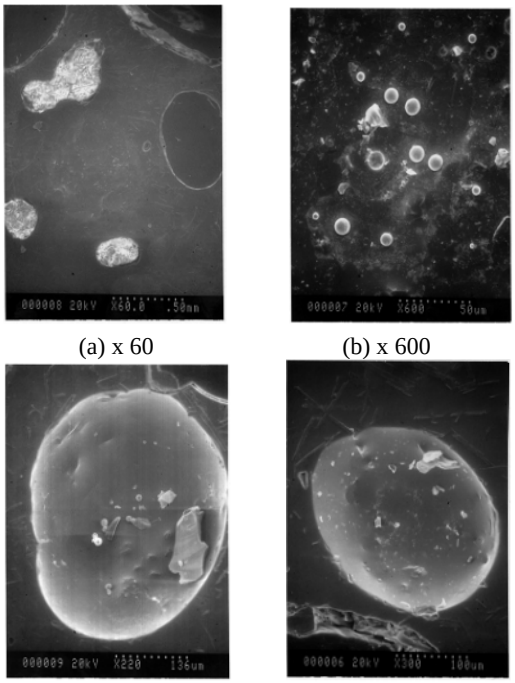

(a) x 60 (b) x 600

(c) Pore at × 220 (d) Pore at ×300

Figure 4. SEM micrographs from the top of Denisovsky coal slag cooled at 10°C/min.

The difference in the extent of swelling of the slag samples from two cooling rates can be explained by the viscosity. When the reduction of iron oxides started, the oxygen bubbles grew more readily in the slag matrix with the lower viscosity.

Conclusions

Reduction of iron oxides to metallic Fe can cause excessive slag foaming by O_2 gas when it occurs in a relatively low viscous glassy slag. Even in the slag with high isothermal viscosity, the low viscous condition can occur under a rapid cooling condition, such as at the slag tap of the gasifier. The slag foaming by iron oxides reduction can cause a serious damage to gasifiers which operate at temperatures around 1300°C. The swelling tests under rapid cooling in a reducing atmosphere must be performed for glassy slags prior to gasification.

Acknowledgement. This work was supported by Korean Ministry of Commerce, Industry and Energy under Contract 1996 N-CO02-P5.

References

(1) Corey, R. C., US Bureau Mines Bull. No. 618, 1964.
(2) Oh, M. S., and 4 others, *Fuel Processing Technol*., **1995**, *44*, 191.
(3) Watt, J. D., and Fereday, F., J. Inst. *Fuel*, **1969**, *42*, 99.
(4) Urbain, G., and 3 *Trans. J. Br. Ceram. Soc.*, **1981**, *80*, 139.
(5) Report to Korean Ministry of Commerce, Industry and Energy, 1996-N-CO02-P-5, **2000** and 2000-N-CO02-P-01, **2003.**
(6) Cho, D. H., Moon, I. S., Whang, S. Y., and Oh, M. S., *Korean J. Ind. Eng. Chem.* **2001**, *7*(1), 30.

Behavior of Minerals During Anthracite Graphitization

Margaret L. Laumb and Steven A. Benson
Microbeam Technologies Incorporated
4300 Dartmouth Drive
Grand Forks, ND 58203

Peter Pappano and Harold H. Schobert
The Energy Institute
Pennsylvania State University
University Park, PA 16803

Introduction

Anthracite coal was heated to three different temperatures to induce graphitization. The goal of the work was to determine how heating affected the mineral content and texture of the coal. This paper will focus on the various mineral transformations underwent during the heating process. The mineral transformations were measured using scanning electron microscopy and x-ray microanalysis.

Heating of the anthracite samples was conducted at Pennsylvania State University (1). Anthracite and heat-treated samples were analyzed by Microbeam Technologies Incorporated (MTI) to determine size, composition, and abundance of mineral and transformed mineral grains using computer-controlled scanning electron microscopy (CCSEM). In addition, morphological analysis was conducted to provide images and chemical compositions of selected features in the anthracite samples (2). The quantities of minerals and transformation products were determined at 2000°C, 2500°C, and 2600°C.

Experimental

LCNN anthracite was heated to three different temperatures: 2000°C, 2500°C, and 2600°C to induce graphitization. The samples were heat-treated in a Centorr Vacuum Industry Series 45 furnace, accurate to ±10°C. Graphite crucibles containing 12 grams of sample under graphite lids were placed in the hot zone of the furnace. The environment of the hot zone was purged by pulling a vacuum, and then backfilling with ultra-high purity argon three times. Following this purge, the samples were heated to 2000, 2500, and 2600° C with a heating rate of 10°C/min and held at the maximum temperature for one hour (in vacuum). The heat-treated samples were prepared and analyzed to determine size, composition, and abundance of mineral grains using CCSEM.

Samples of the raw and heat-treated anthracite were prepared for scanning electron microscopy analysis by mixing two grams of sample material with three grams of melted carnauba wax. This mixture was poured into a small rubber mold and, after solidifying, was backed with epoxy. The epoxy is used to increase the strength of the resulting plug. Plugs were allowed to harden overnight, and polished to expose cross-sections of the particles. Polished plugs were cleaned and coated with carbon to improve conductivity in the electron microscope.

Prepared samples were analyzed to determine size, composition, and abundance of mineral grains using fully automated computer-controlled scanning electron microscopy. The CCSEM technique characterizes up to three thousand individual particles in a single sample. Elemental compositions are used to categorize individual mineral types.

MTI also performed scanning electron microscope (SEM) morphology analysis to obtain representative photographs of the samples and determine variations in inorganic content between the organic matrix and mineral matter. Backscattered electron imaging, which best shows compositional differences, was used to examine the minerals present in the samples.

Results and Discussion

Table 1 shows the results of the CCSEM analyses for a raw anthracite and three heated samples. Mineral content for the raw coal was 6.8 wt%, and ranged from 1.1 wt% (at low temperature) to 0.6 wt% (at high temperature). This indicates significant loss of mineral phases from the coal due to decomposition and vaporization during heating. Figure 1 shows backscattered electron images of polished cross-sections of raw anthracite and heat-treated samples. The images show some changes in the shape of the minerals upon heating. Figure 1c shows void spaces where minerals may have been associated. These minerals likely volatilized during heating.

Mineral assemblages vary considerable between the raw and heated coals. Clays and aluminosilicates are abundant in the raw coal but absent from heated coals. This trend occurs for kaolinite, illite, and aluminosilicate. Calcium aluminosilicate, gypsum containing aluminosilicate (mixture of calcium, sulfur, and aluminosilicates), and unknown or amorphous material are most abundant in the sample heated to 2000°C. Pyrite, a sulfide mineral, is absent from the heated coal samples. Calcite-derived (or calcium oxide) and calcium-rich phase are important minerals in the heated coals, with the highest concentrations in the sample heated to 2500°C. Rutile (TiO_2), which is nearly absent in the raw coal sample and scarce in the 2000°C sample, is a dominant phase in the sample heated to 2500°C. Rutile and calcium oxide are stable at high temperatures and are not prone to volatilize during heating. Quartz and alumina are both present in the raw coal and the coal heated to 2000°C, but alumina is not present in the higher temperature samples, and quartz is not present in the 2600°C sample. Iron oxide increases in abundance as the temperature of treatment increases.

Conclusions

Significant mineral transformations were found when comparing the mineral types and abundance in the raw and heated coals. Clay minerals including kaolinite, illite, and aluminosilicate were abundant in the raw coal but absent from heated coals. These materials interacted with other components to produce calcium aluminosilicate, gypsum-containing aluminosilicate, and unclassified materials. The unclassified materials are typically glassy amorphous phases. Pyrite, a sulfide mineral, was absent from the heated coal samples. As a result of the decomposition of pyrite, iron oxide increases in abundance as the temperature of treatment increases. Calcite-derived (or calcium oxide) and calcium-rich phases are important minerals in the heated coals with the highest concentrations in the sample heated to 2500°C. Rutile and calcium oxide are stable at high temperatures and are not prone to volatilize during heating.

References

1. Pappano, P.J. "A mechanism of Pennsylvania anthracite graphitization involving carbide formation and decomposition." Ph.D. Dissertation. The Pennsylvania State University, University Park, PA. **2003**.
2. Laumb, M.L., Benson, S.A, and Laumb, J.D., Ash Behavior in Utility Boilers: A Decade of Fuel and Deposit Analysis, Proceedings of Engineering Foundation Conference, Production in the 21st Century: Impacts of Fuel Quality and Operations, October 28 - November 2, **2001**, Snowbird, Utah.

Acknowledgement
The authors gratefully acknowledge the support by The Consortium for Premium Carbon Products from Coal at the Pennsylvania State University.

Table 1. CCSEM analysis results for untreated LCNN anthracite and three heated LCNN anthracites. Results are expressed as weight percents normalized to 100% on a mineral basis.

Mineral/ phase	Raw	2000°C	2500°C	2600°C
Quartz	1.2	8	2.5	0.4
Iron oxide	0.5	1.1	1.5	2.8
Periclase	0	1.5	0	0
Rutile	0.8	9	42.7	38.5
Alumina	1.1	3.2	0	0
Calcite/calcite derived	1.6	8.2	12.3	9.2
Dolomite	1.4	0.1	0.4	0.1
Ankerite	0	0	0	0
Kaolinite	60.4	0.2	0.2	0
Montmorillonite	2	0.2	0	0.2
Illite	7.5	0	0.3	0
Fe Al-silicate	1.5	0	0	0
Ca Al-silicate	0.3	16.2	0.1	0.7
Na Al-silicate	0.5	0	0	0
Aluminosilicate	5.3	0.3	0	0
Mixed Al-silica	0.9	0.1	0.8	0
Fe silicate	0	0	0	0
Ca silicate	0	0.9	0.2	0
Ca aluminate	0	0.1	0	0
Pyrite	4.9	0	0	0
Pyrrhotite	0	0	0	0
Oxidized pyrrhotite	0.1	0.2	0	0
Gypsum	0.1	0.9	1.7	0.4
Barite	0	0	0	0
Apatite	0.5	0	0.6	0
Ca Al-P	0.1	0	0	0
KCL	0	0	0	0
Gypsum-Barite	0	0.8	0.1	0.2
Gypsum-Al-silic.	0.1	9.3	0.8	0
Si-rich	0.3	2.3	0.5	0.3
Ca-rich	0.8	6.1	8.5	5
Ca-Si-rich	0	0	0	0
Unknown/amorphous	8.1	31.6	26.9	42

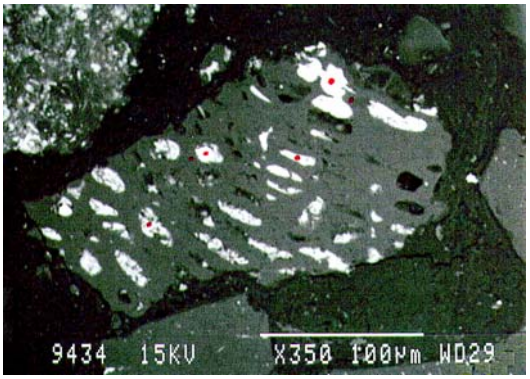

a. Raw anthracite

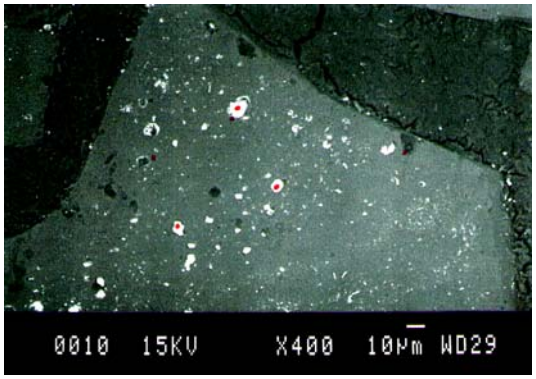

b. Heated to 2000°C

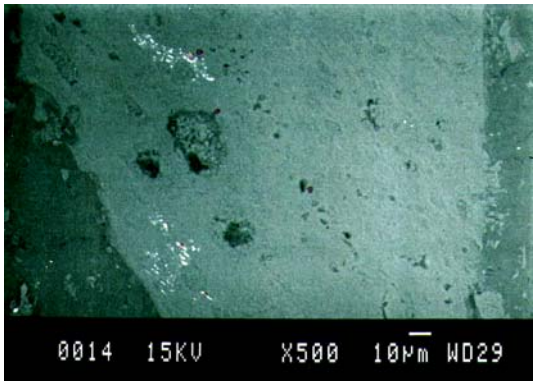

c. Heated to 2500°C

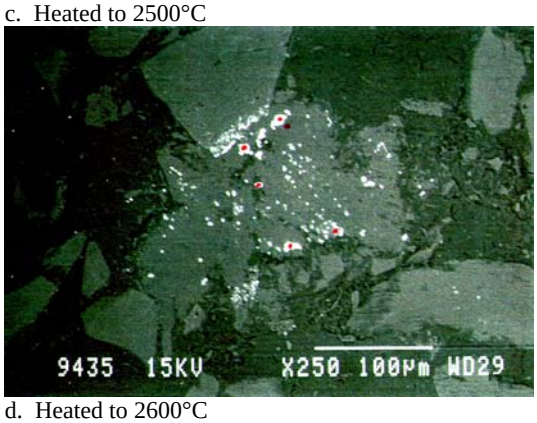

d. Heated to 2600°C

Figure 1. Backscattered electron images of polished cross-sections of raw coal and heat-treated samples.

Sulfur Retention in North Dakota Lignite Coal Ash

Bruce C. Folkedahl and Christopher J. Zygarlicke

Energy &Environmental Research Center
University of North Dakota
15 N. 23rd St.
Grand Forks, ND 58203

Introduction

Emissions from power plants such as particulate and sulfur are regulated by state health agencies and the U.S. Environmental Protection Agency (EPA). Much of the sulfur in the flue gas of coal-fired power plants is in the form of SO_2, with 1%–3% in the form of SO_3. SO_2 can be effectively controlled using commercial flue gas desulfurization (FGD) systems such as wet scrubbers. Sizing of these FGD systems affects the capital cost as well as the operational cost of the units. When the FGD system is sized, a coal analysis provides the amount of sulfur present in the coal, all of which is assumed to be SO_2 at the entrance to the FGD unit. The FGD system is then sized according to this concentration of sulfur. However, during combustion and depositional processes in the combustion system, some of the sulfur is retained in the ash because of reaction with basic oxides in the coal inorganics. The alkali and alkaline-earth elements are primarily responsible for this capture phenomena, with calcium and sodium being the most important. By accounting for the sulfur capture before the FGD, a more accurate determination of the FGD size and efficiency can be made. This report presents data from combustion tests performed at the University of North Dakota (UND) Energy & Environmental Research Center (EERC) on lignite coal, with an emphasis on evaluating the sulfur retention capability of the ash derived from the combustion. Statistical analysis and modeling of the sulfur retention and evaluation of a previous sulfur retention model developed at the EERC by Gronhovd et al. (1) is also presented.

Experimental

Coal Characterization The coal used in this test was obtained from core drilling of a mine area. Samples from the core drilling were contained in plastic bags and ranged from 0.13 to 29.5 lb per sample. Samples were put into three categories according to their sulfur levels. The categories were devised with low-sulfur samples having 0%–0.67% sulfur, medium-sulfur with a sulfur range of 0.68%–1.15% sulfur, and high sulfur having a sulfur content in the coal of greater than 1.16%, all on an as-received, weight percent basis of coal. The individual sample bags were placed into barrels of the three categories. The combined samples were then air-dried and thoroughly mixed. Samples of the three coal divisions were then analyzed using computer-controlled scanning electron microscopy (CCSEM), chemical fractionation, and x-ray fluorescence (XRF) of the ash for bulk oxide content. Table 1 shows the results of the average ultimate analysis for the three sample sulfur levels on an as-received basis. The bulk oxide composition of the ash generated from the coal sample composites as determined by XRF is shown in Table 2.

Table 1. Ultimate Analysis for the Three Composite Samples (as-received basis)

	Low Sulfur	Medium Sulfur	High Sulfur
Hydrogen	6.49	7.12	6.66
Carbon	30.46	33.41	34.25
Nitrogen	0.50	0.56	0.54
Sulfur	0.51	0.95	1.61
Oxygen	47.25	48.24	42.47
Ash	14.78	9.74	14.49
Btu	5830.00	6008.50	5961.50

Table 2. XRF Bulk Oxide Composition of Ash of Coal Sample Composites (weight percent, mineral basis)

	Low Sulfur	Medium Sulfur	High Sulfur
Silica	39.13	23.16	24.18
Aluminum	13.14	8.95	7.66
Iron	1.94	5.65	14.87
Titanium	0.93	0.55	0.43
Phosphorus	0.29	0.19	0.11
Calcium	17.36	18.39	13.14
Magnesium	6.44	6.82	4.77
Sodium	5.31	6.61	4.53
Potassium	0.52	0.40	0.40
Sulfur	14.36	28.92	29.44
Barium	0.58	0.36	0.46

Combustion Tests The coal composite blends were tested in the conversion and environmental process simulator (CEPS), an intermediate-scale downfired combustor that fires 0.5–2.0 kg (1–5 lb)/hr of fuel, simulates conditions of a full-scale utility boiler, and can generate realistic combustion test results for a variety of fuels and combustion conditions. Control of gas temperatures and composition throughout the CEPS is possible, independent of the heat capacity of the fuel, because of its external electric heating. Flue gas temperatures can reach a maximum of 1500°C (2732°F) in the radiant section and can be maintained at 500°–1200°C (932°–2200°F) in the convective pass section and 120°–250°C (248°–482°F) in the baghouse. There is ample access for sampling, observation, and optical diagnostics through access ports located throughout the CEPS. A personal computer displays and records temperature, gas flow, feed rate, and flue gas (O_2, CO_2, CO, SO_2, and NO_x) composition, which is sampled from ports in the radiant section and after the collection device. Figure 1 is a schematic of the CEPS.

The CEPS furnace test conditions were standard operating conditions to simulate pulverized coal (PC)-fired combustion of coal. Coal was fed at a rate of 5 lb per hour, and the first six heated sections were maintained at temperatures of 1000°, 1500°, 1500° 1400°, 1250°, and 1100°C starting at the top of the combustion zone. Air was introduced into the system at the rate of 30 standard liters per minute (SLPM) as primary air and 137 SLPM as secondary air. The ash generated in the system was collected at the baghouse as well as at the horizontal section just after the combustion chamber. This ash was analyzed for sulfur content and the amount of sulfur exiting the system obtained by difference when compared to the total sulfur contained in the coal. These data were used to evaluate the sulfur retention model developed at the EERC in a previous study.

Results and Discussion

Regression Analysis Statistical analyses of nine different samples of recently obtained lignite and 40 other lignite samples from a previous study by Gronhovd et al. (1) have been used to determine the efficacy of a model developed at the EERC in a previous study to predict sulfur emissions. Because calcium seemed either to be heavily affected by other factors or else insignificant, it was not included as a factor in the new model. Instead, silicon and aluminum contents were

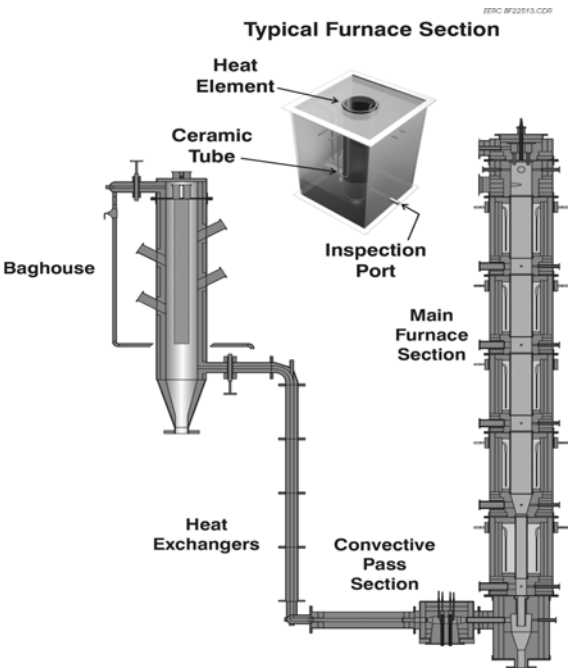

Figure 1. Schematic of the EERC CEPS.

included, which had seemed important to sulfur emissions in the previous tests. Aluminum was later disregarded as neither its effect nor its interactions proved important (the previous tests seemed to find a correlation between Al_2O_3 and sulfur emissions, but this may have been due to a correlation between aluminum and some other element). The final model developed in this study was as follows:

$$173.5!16.77(Na_2O)!2.207(SiO_2)!78.62(S)+0.2608(Na_2O)(SiO_2) +7.898(Na_2O)(S)+1.961(SiO_2)(S)$$

where the Na_2O and SiO_2 are given in weight percent oxide from the bulk ash XRF analysis and the sulfur is from the weighted average ultimate analysis from the three composite samples. The sulfur was computed on a moisture-free basis by weighting the measured sulfur level for each sample that went into the composite by the amount of sample in grams. These values are listed in Table 3 along with the measured sulfur in the collected combustion ash. The model r² term was 0.65, and its standard deviation was 10.1. This r^2 was slightly lower than the model developed previously at the EERC by Gronhovd. Statistically, the new model developed using the Grohovd data and the new lignite data has slightly better accuracy than did Grohovd's previous model. The results of the newly developed model are shown in Figure 2 and Table 4.

Table 3. Sulfur Levels in the Coal and the Collected Combustion Ash

	wt% in Coal (coal basis)	wt% in Combustion Ash (ash basis)
High Sulfur	3.29	2.1
Medium Sulfur	1.57	4.5
Low Sulfur	0.95	4.3

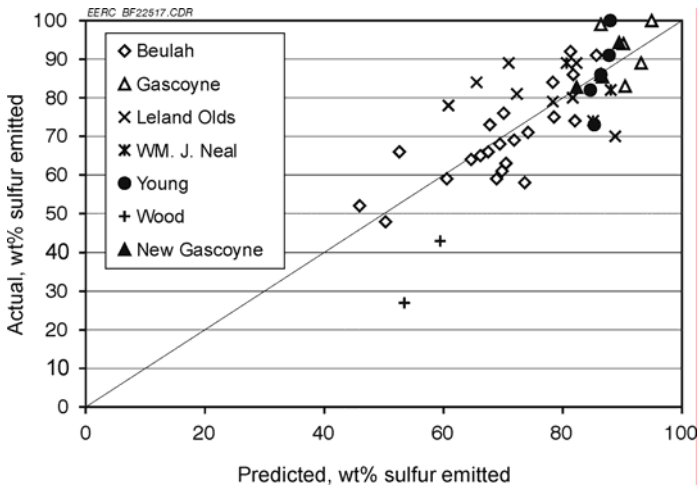

Figure 2. Predicted vs. actual percent sulfur emissions based on our current model.

Table 4. Predicted Versus Actual Sulfur Emitted from the Combustion Tests (percent of sulfur in coal)

	Predicted	Actual
High Sulfur	79	93
Medium Sulfur	70	83
Low Sulfur	87	87

Conclusions. The coal samples used in this study were divided into three composite samples. The coal came from core drilling of the lignite mine area. Core samples ranged in size from 0.13 to 29.5 lb per sample. The three composite samples were compiled according to sulfur levels of low, mid, and high, having values of 0%–0.67%, 0.68%–1.15%, and 1.16% and above, respectively. CCSEM analysis showed increasing amounts of pyrite and pyrrhotite and decreasing quartz and clays as the sulfur level increased. Chemical fractionation data indicate minor differences in the amount of material organically bound and carbonate materials in the three composite samples. The combustion tests of the three composite samples showed sulfur retention in the ash of roughly 7%–17% of the total sulfur in the coal. A new model developed from the data set produced in this study, as well as the data set from Gronhovd's previous study, indicates a slight increase in predictive capability over Gronhovd's previous model.

The regression model indicates that the original model developed by Gronhovd at the EERC in previous studies remains an adequate representation of the sulfur emissions expected from low-rank coals (1). While the newly developed model is statistically superior, the difference is minimal. Another point of the study is that the results from combustion studies performed in the EERC CEPS match the full-scale data from the previous study very well, validating the use of this pilot-scale equipment for modeling reactions in full-scale systems.

References

1. Some Studies on Stack Emissions from Lignite-Fired Powerplants: Technology and Use of Lignites Proceedings: Bureau of Mines, University of North Dakota Symposium 67, North Dakota, May 9–10, **1973**.

SCR CATALYST BLINDING DUE TO SODIUM AND CALCIUM SULFATE FORMATION

Charlene R. Crocker, Steven A. Benson, Jason D. Laumb

Energy & Environmental Research Center
University of North Dakota
15 North 23rd Street
Grand Forks, ND 58203

Introduction

Ash-related impacts on selective catalytic reduction (SCR) catalyst performance depend upon the composition of the coal, the type of firing systems, flue gas temperature, and catalyst design (1–5). The problems currently being experienced on SCR catalysts include the following:

- Formation of sulfate- and phosphate-based blinding materials on the surface of catalysts.
- Carrying of deposit fragments, or popcorn ash, from other parts of the boiler and depositing on top of the SCR catalysts.
- Catalyst poisoning from arsenic.

Licata and others (1) conducted tests on a South African and German Ruhr coal and found that the German Ruhr coal significantly increased the pressure drop across the catalyst because of the accumulation of ash. They found that the German coal produced a highly adhesive ash consisting of alkali (K and Na) sulfates. In addition, they reported that the alkali elements are in a water-soluble form and highly mobile and will migrate throughout the catalyst material, reducing active sites. The water-soluble form is typical of organically associated alkali elements in coals. The German Ruhr Valley coal has about 9.5% ash and 0.9% S on an as-received basis, and the ash consists mainly of Si (38.9%), Al (23.2%), Fe (11.6%), and Ca (9.7%), with lower levels of K (1.85%) and Na (0.85%) (2). Cichanosicz and Muzio (3) summarized the experience in Japan and Germany and indicated that the alkali elements (K and Na) reduced the acidity of the catalyst sites for total alkali content (K+Na+Ca+Mg) of 8%–15% of the ash in European power plants. They also found that alkaline-earth elements such as calcium react with SO_3 on the catalyst, resulting in plugging of pores and a decrease in the ability of NH_3 to bond to catalyst sites. The levels of calcium in the coals that caused blinding ranged from 3% to 5% of the ash. FactSage™ calculations indicate that the concentration of potassium and sodium in the gas stream increases more than proportionally with the addition of secondary fuels such as refuse-derived fuel, poultry litter and meat and bone meal (6). Cofiring 25% e/e poultry litter, in particular, increased the gaseous alkali concentrations dramatically.

The mechanisms for this type of low-temperature deposition have been examined and modeled in detail at the Energy & Environmental Research Center (EERC) in work termed Project Sodium and Project Calcium in the early 1990s; however, the focus of those projects was specific to primary superheater and economizer regions of boilers and not SCR systems (4, 7). Deposit buildup of this type can effectively blind or mask the catalyst, diminishing its reactivity for converting NO_2 to N_2 and water and potentially creating increased ammonia slip (1). In examining deactivation mechanisms related to alkali and alkaline earth metals, Senior et al. reported that vanadium tended not to form sulfates on the SCR catalyst in the presence of SO_2(g) but that the catalyst substrate (anatase) and modifiers (molybdenum) do (8).

Arsenic and phosphates, which are not uncommon in low-rank coals, may also play a role in catalyst degeneration. Arsenic is a known catalyst poison (9) in applications such as catalytic oxidation for pollution control. Phosphates can occur in low-temperature ash deposits to create blinding effects. Beck and others (10) found high concentrations of phosphorus compounds as constituents of the bio-residue (sewage sludge) in cofiring with coal to have a significant effect on the rate of catalyst deactivation. Phosphates also occur with arsenic and can cause catalyst poisoning (7). The blinding process involving pyrosulfates has more liquid-phase materials as compared to the calcium sulfate formation processes reported by Siemens (11) who described sulfate materials blocking catalyst pores with 50% catalyst deactivation after 5000 hours for a Powder River Basin (PRB) coal.

The purpose of this research was to obtain fundamental information on the formation of phases and components that comprise SCR blinding deposits. Calcium aluminum phosphate minerals have been observed in North Dakota lignites and PRB coals. Information on how these phosphate-rich phases develop and form will be invaluable for predicting SCR deposition and formulating ash deposit mitigation measures.

Experimental

Several coals were selected for testing based on coal type, geographical origin, and phosphorus-mineral-bearing content to obtain a variety of samples types. All test coals were analyzed for proximate, ultimate, heating value, and bulk inorganic composition using standard American Society for Testing and Materials procedures. Among the coals selected for the test matrix were a 48/52 blend of low-sulfur U.S. bituminous and PRB coals (LSUS–PRB) and a 100% PRB coal. Ash from the coals was produced under simulated combustion conditions in the conversion and environmental process simulator (CEPS), a down-fired combustion system that burns 2–4 lb/hr of fuel (Figure 1). The ash was collected and size fractioned using 3-stage cyclone to partition the ash. The 1–3-µm particles were characterized using scanning electron microscopy (SEM) to determine the distribution of elements as a function of particle size and vapor phase.

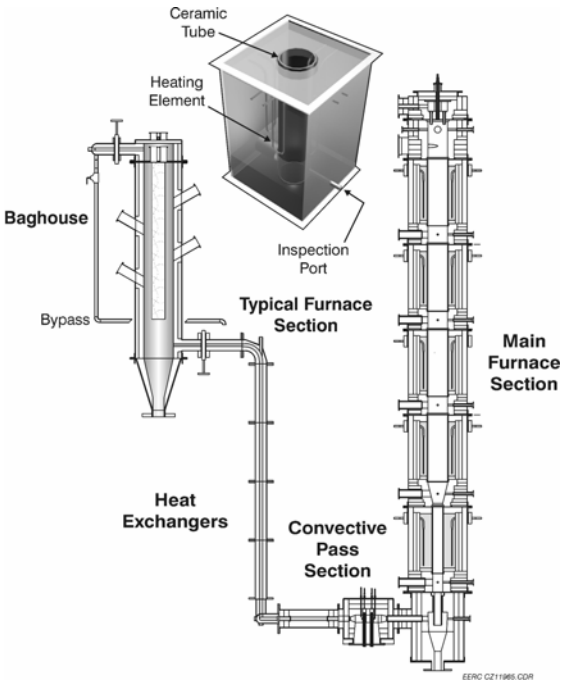

Figure 1. Schematic of the CEPS with furnace section detail.

The impacts of temperature and the presence of the catalyst on the ability of ash to form sulfates were examined. Isothermal tests to develop reaction rate as a function of temperature and gas composition were conducted using thermogravimetric analysis (TGA) with a DuPont model 951 module interfaced to a TA 2100 thermoanalyzer and data processor. The instrument has a 100-mg capacity and a maximum heat-up rate of 100°C/minute. TGA testing was conducted on the 1–3-µm-size fraction of ash produced from the LSUS–PRB and 100% PRB coals and exposing them to vapor-phase sulfur dioxide with and without catalyst at several temperatures. Testing was conducted to determine the weight gain with flue gas containing ammonia. Gas composition for the TGA tests was 74% N_2, 8% H_2O, 14% CO_2, 4% O_2, 100–300 ppm NH_3, 0.04% SO_2, 1–1000 ppm P.

Scanning Electron Microscopy. The SEM method utilizes electron probe microanalysis techniques to chemically analyze individual ash particles. Particles collected in the 3-stage cyclone of the CEPS and exposed in the TGA analyzer were finely dispersed on carbon tape and analyzed for major and minor elements using the ZAF method, which corrects x-ray intensities for differences in the atomic number (Z), absorption (A), and fluorescent (F) effects of the calibration standards relative to the sample. The chemical composition obtained in this manner is semiquantitative at best because of the short x-ray counting time employed (10 s), the use of flat mineral standards for calibration, and the fact that no matrix corrections for particle diameter, shape, or density were applied.

Results and Discussion

Table 1 contains the proximate and ultimate analysis of the selected test materials. The 100% PRB coal had twice the moisture (24.1 vs. 12.9 wt%) of the LSUS–PRB blend. It also contained about 14 wt% more oxygen and 7.5 wt% fixed carbon. Hydrogen and nitrogen content were similar between the coals. The percent ash of the LSUS–PRB blend was about 3.5 wt% higher than the 100% PRB. The sulfur content was also higher (8.3 vs. 5.6 wt% of the ash). Table 2 shows the ratio of mineral constituents in the as-received coals. The 100% PRB coal ash has a higher proportion of Ca than Al and Si. The ashed coal also contained S, Mg, Fe, and small amounts of Ti, Na, and K. The P content was less than 1%. The greatest change resulting from the blending of the PRB with LSUS was the aluminosilicate nature of the ashed blend. The Ca content was one third that of the 100% PRB, and the Mg was half the PRB content. The rest of the elements were present in similar proportion to the 100% PRB coal ash

Table 1. Proximate and Ultimate Analysis of Coal, as received

	100% PRB	LSUS–PRB
Air Dry Loss, %	17.58	9.86
Moisture, %	24.1	12.9
Volatile Matter, %	35.6	35.72
Fixed Carbon, %[1]	36.03	43.59
Ash, %	4.27	7.8
H, %	6.19	5.44
C, %	52.06	62.48
N, %	1.26	1.61
S, %	0.24	0.65
S, % of mineral constituents	5.6	8.3
O, %[1]	35.99	22.03
Calculated Calorific Value	8904	10,830

[1] By difference.

Table 2. SEM Analysis of the Mineral Content of the Coals

Oxide content, SO_3 free	100% PRB	LSUS–PRB
Al_2O_3	32.0	48.3
CaO	20.3	29.7
Fe_2O_3	7.1	5.3
K_2O	1.7	1.8
MgO	1.1	0.4
Na_2O	28.5	9.5
P_2O_5	7.6	2.9
SiO_2	1.1	0.8
TiO_2	0.5	1.3
Al_2O_3	32.0	48.3

The aim of the TGA testing was to determine the potential of the formation of sulfates to cause particle-to-particle bonding that leads to the formation of deposits in the temperature range where SCR catalysts are used. The TGA testing is focused on determining the reactivity of the 1–3-µm ash produced from the LSUS–PRB and 100% PRB coals to sulfur dioxide and gas-phase phosphorus species as a function of temperature. Testing was conducted to determine the weight gain with flue gas containing ammonia. The impact temperature on the weight gain due to the formation of sulfates for the LUSU–PRB blend is shown in Figure 2. The rates of sulfation were found to increase with increased temperature. The increase in the weight gains was magnified when ammonia and phosphorus were added. Ground catalyst was mixed with the 100% PRB ash in the TGA. Increases in weight gain were observed when catalyst was added as compared to baseline cases for 100% PRB, as shown in Figure 3. The presence of catalyst enhances the formation of sulfates.

The ash exposed in the TGA was examined using the SEM. Figure 4 shows the LSUS–PRB blend. The analysis included points at the margins of the spheres to identify coating elements and points in the center of the large spheres to excite as much of the underlying particle as possible. A comparison of the coating and ash particle composition (Table 3) shows higher Ca and S content in the coating material, supporting evidence of sulfate—as $CaSO_4$—formation on the ash particles under SCR reactor conditions.

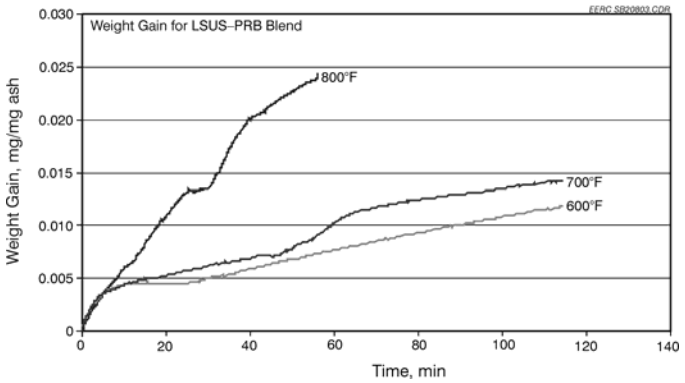

Figure 2. Weight changes for LSUS–PRB coal ash exposed to simulated flue gases and ammonia at three temperatures.

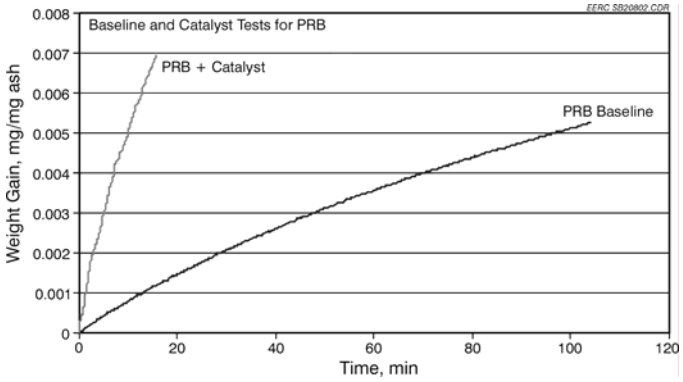

Figure 3. Weight changes for 100% PRB coal ash exposed to simulated flue gases and ammonia as with and without SCR catalyst present at 800°F.

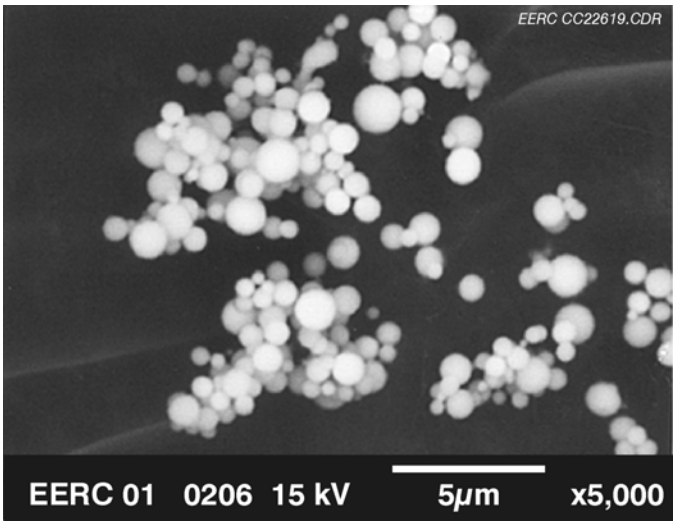

Figure 4. SEM micrograph of LSUS–PRB-blend coal ash exposed to simulated flue gases and ammonia at 800°F (no catalyst present).

Table 3. SEM Analysis of the LSUS–PRB Ash Exposed to Simulated Flue Gas, Ammonia, and Phosphorus in the TGA

Elemental Content	Coating, wt%	Particle and Coating, wt%
Al	15.9	12.6
Ba	0.0	1.0
Ca	20.0	10.6
Cl	0.1	0.0
Cr	0.0	0.0
Fe	4.9	5.6
K	1.7	1.0
Mg	2.1	3.1
Na	0.4	0.5
P	2.0	4.0
S	1.0	0.0
Si	14.5	21.8
Ti	0.9	3.0
O	36.4	36.5

Conclusions

The following observations were noted from the bench-scale phase of this research:

- PRB and lignite coals have the potential to blind SCR catalysts.
- A high blinding potential exists for LSUS–PRB blends.
- The addition of ammonia, phosphorus, and catalyst enhances the formation of phosphates and sulfates.
- Morphology analysis of fly ash exposed to SO_2, ammonia, and P in the TGA shows that sulfates and phosphates accumulated on the surface of the ash.

Acknowledgment. This investigation was supported by Alliant Energy, AmerenUE, Dynegy Midwest Generation, Kinectrics Inc., Ontario Power Generation, Otter Tail Power Company, EPRI, the Industrial Commission of North Dakota, Hitachi, Haldor-Topsoe, and Cormetech through the EERC Jointly Sponsored Research Program, which is supported by the U.S. Department of Energy National Energy Technology Laboratory under Cooperative Agreement No. DE-FC26-98FT40321.

References

(1) Licata, A.; Hartenstein, H.U.; Gutberlet, H. Utility Experience with SCR in Germany. 16th Annual International Pittsburgh Coal Conference, Pittsburgh, PA. Oct 11–15, 1999.

(2) Cichanovicz, J.E.; Broske, D.R. An Assessment of European Experience with Selective Catalytic Reduction in Germany and Denmark. EPRI–DOE–EPA Combined Utility Air Pollution Control Symposium: The MEGA Symposium, Atlanta, Georgia, Aug 16–20, 1999.

(3) Cichanovicz, J.E.; Muzio, L.J. Twenty-Five Years of SCR Evolution: Implications for U.S. Applications and Operation. EPRI–DOE–EPA Combined Utility Air Pollution Control Symposium: The MEGA Symposium, AWMA, Chicago, IL, Aug 20–23, 2001.

(4) Benson, S.A.; Fegley, M.M.; Hurley, J.P.; Jones, M.L.; Kalmanovitch, D.P.; Miller, B.G.; Miller, S.F.; Steadman, E.N.; Schobert, H.H.; Weber, B.J.; Weinmann, J.R.; Zobeck, B.J. *Project Sodium: A Detailed Evaluation of sodium Effects in Low Rank Coal Combustion Systems;* Final Technical Report; EERC publication, July 1988.

(5) Franklin, H.N. The Effect of Fuel Properties and Characteristics on Selective Catalytic Reduction Systems. In *Proceedings of the 1996 Joint Power Generation Conference*; Volume 1, ASME 1996, EC-Vol. 4/Fact-Vol. 21, pg. 421–428.

(6) Vredenbregt, L.H.J.; Meijer, R. The Effect of Cofiring Large Amounts of Secondary Fuels on SCR Deactivation. In the National Energy Technology Laborabory Web site. http://www.netl.doe.gov/ (accessed 12/10/03). In *Proceedings of the 2003 Conference on Selective Catalytic Reduction and Non-Catalytic Reduction for NO_x Control*, Pittsburgh, PA, October 29–30, 2003.

(7) Hurley, J.P.; Erickson, T.A.; Benson, S.A.; Brobjorg, J.N.; Steadman, E.N.; Mehta, A.K.; Schmidt, C.E. Ash Deposition at Low Temperatures in Boilers Firing Western U.S. Coals. International Joint Power Generation Conference; Elsevier Science, 1991; pp 1–8.

(8) Senior, C.;Linjewile, T.; Bockelie, M.; Baxter, L.; Bartholomew, C.; Hecker, W.; K. Whitty, K.; Eddings, E.. SCR Deactivation Mechanisms Related to Alkali & Alkaline Earth Elements. In the National Energy Technology Laborabory Web site. http://www.netl.doe.gov/ (accessed 12/10/03). In *Proceedings of the 2003 Conference on Selective Catalytic Reduction and Non-Catalytic Reduction for NO_x Control*, Pittsburgh, PA, October 29–30, 2003.

(9) Bullock, D.W.; Hartenstein, H. Full-Scale Catalyst Regeneration Experience of a Coal-Fired U.S. Merchant Plant. In the National Energy Technology Laboratory Web site. http://www.netl.doe.gov/ (accessed 12/10/03). In *Proceedings of the 2003 Conference on Selective Catalytic Reduction and Non-Catalytic Reduction for NO_x Control*, Pittsburgh, PA, October 29–30, 2003.

(10) Beck, J.; Unterberger, S.; Hein, K.R.G. Deactivation Mechanisms of SCR Catalysts During the Co-Combustion of Bio-Residues. In the National Energy Technology Laborabory Web site. http://www.netl.doe.gov/ (accessed 12/10/03). In *Proceedings of the 2003 Conference on Selective Catalytic Reduction and Non-Catalytic Reduction for NO_x Control*, Pittsburgh, PA, October 29–30, 2003.

(11) Rigby, K.; Johnson, R.; Neufort, R.; Gunther, P.; Hurns, E.; Katt, A.; Sigling, R. SCR Catalyst Design Issues and Operating Experience: Coals with High Arsenic Concentrations and Coals from the Powder River Basin. Presented at the International Joint Power Generation Conference, IJPGC2000-15067, July 23–26, 2000.